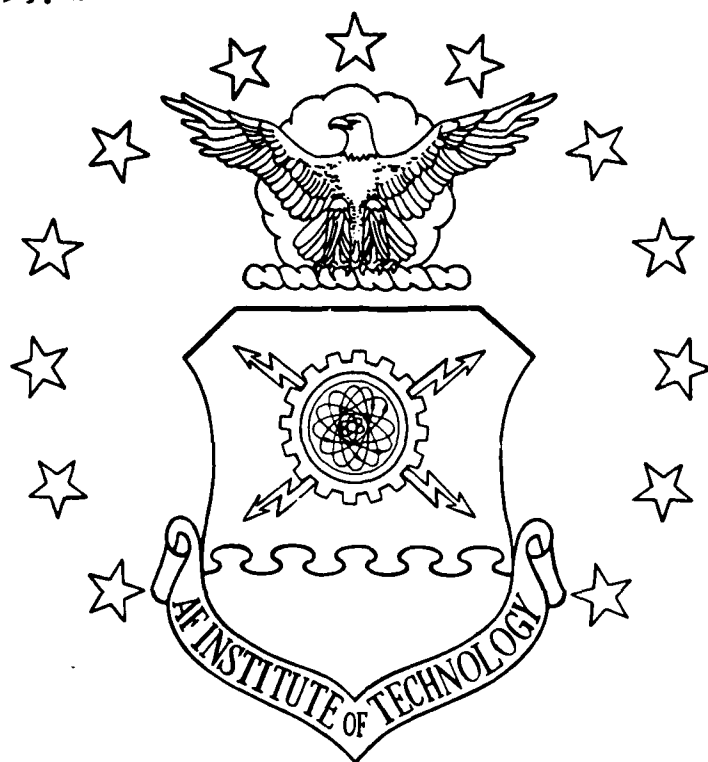


DTIC FILE COPY

1

AD-A216 411



MULTICELLULAR NATURAL CONVECTION  
IN A NARROW VERTICAL SLOT

THESIS

AFIT/GAE/ENY/89D-16

DAVID C. JARMAN

DTIC  
ELECTE  
JAN 03 1990

Dcs

DISTRIBUTION STATEMENT A

Approved for public release  
Distribution Unlimited

DEPARTMENT OF THE AIR FORCE  
AIR UNIVERSITY

**AIR FORCE INSTITUTE OF TECHNOLOGY**

Wright-Patterson Air Force Base, Ohio

90 01 02 098

①

DTIC  
ELECTE  
JAN 6 1980  
S D

MULTICELLULAR NATURAL CONVECTION  
IN A NARROW VERTICAL SLOT

THESIS

AFIT/GAE/ENY/89D-16      DAVID C. JARMAN

DISTRIBUTION STATEMENT A  
Approved for public release;  
Distribution Unlimited

MULTICELLULAR NATURAL CONVECTION IN  
A NARROW VERTICAL SLOT

THESIS

Presented to the Faculty of the School of Engineering  
of the Air Force Institute of Technology  
Air University  
In Partial Fulfillment of the  
Requirements for the Degree of  
Master of Science in Aeronautical Engineering

David C. Jarman  
Captain, USAF

December 1989



Accession For	
NTIS	CRA&I
DTIC	1AB
Unannounced	
Justification	
By _____	
Distribution/	
Availability Codes*	
Dist	Available for Special
A-1	

Approved for public release; distribution unlimited

## Preface

The purpose of this thesis is to study the influence of Prandtl number on multicellular flow in a narrow vertical slot. Research such as this has practical applications in technology systems that cool or insulate critical components. Some examples include nuclear reactor design, materials processing, aircraft cabin insulation, and actively cooled aircraft structures.

Both low Prandtl number ( $Pr \leq 0.1$ ) and high Prandtl number ( $Pr \geq 10$ ) fluids were investigated; including, Prandtl number of order one and the limiting condition of  $Pr \rightarrow 0$ . Due to lack of time, the solution for  $Pr \rightarrow \infty$  was not accomplished. Only the analytical and numerical equations governing this type of fluid behavior were formulated ( and should be investigated in any follow-on study ).

In preparing this thesis, I am eternally grateful for the assistance of others who helped me through this project. Especially, to Capt Daniel B. Fant, whose superb knowledge, technical expertise, and patience enabled me to accomplish my goal. I also wish to thank the other members of my thesis committee, Dr. Franke, and Dr Hitchcock. And finally, thanks to my wife, Maria, whose love and devotion made all this possible.

David C. Jarman

## Table of Contents

	page
Preface . . . . .	ii
List of Figures . . . . .	v
List of Symbols . . . . .	viii
Abstract . . . . .	xii
I. Introduction . . . . .	I - 1
Literature Review . . . . .	I - 3
II. Mathematical Analysis . . . . .	II - 1
Physical Model . . . . .	II - 1
Dimensional Formulation . . . . .	II - 3
Dimensionless Formulation . . . . .	II - 6
III. Analytical Analysis . . . . .	III - 1
Boundary Layer Equations for Low Prandtl Number ( $Pr \leq 0.1$ ) . . . . .	III - 1
Boundary Layer Equations for High Prandtl Number ( $Pr \geq 10.0$ ) . . . . .	III - 18
IV. Numerical Analysis . . . . .	IV - 1
Numerical Method . . . . .	IV - 2
Computational Procedure . . . . .	IV - 14
V. Results and Discussion . . . . .	V - 1
Zero Prandtl Number . . . . .	V - 1
Low Prandtl Number . . . . .	V - 5
Prandtl Number of Order One . . . . .	V - 7
High Prandtl Number . . . . .	V - 10
VI. Conclusions and Recommendations . . . . .	VI - 1
Conclusions . . . . .	VI - 1
Recommendations . . . . .	VI - 4

Appendix A: Supplementary Analytical Results . . . . .	A - 1
Bibliography . . . . .	B - 1
Vita . . . . .	C - 1

## List of Figures

Figure	Page
1. 2-D Vertical Slot Geometry . . . . .	II - 2
2. Computational Mesh with Variable Increments . . . .	IV - 3
3. Stream Function Contours for $Pr = 0$ . . . . .	V - 14
4. Stream Function Variation at the Horizontal Centerline . . . .	V - 15
5. Stream Function Relative Error . . . . .	V - 16
6. Vorticity Contours for $Pr = 0$ . . . . .	V - 17
7. Vorticity Variation at the Horizontal Centerline . . . . .	V - 18
8. Vorticity Relative Error . . . . .	V - 19
9. Stream Function Contours for $Pr = 0.02$ . . . . .	V - 20
10. Stream Function Variation at the Horizontal Centerline . . . .	V - 21
11. Stream Function Relative Error . . . . .	V - 22
12. Vorticity Contours for $Pr = 0.02$ . . . . .	V - 23
13. Vorticity Variation at the Horizontal Centerline . . . . .	V - 24
14. Vorticity Relative Error . . . . .	V - 25
15. Temperature Contours for $Pr = 0.02$ . . . . .	V - 26
16. Temperature Variation at the Horizontal Centerline . . . . .	V - 27
17. Temperature Relative Error . . . . .	V - 28
18. Stream Function Contours for $Pr = 0.706$ . . . . .	V - 29
19. Vorticity Contours for $Pr = 0.706$ . . . . .	V - 30
20. Temperature Contours for $Pr = 0.706$ . . . . .	V - 31

21.	Stream Function Variation at the Horizontal Centerline . . .	V - 32
22.	Stream Function Relative Error . . . . .	V - 33
23.	Vorticity Variation at the Horizontal Centerline . . . . .	V - 34
24.	Vorticity Relative Error . . . . .	V - 35
25.	Temperature Variation at the Horizontal Centerline . . . . .	V - 36
26.	Temperature Relative Error . . . . .	V - 37
27.	Stream Function Contours for $Pr = 1000$ . . . . .	V - 38
28.	Vorticity Contours for $Pr = 1000$ . . . . .	V - 39
29.	Temperature Contours for $Pr = 1000$ . . . . .	V - 40
30.	Stream Function Variation at the Horizontal Centerline . . .	V - 41
31.	Stream Function Relative Error . . . . .	V - 42
32.	Vorticity Variation at the Horizontal Centerline . . . . .	V - 43
33.	Vorticity Relative Error . . . . .	V - 44
34.	Temperature Variation at the Horizontal Centerline . . . . .	V - 45
35.	Temperature Relative Error . . . . .	V - 46
36.	Stream Function Variation at Node 12 . . . . .	A - 1
37.	Stream Function Relative Error . . . . .	A - 2
38.	Vorticity Variation at Node 12 . . . . .	A - 3
39.	Vorticity Relative Error . . . . .	A - 4
40.	Temperature Variation at Node 12 . . . . .	A - 5
41.	Temperature Relative Error . . . . .	A - 6
42.	Stream Function Variation at Node 32 . . . . .	A - 7
43.	Stream Function Relative Error . . . . .	A - 8



44.	Vorticity Variation at Node 32 . . . . .	A - 9
45.	Vorticity Relative Error . . . . .	A - 10
46.	Temperature Variation at Node 32 . . . . .	A - 11
47.	Temperature Relative Error . . . . .	A - 12
48.	Stream Function Variation at Node 50 . . . . .	A - 13
49.	Stream Function Relative Error . . . . .	A - 14
50.	Vorticity Variation at Node 50 . . . . .	A - 15
51.	Vorticity Relative Error . . . . .	A - 16
52.	Temperature Variation at Node 50 . . . . .	A - 17
53.	Temperature Relative Error . . . . .	A - 18

### List of Symbols

$C_0 - C_4$	Finite-difference expressions
$c$	Specific heat
$E$	Error term in finite-difference
$f$	$\bar{f}/\nu$ , dimensionless stream function in N-S equations
$\tilde{f}$	Dimensionless stream function in low-, high-, and infinite-Pr boundary-layer equations
$\bar{f}$	Dimensionless stream function in infinite-Pr analytical equations
$F$	Dimensionless stream function in zero-Pr boundary-layer equations
$\bar{F}$	Dimensional body force term
$g$	Acceleration of gravity
$G$	$l/L$ , dimensionless gap number in N-S equations
$\tilde{G}$	$Ra^{1/4} G$ , dimensionless scaled gap number in low-, high-, and infinite-Pr boundary-layer equations
$\hat{G}$	$(Ra/Pr)^{1/4} G$ , Dimensionless scaled gap number in zero-Pr boundary-layer equations
$H$	$h_f/h_b$ , horizontal increment ratio
$h_b, h_f$	Variable horizontal increments
$\hat{i}$	Unit vector in the horizontal ( X ) direction
$\hat{j}$	Unit vector in the vertical ( Y ) direction
$k$	Coefficient of thermal conductivity
$k_b, k_{b1}, k_f, k_{f1}$	Variable vertical increments
$L$	Width of the vertical slot

$l$	Length of the vertical slot
$NR$	Number of nodes in the horizontal direction
$NS$	Number of nodes in the vertical direction
$P, Q$	Dummy variables
$\bar{P}$	Pressure
$Pr$	$\nu/\alpha$ , Prandtl number
$Ra$	$\frac{g \beta l^3 \Delta T}{\nu \alpha}$ , Rayleigh number based on the length ( $l$ ) of the vertical slot
$S$	Source term in numerical method
$t$	$\bar{t} \nu/l^2$ , dimensionless time
$\tilde{t}$	$Ra^{1/2} t$ , dimensionless scaled time in low-, high-, and infinite-Pr boundary-layer equations
$\hat{t}$	$(Ra/Pr)^{1/2} t$ , dimensionless scaled time in zero-Pr boundary-layer equations
$T$	$(\bar{T} - T_o) / (T_i - T_o)$ , dimensionless temperature in N-S equations or zero-Pr boundary-layer equations
$\bar{T}$	Dimensionless temperature in infinite-Pr analytical equations or dimensional temperature in N-S equations
$\tilde{T}$	Dimensionless temperature in low-, high-, and infinite-Pr boundary-layer equations
$T_i$	Temperature at the left vertical wall
$T_o$	Temperature at the right vertical wall
$u$	$\bar{u} l/\nu = -\partial \bar{f}/\partial \bar{y}$ , dimensionless horizontal velocity in N-S equations
$\tilde{u}$	Dimensionless horizontal velocity in boundary-layer equations

$\bar{v}$	$\bar{v} L/\nu = \partial \bar{f} / \partial \bar{x}$ , dimensionless vertical velocity in N-S equations
$\tilde{v}$	Dimensionless vertical velocity in boundary-layer equations
$\bar{w}$	$\bar{w} ( l^2/\nu )$ , dimensionless vorticity in N-S equations or zero-Pr boundary-layer equations
$\tilde{w}$	Dimensionless vorticity in low-, high-, and infinite-Pr boundary-layer equations
$\bar{w}$	Dimensionless vorticity in infinite-Pr analytical equations or dimensional vorticity in N-S equations
$\bar{x}$	$\bar{x}/L$ , dimensionless horizontal coordinate
$\bar{y}$	$\bar{y}/l$ , dimensionless vertical coordinate
$\alpha$	$k/\rho c$ , thermal diffusivity
$\beta$	Coefficient of thermal expansion
$\epsilon$	Convergence criterion
$\lambda$	Parameter in finite-difference equations
$\mu$	Dynamic viscosity, or parameter in finite-difference equations
$\nu$	$\mu/\rho$ , momentum diffusivity
$\rho$	Density
$\tau$	Time increment in numerical method
$\phi$	Arbitrary dependent variable
$\Gamma$	Parameter in finite-difference equations
$\Omega_1$ , $\Omega_2$	Relaxation parameters in numerical method
$\bar{\nabla}$	Gradient differential operator
$\tilde{\Delta}$ , $\Delta_1$ , $\Delta_2$	Parameters in finite-difference equations
$\nabla^2$ , $\nabla_2^2$ ,	Second-order differential operators

### Superscripts

m                      Iteration number

n                      Time level

### Subscripts

i                      Horizontal position or heated vertical wall

j                      Vertical position

•                      Cooled vertical wall

0,1,....,10,12        Node position in computational molecule

## Abstract

The purpose of this study is to investigate the influence of Prandtl number on steady, or unsteady, flow behavior in a narrow vertical slot. The focus is to examine the effects of Prandtl number on natural convective flows, and the formation of single and multiple cells, over a range of Prandtl numbers from  $Pr = 0$  to  $Pr = \infty$ . Both numerical as well as analytical approaches are undertaken in studying these phenomena.

By assuming a large Rayleigh number and small gap, the two-dimensional Navier-Stokes equations are reduced to the simpler boundary-layer form. Boundary-layer equations are then derived for both the low ( $Pr \leq 0.1$ ) and high ( $Pr \geq 10$ ) Prandtl number regimes, including the limiting conditions of  $Pr \rightarrow 0$  and  $Pr \rightarrow \infty$ . Furthermore, the equations obtained for the low Prandtl number regime also hold for any finite Prandtl number in the range  $0 < Pr \leq 1.0$ .

Numerical solutions to these equations are obtained by using a stable, second-order, fully-implicit, time-accurate, Gauss-Siedel iterative procedure. In addition to numerical solutions, steady-state analytical solutions are derived using perturbative methods.

For most of the Prandtl numbers studied, the boundary-layer approximations produced results that compared well with those

obtained by other researchers using the complete Navier-Stokes equations and more sophisticated numerical and analytical techniques. The exception is in the high Prandtl number regime, which may have been due to neglecting the streamwise viscous terms. However, the results show that the boundary-layer approach captures all of the important physics of low Prandtl number fluid flows, flows where  $Pr \sim 1.0$ , and a significant portion of that involved with fluids of high Prandtl number.

Due to lack of time, the limiting condition where  $Pr \rightarrow \infty$  was not accomplished. However, the equations for this type of fluid are developed and presented in Chapter III. The  $Pr \rightarrow \infty$  case should be investigated in any follow-on studies that are conducted.

# MULTICELLULAR NATURAL CONVECTION IN A VERTICAL SLOT

## I. Introduction

The study of natural convection in vertical slots has received considerable attention from researchers over the past few decades. Practical applications of this research include nuclear reactor design, aircraft cabin insulation, cooling of electronic equipment, thermal storage systems, and material processing. At present, particular emphasis is being placed on the design of hypersonic vehicle airframe structures where the outer skin is cooled by the aircraft's fuel. Knowledge of the boundary conditions that generate multicellular flows is critical to the design of such vehicles since the formation of convective cells is the primary mechanism for heat transfer.

A complete understanding and analysis of the flow in the boundary-layer regime, corresponding to the limiting conditions of high Rayleigh number and small gap width, is still lacking. In addition, the influence of Prandtl number on the flow field is not well understood. In most cases, the focus of previous investigations has been on numerical studies of fluids with low Rayleigh numbers or high Prandtl numbers ( $Pr \geq 10.0$ ).

This thesis investigates the steady, or unsteady, flow behavior in a narrow vertical slot induced solely by buoyancy effects. The intent of this study is to examine the character-



istics of natural convective flows over a range of Prandtl numbers from  $Pr = 0$  to  $Pr = \infty$  -- including low Prandtl numbers ( $Pr \leq 0.1$ ), Prandtl number of order one ( $Pr \sim 1.0$ ), and high Prandtl numbers ( $Pr \geq 10.0$ ) -- and how the nature of the flow instability changes with Prandtl number.

In low Prandtl number fluids thermal diffusivity dominates, therefore the instabilities are hydrodynamic in nature. Whereas, in high Prandtl number fluids momentum diffusivity dominates and the instabilities are more thermal in nature.

Two approaches are used to accomplish the objectives of this thesis. First, the 2-D Navier-Stokes equations are simplified for the conditions of large Rayleigh number and small gap width. This reduces the equations to a 2-D boundary-layer form. Finite-differencing techniques are used to discretize the equations, which are then solved by computer (Vax 8650) to obtain the stream function, vorticity, and temperature distributions within the vertical slot.

It should be noted, there was considerable doubt that the boundary-layer form of the Navier-Stokes equations would capture the instabilities present in natural convective flow. This is because the streamwise viscous terms are neglected and it was believed that these terms play an important role in generating the multicellular instability. Fant (1987)

demonstrated that this is not true for flow through an annulus with a small radial gap. All of the physical properties of the flow were reproduced and compared well with experimental data. The same should also be true for the vertical slot as long as the gap is narrow and the Rayleigh number is large.

Second, perturbation methods are used to determine the analytical steady-state solution to the boundary-layer equations. These solutions are then compared to the numerical results and serve to reinforce confidence in the numerical algorithm and procedure.

#### Literature Review

Before discussing the details of this thesis, a review of related literature in this field of study is appropriate.

De Vahl Davis and Mallinson ( 1975 ) studied natural convection in a vertical slot for a fluid with  $Pr = 1000$  by numerically solving the conservative, second-order, finite-difference approximations to the steady-state Boussinesq equations. The left vertical wall was hot, while the right one was cool. The flow was assumed to be skew-symmetric about the horizontal centerline and no attempt was made to perturb the flow. Random occurrence of round-off errors in the computations was sufficient to initiate secondary motion. Several stream function and temperature plots were generated for increasing

values of Rayleigh number. Their results show that a temperature inversion within the flow field occurs when convective cells are formed in fluids with high Prandtl numbers.

Lee and Korpela ( 1983 ) studied the behavior of fluids in a narrow vertical slot. Their success in numerically resolving the multicellular flow field was attributed to the fourth-order differencing of Arakawa ( 1966 ), which was used to approximate the nonlinear, convective terms. However, they solved the complete Navier-Stokes system of equations:

$$\frac{\partial \zeta}{\partial t} = \frac{G}{H} J ( \zeta, \psi ) - \frac{\partial T}{\partial X} + \nabla^2 \zeta$$

$$\frac{\partial T}{\partial t} = \frac{G}{H} J ( T, \psi ) + \frac{1}{Pr} \nabla^2 T$$

$$\nabla^2 \psi = - \zeta$$

where  $G$  is the Grashof number,  $Pr$  is the Prandtl number,  $H$  is the aspect ratio,  $T$  is the temperature,  $J$  is the Jacobian,  $\zeta$  is the vorticity, and  $\psi$  is the stream function. Steady, multicellular flow for Prandtl numbers ranging from 0 to 1000 was obtained. However, as Prandtl number increased, the aspect ratio had to be increased to trigger the formation of multiple cells.

Chait and Korpela ( 1989 ) numerically simulated the multicellular flow between two vertical parallel plates using a time-splitting, pseudospectral method. The spectral approxi-

mation was obtained by expressing the flow variables as a double sum:

$$Q(x, y, t) = \text{Re} \left[ \sum_{k=-K+1}^K \sum_{n=0}^N \hat{Q}(n, k, t) T_n(x) e^{2\pi i k y / \lambda} \right].$$

in which Re denotes the real part of the expression that follows. This representation uses a spectral sum of Chebyshev polynomials,  $T_n(X)$ , in  $X$  and a Fourier expansion in  $Y$ . The parameter  $\lambda$  is the non-dimensional wavelength of the multicellular structure. The steady flow of air ( $Pr = 0.7$ ) and time-periodic flow of oil ( $Pr = 1000$ ) were investigated. The authors stated that the spectral transfer of kinetic energy and thermal variance for air was smooth and dominated by viscous forces; while that for oil was bumpier.

Henkes and Hoogendoorn (1989) submitted a paper this year on a numerical study of laminar natural convection in a square cavity for air ( $Pr = 0.71$ ) and water ( $Pr = 7.0$ ) using the unsteady, 2-D Navier-Stokes equations. The cavity consisted of a hot vertical wall and either conducting or adiabatic horizontal walls. In the case of conducting walls, stability was lost at a lower Rayleigh number than that for the case of adiabatic walls. The flow of water was found to be more stable than that of air. Above the critical Rayleigh number, the unsteady flow had a single frequency oscillation; except for air, which displayed two distinct frequencies when both the

horizontal walls were adiabatic. The authors stated that the instability seemed to be related to a hydraulic-jump instability. Whereas, for the case of conducting and adiabatic horizontal walls, the instability seemed to be related to a Rayleigh-Taylor/Bénard and Tollmien-Schlichting instability.

Keyhani, Prasad, and Cox ( 1988 ) performed an experimental study of natural convection heat transfer in a vertical cavity with discrete heat sources. One vertical wall was isothermally cooled. The opposing wall had eleven alternately unheated and flush-heated sections of equal height. The cavity was filled with ethylene glycol (  $Pr \sim 20$  ) and flow visualization pictures were obtained showing the primary, secondary, and tertiary flow patterns. Their study indicated that the local Nusselt numbers obtained in the enclosure are nearly the same as those reported for a wide flush-mounted heater on a vertical plate.

Elder ( 1965 ) performed an experimental study of natural convection for a liquid (  $Pr = 1000$  ) in vertical slots with isothermal walls. Single cell flows resulted when the Rayleigh number was less than  $10^5$ . For larger aspect ratios, a steady secondary flow was superimposed on the basic single cell. Increasing the Rayleigh number to above  $10^6$ , produced tertiary flow with counter-rotation.

Elder ( 1966 ) numerically solved the same problem described above for a moderate-size vertical slot. He dupli-

cated the basic flow field obtained in the experiment, but was unable to capture the secondary flow. Elder stated that the nonlinear terms began to dominate the motion as the Rayleigh number was increased; and was able to numerically show the development of the boundary-layers and fully developed boundary-layer flow.

Vest and Arpaci ( 1969 ) performed an analytical investigation of natural convection in a narrow vertical slot using linearized hydrodynamic stability theory. They obtained a neutral stability curve for the conduction-dominated flow regime. In addition, stream function plots for the secondary flow fields were obtained that qualitatively agreed with experimental results.

Korpela et al. ( 1973 ) used linear stability theory to examine the stability of the conduction regime for natural convection in a vertical slot. They claimed that instability set in as horizontal cells for  $Pr < 12.7$  . The instability was thought to be hydrodynamic in origin, resulting from the vorticity distribution of the base flow.

Korpela ( 1974 ) studied the problem of the narrow slot inclined at an angle  $\delta$ , from the vertical. Instabilities set in as transverse, traveling waves for small angles of inclination; whereas longitudinal cells formed as  $\delta$  reached a certain value.

For  $Pr < 0.24$ , Korpela claimed that only horizontal cells were possible and that the stability of the flow was mainly a function of  $Pr \tan \delta$ .

Pepper and Harris ( 1977 ) numerically obtained 2-D natural convective flow patterns in rectangular and annular vertical cavities. The energy and vorticity equations, in divergence form, were solved using central-differencing and a strongly implicit procedure. A weak multicellular flow pattern was obtained for  $Pr = 1000$  and  $Ra = 5 \times 10^5$ .

Seki et al. ( 1978 ) performed an experimental analysis of natural convection in narrow vertical rectangular cavities. Transformer oil, water, and glycerin were used as working fluids. Multicellular secondary flow was observed in each case. In the case for oil, as the temperature was increased, tertiary flow with counter-rotating cells developed until the flow near the upper region of the hot wall became unsteady and turbulent. They concluded that the flow more easily shifted from laminar to turbulent as the Prandtl number decreased and the cavity width increased.

From the literature search, it is evident that there is considerable interest in studying the multicellular flow phenomenon. Many theoretical, numerical, and experimental studies have been accomplished. However, none have used the

boundary-layer approach to solving the Navier-Stokes equations  
for the vertical slot geometry.

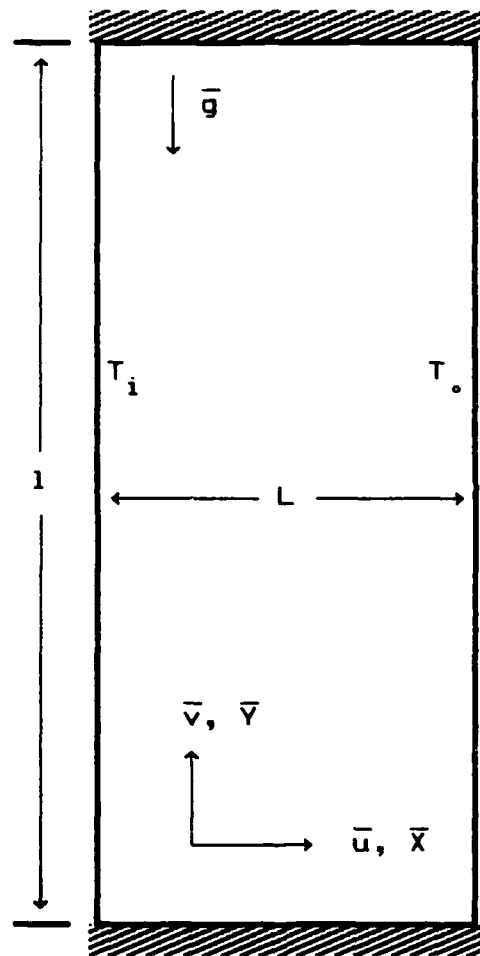


## II. Mathematical Analysis

This chapter describes a vorticity-stream function formulation of the Navier-Stokes equations in dimensionless form. Using this approach, the pressure terms are eliminated and the conservation of mass principle is automatically satisfied. The solutions to these equations are used to generate stream function, vorticity, and temperature contours that are useful for visualizing and analyzing the flow field. The final form of the equations is presented in Eqs ( 2.30 - 2.32 ) and ( 2.44 - 2.46 ).

### Physical Model

- a. The flow is unsteady and two-dimensional  
(see Figure 1).
- b. The fluid is initially at rest.
- c. The left vertical wall is isothermally heated, the right vertical wall is isothermally cooled.
- d. The fluid is Newtonian and laminar fluid motion is induced solely by buoyancy effects.
- e. All material properties are constant and density variations are allowed to occur by means of the Boussinesq approximation.




 ..... Adiabatic Wall

Figure 1. 2-D Vertical Slot Geometry.

## Dimensional Formulation

Governing Equations Using the Vorticity-Stream Function Approach. The vorticity-transport equation is obtained by taking the curl of the Navier-Stokes equations ( ref Incompressible Flow , p 328 ). This equation can be written as

$$\frac{\partial \bar{\omega}}{\partial t} + (\bar{v} \cdot \bar{\nabla}) \bar{\omega} = (\bar{\omega} \cdot \bar{\nabla}) \bar{v} + \nu \bar{\nabla}^2 \bar{\omega} + \bar{\nabla} \times \bar{F}_B, \quad (2.1)$$

where the bar over the variable indicates a dimensional quantity.  $\bar{\omega}$  and  $\bar{v}$  represent the dimensional form of the vorticity and velocity vectors, respectively.

The left side of the equation is the total rate of change of particle vorticity. The term  $(\bar{\omega} \cdot \bar{\nabla}) \bar{v}$  is identically zero for 2-D flows because the vorticity vector is always perpendicular to the plane of flow. The term  $\nu \bar{\nabla}^2 \bar{\omega}$  is the net rate of vorticity diffusion due to viscosity. The last term,  $\bar{\nabla} \times \bar{F}_B$ , is the rate of inertial vorticity generated by the body forces which result from density perturbations in natural convective flows.

It is interesting to note that the pressure (  $\bar{P}$  ) terms do not appear explicitly in Eq ( 2.1 ), since  $\bar{\nabla} \times \bar{\nabla} \bar{P} = 0$ . Therefore, the flow field can be determined without knowledge of the pressure distribution. Using the Boussinesq approximation, the net body force can be obtained. The resulting expression

is

$$\bar{F}_B = -g\beta(\bar{T} - T_0)\hat{j} , \quad (2.2)$$

where  $T_0$  is a known initial temperature,  $\beta$  is the coefficient of thermal expansion, and  $g$  is the acceleration due to gravity.

Making this substitution, the final form of the vorticity-transport equation becomes

$$\frac{\partial \bar{W}}{\partial \bar{t}} + \frac{\partial(\bar{f}, \bar{W})}{\partial(\bar{X}, \bar{Y})} = g\beta \frac{\partial \bar{T}}{\partial \bar{X}} + \nu \bar{\nabla}^2 \bar{W} , \quad (2.3)$$

and the thermal energy and stream function equations are

$$\frac{\partial \bar{T}}{\partial \bar{t}} + \frac{\partial(\bar{f}, \bar{T})}{\partial(\bar{X}, \bar{Y})} = \alpha \bar{\nabla}^2 \bar{T} , \quad (2.4)$$

and

$$\bar{W} = \bar{\nabla}^2 \bar{f} . \quad (2.5)$$

In the above equations,  $\bar{X}$  and  $\bar{Y}$  are the coordinate positions in the  $\hat{i}$  and  $\hat{j}$  directions,  $\bar{T}$  is the dimensional temperature variable, and  $\bar{t}$  is dimensional time.  $\nu$  and  $\alpha$  are the momentum and thermal diffusivities, respectively. The spacial velocities  $\bar{u}$  and  $\bar{v}$  have been written in terms of the stream function,  $\bar{f}$ , defined as

$$\bar{u} = - \frac{\partial \bar{f}}{\partial \bar{Y}} \quad \text{and} \quad \bar{v} = \frac{\partial \bar{f}}{\partial \bar{X}} . \quad (2.6)$$

This reduces the number of dependent variables by one. The convective terms are represented by the Jacobian,  $\partial(P,Q)/\partial(X,Y)$ ,

where

$$\frac{\partial(P,Q)}{\partial(X,Y)} = \frac{\partial P}{\partial X} \frac{\partial Q}{\partial Y} - \frac{\partial P}{\partial Y} \frac{\partial Q}{\partial X} . \quad ( 2.7 )$$

These three coupled equations ( Eqs 2.3 - 2.5 ) describe the vorticity, temperature, and stream function for the vertical slot.

Boundary Conditions. For temperature, the left and right vertical walls are isothermally heated and cooled, respectively. The top and bottom horizontal walls are adiabatic. Therefore, the boundary conditions are:

$$\bar{T}(0,\bar{Y}) = T_i \quad ( 2.8 )$$

$$\bar{T}(L,\bar{Y}) = T_o \quad ( 2.9 )$$

$$\frac{\partial \bar{T}}{\partial \bar{Y}}(\bar{X},0) = \frac{\partial \bar{T}}{\partial \bar{Y}}(\bar{X},1) = 0 . \quad ( 2.10 )$$

The velocity components,  $\bar{u}$  and  $\bar{v}$ , are identically zero along the vertical and horizontal walls. This requirement gives the boundary conditions for stream function and vorticity:

$$\bar{f}(0,\bar{Y}) = \bar{f}(L,\bar{Y}) = \bar{f}(\bar{X},0) = \bar{f}(\bar{X},1) = 0 \quad ( 2.11 )$$

$$\bar{w} = \left. \frac{\partial^2 \bar{f}}{\partial \bar{X}^2} \right|_{\bar{X}=0,L} \quad ( 2.12 )$$

$$\bar{w} = \left. \frac{\partial^2 \bar{f}}{\partial \bar{Y}^2} \right|_{\bar{Y}=0,1} . \quad ( 2.13 )$$

Initial Conditions. Since the fluid is initially at rest,

$$\bar{f} = \bar{w} = 0 \text{ and } \bar{T} = T_0 \quad ( 2.14 )$$

throughout the vertical slot, except at the left wall where

$$\bar{T} = T_i \quad ( 2.15 )$$

is enforced.

### Dimensionless Formulation

Writing equations in dimensionless form has three distinct advantages:

- a. it simplifies the mathematical or numerical expressions, allowing for better interpretation
- b. measurement scales are no longer an intrinsic part of the physical quantities, therefore, any laws governing physical variables are valid for all different measurement systems  
( Fant, 1987 )
- c. fewer variables are used and the proper dimensionless groups characterizing a particular flow model become evident.

Coordinate Transformation. The  $\bar{X}$  and  $\bar{Y}$  spacial coordinates are non-dimensionalized using the appropriate length scales from the vertical slot geometry,

$$X = \frac{\bar{X}}{L} \text{ and } Y = \frac{\bar{Y}}{1} . \quad ( 2.16 )$$

Time, the other independent variable, is non-dimensionalized as

$$t = \frac{\bar{t}\nu}{l^2} \quad \text{or} \quad \frac{\bar{t}\alpha}{l^2} . \quad ( 2.17 )$$

The dimensionless gap,  $G$ , is defined as

$$G = \frac{L}{l} . \quad ( 2.18 )$$

Also,

$$Pr = \frac{\nu}{\alpha} \quad ( 2.19 )$$

and

$$Ra = \frac{g\beta l^3 (T_i - T_o)}{\nu\alpha} . \quad ( 2.20 )$$

#### Navier-Stokes Equations for Low Prandtl Number

(  $Pr \leq 0.1$  ). In dimensionless form, the dependent variables are written as:

$$T = \frac{\bar{T} - T_o}{T_i - T_o} \quad (\text{temperature}) \quad ( 2.21 )$$

$$W = \frac{\bar{W}l^2}{\nu} \quad (\text{vorticity}) \quad ( 2.22 )$$

$$f = \frac{\bar{f}}{\nu} \quad (\text{stream function}). \quad ( 2.23 )$$

In addition,

$$\frac{\partial}{\partial \bar{X}} = \frac{\partial X}{\partial \bar{X}} \frac{\partial}{\partial X} = \frac{1}{L} \frac{\partial}{\partial X} \quad ( 2.24 )$$

$$\frac{\partial}{\partial \bar{Y}} = \frac{\partial Y}{\partial \bar{Y}} \frac{\partial}{\partial Y} = \frac{1}{l} \frac{\partial}{\partial Y} \quad ( 2.25 )$$

$$\frac{\partial^2}{\partial \bar{X}^2} = \frac{1}{L^2} \frac{\partial^2}{\partial X^2} \quad (2.26)$$

$$\frac{\partial^2}{\partial \bar{Y}^2} = \frac{1}{l^2} \frac{\partial^2}{\partial Y^2} \quad (2.27)$$

$$\bar{u} = - \frac{\partial \bar{f}}{\partial \bar{Y}} = - \frac{\nu u}{l} \quad (2.28)$$

$$\bar{v} = \frac{\partial \bar{f}}{\partial \bar{X}} = \frac{\nu v}{L} \quad (2.29)$$

When Eqs ( 2.16 - 2.29 ) are substituted into Eqs ( 2.3 - 2.5 ), the following non-dimensional form of the Navier Stokes equations result

Energy:

$$G^2 \frac{\partial T}{\partial \bar{t}} + G \left\{ \frac{\partial f}{\partial \bar{X}} \frac{\partial T}{\partial \bar{Y}} - \frac{\partial f}{\partial \bar{Y}} \frac{\partial T}{\partial \bar{X}} \right\} = \frac{1}{Pr} \left\{ \frac{\partial^2 T}{\partial \bar{X}^2} + G^2 \frac{\partial^2 T}{\partial \bar{Y}^2} \right\} \quad (2.30)$$

Vorticity:

$$\begin{aligned} Pr \left\{ G^2 \frac{\partial W}{\partial \bar{t}} + G \left[ \frac{\partial f}{\partial \bar{X}} \frac{\partial W}{\partial \bar{Y}} - \frac{\partial W}{\partial \bar{X}} \frac{\partial f}{\partial \bar{Y}} \right] \right\} &= G Ra_1 \frac{\partial T}{\partial \bar{X}} \\ &+ Pr \left\{ \frac{\partial^2 W}{\partial \bar{X}^2} + G^2 \frac{\partial^2 W}{\partial \bar{Y}^2} \right\} \end{aligned} \quad (2.31)$$

Stream Function:

$$W = \frac{1}{G^2} \frac{\partial^2 f}{\partial \bar{X}^2} + \frac{\partial^2 f}{\partial \bar{Y}^2} = \nabla^2 f, \quad (2.32)$$



where

$$\nabla^2 = \frac{1}{G^2} \frac{\partial^2}{\partial X^2} + \frac{\partial^2}{\partial Y^2} . \quad ( 2.33 )$$

G, Pr, and Ra are three dimensionless parameters that arise from this analysis and are used to simulate various flow conditions and geometries. The gap number, G, defines the vertical slot geometry. It is analagous to the aspect ratio used to define other geometries, such as airfoils. The Prandtl number, Pr, characterizes the fluid and is the ratio of momentum to thermal diffusivity. The Rayleigh number, Ra, is the ratio of the buoyant forces, which are destabilizing, to the viscous forces, which tend to stabilize the flow. The magnitude of Ra can be used to predict the onset of thermal and/or hydrodynamic instability, since the transition to instability usually occurs at some critical value of Ra.

The variables W, f, and t, in Eqs ( 2.30 - 2.32 ), are non-dimensionalized with  $\nu$ , instead of  $\alpha$ , to reflect a thermal-diffusion dominated energy equation for small Prandtl numbers. Later on in this thesis, when high Prandtl number flows are investigated,  $\alpha$  will be used to non-dimensionalize the equations to reflect momentum-diffusion dominated flows.

Non-dimensional Boundary Conditions. The non-dimensionalized boundary conditions for the vertical slot are obtained by substituting Eqs ( 2.21 - 2.23 ) into Eqs ( 2.11 - 2.13 ) and

noting that:

at  $\bar{X} = 0$ ,

$$X = 0 \quad \text{and} \quad T = 1;$$

at  $\bar{X} = L$ ,

$$X = 1 \quad \text{and} \quad T = 0;$$

at  $\bar{Y} = 0$ ,

$$Y = 0 \quad \text{and} \quad \frac{\partial T}{\partial Y} = 0;$$

at  $\bar{Y} = 1$ ,

$$Y = 1 \quad \text{and} \quad \frac{\partial T}{\partial Y} = 0.$$

The boundary conditions are:

$$f(0,Y) = f(1,Y) = f(X,0) = f(X,1) = 0 \quad (2.34)$$

$$\left. \frac{\partial f}{\partial X} \right|_{X=0,1} = \left. \frac{\partial f}{\partial Y} \right|_{Y=0,1} = 0 \quad (2.35)$$

$$T(0,Y) = 1, \quad T(1,Y) = 0 \quad (2.36)$$

$$\left. \frac{\partial T}{\partial Y} \right|_{Y=0,1} = 0 \quad (2.37)$$

$$W = \frac{1}{G^2} \left. \frac{\partial^2 f}{\partial X^2} \right|_{X=0,1} \quad (2.38)$$

and

$$W = \left. \frac{\partial^2 f}{\partial Y^2} \right|_{Y=0,1}. \quad (2.39)$$

Non-dimensional Initial Conditions. The dimensionless initial conditions are similar to Eqs ( 2.14 - 2.15 ) for the entire vertical slot,

$$f = W = T = 0 . \quad ( 2.40 )$$

Except, at the left vertical wall where

$$T = 1 . \quad ( 2.41 )$$

Note that at rest,  $Ra = 0$ , and the problem becomes one of steady-state conduction. Initial conditions other than zero are also used, and will be explained in Chapter IV.

Navier-Stokes Equations for High Prandtl Number (  $Pr \geq 10.0$  ). The procedure for formulating the high Prandtl number equations is similar to that for small Prandtl number.  $\alpha$  replaces  $\nu$  as the non-dimensionalizing parameter to reflect a momentum-diffusion dominated vorticity equation. Dimensionless vorticity, stream function, and time are

$$W = \frac{\bar{W} l^2}{\alpha}, \quad f = \frac{\bar{f}}{\alpha}, \quad \text{and} \quad t = \frac{\bar{t} \alpha}{l^2} . \quad ( 2.43 )$$

The dimensionless form of the energy, vorticity, and stream function equations become

Energy:

$$\begin{aligned} G^2 \frac{\partial T}{\partial t} + G \left\{ \frac{\partial f}{\partial X} \frac{\partial T}{\partial Y} - \frac{\partial f}{\partial Y} \frac{\partial T}{\partial X} \right\} \\ = \frac{\partial^2 T}{\partial X^2} + G^2 \frac{\partial^2 T}{\partial Y^2} \end{aligned} \quad ( 2.44 )$$

Vorticity:

$$\begin{aligned} G^2 \frac{\partial W}{\partial t} + G \left\{ \frac{\partial f}{\partial X} \frac{\partial W}{\partial Y} - \frac{\partial f}{\partial Y} \frac{\partial W}{\partial X} \right\} \\ = Pr \left\{ G Ra_1 \frac{\partial T}{\partial X} + \frac{\partial^2 W}{\partial X^2} + G^2 \frac{\partial^2 W}{\partial Y^2} \right\} \end{aligned} \quad ( 2.45 )$$

Stream Function:

$$W = \frac{1}{G^2} \frac{\partial^2 f}{\partial X^2} + \frac{\partial^2 f}{\partial Y^2} . \quad ( 2.46 )$$

Compare these equations with Eqs ( 2.30 - 2.32 ). The energy equation is no longer dependent on Prandtl number; but a strong dependency now exists on the diffusion side of the vorticity equation. Boundary and initial conditions are the same ( Eqs 2.34 - 2.41 ).

### III. Analytical Analysis

In this chapter, simplified boundary-layer equations are derived from the 2-D Navier-Stokes equations for certain limiting conditions. Analytical steady-state solutions to these equations are then determined. The best approach to this analysis was taken from Fant ( 1987 ).

#### Boundary-Layer Equations for Low Prandtl Number ( $Pr \leq 0.1$ ).

Using a high Rayleigh number/small-gap asymptotic expansion, Fant ( 1987 ) derived simplified, boundary-layer equations from the 2-D Navier-Stokes equations that modeled a narrow cylindrical annulus. These equations were valid in the double limit as  $Ra \rightarrow \infty$  and  $G \rightarrow 0$  . The following expansions for the dimensionless velocity components, vorticity, stream function, and temperature were obtained:

$$u = Ra^{1/4} \tilde{u} + O(Ra^{-1/4}) \quad ( 3.1 )$$

$$v = Ra^{1/4} \tilde{v} + O(1) \quad ( 3.2 )$$

$$W = Ra^{3/4} \tilde{W} + O(Ra^{1/4}) \quad ( 3.3 )$$

$$f = Ra^{1/4} \tilde{f} + O(Ra^{-1/4}) \quad ( 3.4 )$$

$$T = \tilde{T} + O(Ra^{-1/2}) \quad ( 3.5 )$$

The tilde over the variable is used to indicate a scaled dimensionless quantity. These scalings are a result of the

boundary layer thickness being of order

$$\delta \sim Ra^{-1/4} . \quad ( 3.6 )$$

The above scalings will be incorporated into the present study to obtain boundary-layer equations that model the narrow vertical slot geometry. Since the left and right wall boundary layers merge as  $G \rightarrow 0$ , the point at which they just begin to contact each other is

$$2\delta = L . \quad ( 3.7 )$$

Substituting Eq ( 2.18 ) into Eq ( 3.7 ) gives the relationship between gap number and boundary-layer thickness.

$$2\delta = Gl \quad \text{or} \quad G = \frac{2}{1} \delta . \quad ( 3.8 )$$

But,  $\delta \sim Ra^{-1/4}$ . Therefore,  $G \sim Ra^{-1/4}$ . With this result, the proper scale for gap number is

$$G = \tilde{G} Ra^{-1/4} . \quad ( 3.9 )$$

To maintain the unsteady terms in Eqs ( 2.30 - 2.31 ), the appropriate scale for time is

$$t = \tilde{t} Ra^{-1/2} . \quad ( 3.10 )$$

Eqs ( 3.3 - 3.5 ) and ( 3.9 - 3.10 ) can now be substituted into Eqs ( 2.30 - 2.32 ). Starting with the energy equation ( Eq 2.30 ),

$$\frac{\tilde{G}^2}{Ra^{1/2}} (Ra^{1/2}) \frac{\partial \tilde{T}}{\partial \tilde{t}} + \frac{\tilde{G}}{Ra^{1/4}} \left\{ Ra^{1/4} \frac{\partial \tilde{f}}{\partial X} \frac{\partial \tilde{T}}{\partial Y} - Ra^{1/4} \frac{\partial \tilde{f}}{\partial Y} \frac{\partial \tilde{T}}{\partial X} \right\}$$

$$= \frac{1}{Pr} \left\{ \frac{\partial^2 \tilde{T}}{\partial X^2} + \frac{\tilde{G}^2}{Ra^{1/2}} \frac{\partial^2 \tilde{T}}{\partial Y^2} \right\} ,$$

which reduces to

$$\tilde{G}^2 \frac{\partial \tilde{T}}{\partial \tilde{t}} + \tilde{G} \left\{ \frac{\partial \tilde{f}}{\partial X} \frac{\partial \tilde{T}}{\partial Y} - \frac{\partial \tilde{f}}{\partial Y} \frac{\partial \tilde{T}}{\partial X} \right\}$$

$$= \frac{1}{Pr} \left\{ \frac{\partial^2 \tilde{T}}{\partial X^2} + \frac{\tilde{G}^2}{Ra^{1/2}} \frac{\partial^2 \tilde{T}}{\partial Y^2} \right\} . \quad ( 3.11 )$$

Likewise, substituting into the vorticity equation ( Eq 2.31 ) gives

$$Pr \tilde{G}^2 \frac{\partial \tilde{W}}{\partial \tilde{t}} + \tilde{G} Pr \left\{ \frac{\partial \tilde{f}}{\partial X} \frac{\partial \tilde{W}}{\partial Y} - \frac{\partial \tilde{W}}{\partial X} \frac{\partial \tilde{f}}{\partial Y} \right\}$$

$$= \tilde{G} \frac{\partial \tilde{T}}{\partial \tilde{t}} + Pr \left\{ \frac{\partial^2 \tilde{W}}{\partial X^2} + \frac{\tilde{G}^2}{Ra^{1/2}} \frac{\partial^2 \tilde{W}}{\partial Y^2} \right\} . \quad ( 3.12 )$$

And, the stream function equation ( Eq 2.32 ) becomes

$$\frac{\partial^2 \tilde{f}}{\partial X^2} + \frac{\tilde{G}^2}{Ra^{1/2}} \frac{\partial^2 \tilde{f}}{\partial Y^2} = \tilde{G}^2 \tilde{W} . \quad ( 3.13 )$$

For large Rayleigh number and small gap, the following orders of magnitude are evident:

$$\frac{\tilde{G}^2}{Ra^{1/2}} \frac{\partial^2 \tilde{f}}{\partial Y^2} \ll \frac{\partial^2 \tilde{f}}{\partial X^2}$$

$$\frac{\tilde{G}^2}{Ra^{1/2}} \frac{\partial^2 \tilde{W}}{\partial Y^2} \ll \frac{\partial^2 \tilde{W}}{\partial X^2}$$

$$\frac{\tilde{G}^2}{Ra^{1/2}} \frac{\partial^2 \tilde{f}}{\partial Y^2} \ll \frac{\partial^2 \tilde{f}}{\partial X^2} .$$

Neglecting these higher order terms, the Navier-Stokes equations for low Prandtl numbers reduce to the simplified boundary-layer form

Energy:

$$\tilde{G}^2 \frac{\partial \tilde{T}}{\partial \tilde{t}} + \tilde{G} \left\{ \frac{\partial \tilde{f}}{\partial X} \frac{\partial \tilde{T}}{\partial Y} - \frac{\partial \tilde{f}}{\partial Y} \frac{\partial \tilde{T}}{\partial X} \right\} = \frac{1}{Pr} \frac{\partial^2 \tilde{T}}{\partial X^2} \quad ( 3.14 )$$

Vorticity:

$$\begin{aligned} Pr \tilde{G}^2 \frac{\partial \tilde{W}}{\partial \tilde{t}} + \tilde{G} Pr \left\{ \frac{\partial \tilde{f}}{\partial X} \frac{\partial \tilde{W}}{\partial Y} - \frac{\partial \tilde{W}}{\partial X} \frac{\partial \tilde{f}}{\partial Y} \right\} \\ = \tilde{G} \frac{\partial \tilde{T}}{\partial X} + Pr \frac{\partial^2 \tilde{W}}{\partial X^2} \end{aligned} \quad ( 3.15 )$$

Stream Function:

$$\frac{1}{\tilde{G}^2} \frac{\partial^2 \tilde{f}}{\partial X^2} = \tilde{W} . \quad ( 3.16 )$$

Eqs ( 3.14 - 3.16 ) are valid only for large Rayleigh and small gap numbers. They also hold for any finite Prandtl number less than or equal to one. Furthermore, there is no longer any dependency on  $\partial^2/\partial Y^2$  terms. Thus, the number of terms are



reduced, as well as the boundary and initial conditions that go with them. The boundary conditions are:

$$\tilde{f}(0,Y) = \tilde{f}(1,Y) = \tilde{f}(X,0) = \tilde{f}(X,1) = 0 \quad (3.17)$$

$$\left. \frac{\partial \tilde{f}}{\partial X} \right|_{X=0,1} = \left. \frac{\partial \tilde{f}}{\partial Y} \right|_{Y=0,1} = 0 \quad (3.18)$$

$$\tilde{T}(0,Y) = 1, \quad \tilde{T}(1,Y) = 0 \quad (3.19)$$

$$\left. \frac{\partial \tilde{T}}{\partial Y} \right|_{Y=0,1} = 0 \quad (3.20)$$

$$\left. \frac{\partial^2 \tilde{f}}{\partial X^2} \right|_{X=0,1} = \tilde{G}^2 \tilde{W} . \quad (3.21)$$

The initial conditions are:

$$\tilde{f} = \tilde{W} = \tilde{T} = 0 , \quad (3.22)$$

except at the left vertical wall where

$$\tilde{T} = 1 . \quad (3.23)$$

#### Steady-State Analytical Solution for Low Prandtl Number .

To a leading order, in the limit as  $\tilde{G} \rightarrow 0$ , Eqs ( 3.14 - 3.16 ) reduce to

Energy:

$$\frac{\partial^2 \tilde{T}}{\partial Y^2} = 0 \quad (3.24)$$

Vorticity:

$$\frac{\partial^2 \tilde{W}}{\partial X^2} = 0 \quad (3.25)$$

Stream Function:

$$\frac{\partial^2 \tilde{f}}{\partial x^2} = 0 \quad (3.26)$$

Therefore, the energy equation ( Eq 3.14 ) simplifies to the steady-state, 1-D conduction equation, which can then be integrated to obtain

$$\tilde{T} = 1 - x \quad (3.27)$$

for the boundary conditions of this problem.

From the no-slip condition, the vorticity and velocity components are identically zero at the walls. The convective terms can thus be ignored and the temperature distribution is completely determined by the linear relationship of Eq ( 3.27 ). With these results, and assuming steady-state (  $\partial/\partial t$  ) conditions, the following asymptotic expansions are obtained ( Fant, 1987 ):

$$\tilde{T} = ( 1 - x ) + \tilde{G}^4 T_1 + \tilde{G}^8 T_2 + O(\tilde{G}^{16}) \quad (3.28)$$

$$\tilde{W} = \tilde{G} W_1 + \tilde{G}^5 W_2 + O(\tilde{G}^9) \quad (3.29)$$

$$\tilde{f} = \tilde{G}^3 f_1 + \tilde{G}^7 f_2 + O(\tilde{G}^9) \quad (3.30)$$

Rearranging the stream function equation for low Pr ( Eq 3.16 ) results in the following expression for vorticity:

$$\tilde{W} = \frac{1}{\tilde{G}^2} \frac{\partial^2 \tilde{f}}{\partial x^2} \quad (3.31)$$

Assuming steady-state conditions and substituting  
Eq ( 3.31 ) into Eq ( 3.15 ) now gives

$$\frac{1}{\tilde{G}} \text{Pr} \left\{ \frac{\partial \tilde{f}}{\partial x} \frac{\partial^3 \tilde{f}}{\partial x^2 \partial y} - \frac{\partial^3 \tilde{f}}{\partial x^3} \frac{\partial \tilde{f}}{\partial y} \right\} = \tilde{G} \frac{\partial \tilde{T}}{\partial x} + \text{Pr} \frac{\partial^4 \tilde{f}}{\partial x^4} . \quad ( 3.32 )$$

Substituting Eq ( 3.30 ) into this expression and equating  
like coefficients yields

$$\tilde{G} : \quad \frac{\partial^4 f_1}{\partial x^4} = \frac{1}{\text{Pr}} \quad ( 3.33 )$$

$$\begin{aligned} \tilde{G}^5 : \quad \text{Pr} \left\{ \frac{\partial f_1}{\partial x} \frac{\partial^3 f_1}{\partial x^2 \partial y} - \frac{\partial^3 f_1}{\partial x^3} \frac{\partial f_1}{\partial y} + \frac{\partial^4 f_2}{\partial x^4} \right\} \\ + \frac{\partial \tilde{T}_1}{\partial x} = 0 \end{aligned} \quad ( 3.34 )$$

$$\begin{aligned} \tilde{G}^9 : \quad \text{Pr} \left\{ \frac{\partial^3 f_1}{\partial x^2 \partial y} \frac{\partial f_2}{\partial x} + \frac{\partial f_1}{\partial x} \frac{\partial^3 f_2}{\partial x^2 \partial y} - \frac{\partial^3 f_2}{\partial x^3} \frac{\partial f_1}{\partial y} \right. \\ \left. - \frac{\partial^3 f_1}{\partial x^3} \frac{\partial f_2}{\partial y} \right\} + \frac{\partial \tilde{T}_2}{\partial x} = 0 \end{aligned} \quad ( 3.35 )$$

$$\tilde{G}^{13} : \quad \text{Pr} \left\{ \frac{\partial f_2}{\partial x} \frac{\partial^3 f_2}{\partial x^2 \partial y} - \frac{\partial^3 f_2}{\partial x^3} \frac{\partial f_2}{\partial y} \right\} = 0 . \quad ( 3.36 )$$

An expression for  $f_1(x)$ , in terms of the Prandtl number,  
can be obtained by integrating Eq ( 3.33 ).

$$f_1(X) = \frac{1}{4!Pr} X^4 + \frac{C_1}{3!} X^3 + \frac{C_2}{2} X^2 + C_3 X + C_4 . \quad (3.37)$$

Applying the boundary conditions ( Eqs 3.17 - 3.18 ) yields the final result for  $f_1(X)$  .

$$f_1(X) = \frac{1}{24 Pr} X^2 (X - 1)^2 . \quad (3.38)$$

Equation ( 3.38 ) can be differentiated twice to obtain an expression for  $w_1(X)$  .

$$w_1(X) = \frac{\partial^2 f_1}{\partial X^2} = \frac{1}{2 Pr} (X^2 - X + \frac{1}{6}) . \quad (3.39)$$

Using Eq ( 3.34 ), and noting the  $\partial f_1 / \partial Y = 0$  and  $\partial T_1 / \partial X = 0$ , leads to

$$f_2 = w_2 = 0 .$$

Substituting Eq ( 3.38 ) into Eq ( 3.30 ) and Eq ( 3.39 ) into Eq ( 3.29 ) gives the final result for stream function and vorticity.

$$\tilde{f} = \frac{\tilde{G}^3}{24 Pr} X^2 (X - 1)^2 \quad (3.40)$$

$$\tilde{w} = \frac{\tilde{G}}{2 Pr} \left\{ X^2 - X + \frac{1}{6} \right\} . \quad (3.41)$$

The temperature is ( see Fant, 1987 )

$$\tilde{T} = (1 - X) + \tilde{G}^8 T_2 , \quad (3.42)$$

where

$$T_2 = \frac{-1}{96 \text{ Pr}} \left\{ A_1 + \frac{A_2}{\text{Pr}} \right\} + \frac{A_3}{34560} \quad (3.43)$$

$$A_1 = \frac{-x^{11}}{415800} + \frac{x^{10}}{75600} + \frac{-x^9}{45360} + \frac{x^6}{10800} + \frac{-x^5}{6900} \\ + \frac{x^4}{15120} + \frac{-x}{387701} \quad (3.44)$$

$$A_2 = \frac{x^{11}}{83160} + \frac{-x^{10}}{15120} + \frac{x^9}{6480} + \frac{-x^8}{5040} + \frac{x^7}{7560} \\ + \frac{-x^5}{15120} + \frac{x^4}{30240} + \frac{-x}{997934} \quad (3.45)$$

$$A_3 = \frac{-4}{55} x^{11} + \frac{2}{5} x^{10} + \frac{-5}{6} x^9 + \frac{3}{4} x^8 + \frac{-5}{21} x^7 \\ + \frac{2}{15} x^6 + \frac{-3}{10} x^5 + \frac{x^4}{6} + \frac{-x}{171} \quad (3.46)$$

It is important to note that the above analytical expressions are valid for any finite Prandtl number less than or equal to one.

Limiting Equations for Zero Prandtl Number. One of the primary objectives of this thesis is to study the behavior of very low Prandtl number fluids, which is characteristic of liquid metals, in a vertical slot. To accomplish this, the low Prandtl number boundary-layer equations are simplified for the

limiting condition of  $Pr \rightarrow 0$ . Although numerical studies of such flows have been done before, none have used the boundary-layer equation approach.

First, let  $Pr \rightarrow 0$  and assume the temperature is  $O(1)$ . Next, assume that the vorticity and stream functions have the form

$$\tilde{w} = \lambda_1 W + \dots \quad (3.47)$$

$$\tilde{f} = \lambda_2 F + \dots \quad (3.48)$$

And, from the stream function equation ( Eq 3.16 ),

$$\lambda_2 \sim \tilde{G}^2 \lambda_1 \quad (3.49)$$

By substituting these expressions into Eqs ( 3.14 - 3.16 ), the energy equation can be written as

$$\tilde{G}^2 \frac{\partial \tilde{T}}{\partial \tilde{t}} + \tilde{G} \lambda_2 \left\{ \frac{\partial F}{\partial X} \frac{\partial \tilde{T}}{\partial Y} - \frac{\partial F}{\partial Y} \frac{\partial \tilde{T}}{\partial X} \right\} = \frac{1}{Pr} \frac{\partial^2 \tilde{T}}{\partial X^2} \quad (3.50)$$

Likewise, the vorticity equation becomes

$$\begin{aligned} Pr \tilde{G}^2 \lambda_1 \frac{\partial W}{\partial \tilde{t}} + Pr \tilde{G} \lambda_2 \lambda_1 \left\{ \frac{\partial F}{\partial X} \frac{\partial W}{\partial Y} - \frac{\partial F}{\partial Y} \frac{\partial W}{\partial X} \right\} \\ = \tilde{G} \frac{\partial \tilde{T}}{\partial X} + Pr \lambda_1 \frac{\partial^2 W}{\partial X^2} \end{aligned} \quad (3.51)$$

And, the stream function equation is

$$\lambda_1 W = \frac{1}{\tilde{G}^2} \lambda_2 \frac{\partial^2 F}{\partial x^2} . \quad ( 3.52 )$$

To retain the physics of the flow, it becomes evident that

$$\frac{\tilde{G}^2 \text{Pr} \lambda_1}{\tilde{t}} \sim \text{Pr} \tilde{G} \lambda_2 \lambda_1 \sim \text{Pr} \lambda_1 \sim \tilde{G} . \quad ( 3.53 )$$

By equating the first and third terms,

$$\frac{\tilde{G}^2 \text{Pr} \lambda_1}{\tilde{t}} \sim \text{Pr} \lambda_1 , \quad ( 3.54 )$$

it is apparent that

$$\tilde{t} \sim \tilde{G}^2 . \quad ( 3.55 )$$

Balancing the viscous and buoyancy terms now gives:

$$\lambda_1 \sim \frac{\tilde{G}}{\text{Pr}} . \quad ( 3.56 )$$

Substituting this expression into Eq ( 3.49 ) yields:

$$\lambda_2 \sim \frac{\tilde{G}^3}{\text{Pr}} . \quad ( 3.57 )$$

But, since  $\text{Pr} \tilde{G} \lambda_1 \lambda_2 \sim \tilde{G}$  ( Eq 3.51 ),

$$\text{Pr} \tilde{G} \left( \frac{\tilde{G}}{\text{Pr}} \right) \left( \frac{\tilde{G}^3}{\text{Pr}} \right) \sim \tilde{G} \quad ( 3.58 )$$

$$\text{or, } \tilde{G} \sim \text{Pr}^{1/4} . \quad ( 3.59 )$$

From this and Eq ( 3.55 ), it can be seen that

$$\tilde{t} \sim Pr^{1/2} . \quad ( 3.60 )$$

Using these relations and Eqs ( 3.9 ) and ( 3.10 ) , a new set of scaled variables can be defined.

$$\hat{G} = \tilde{G} Pr^{-1/4} = G \left[ \frac{Ra}{Pr} \right]^{1/4} \quad ( 3.61 )$$

$$\hat{t} = \tilde{t} Pr^{-1/2} = t \left[ \frac{Ra}{Pr} \right]^{1/2} . \quad ( 3.62 )$$

Also, from Eqs ( 3.56 ), ( 3.57 ), and ( 3.59 ),

$$\lambda_1 \sim Pr^{-3/4} \quad ( 3.63 )$$

$$\lambda_2 \sim Pr^{-1/4} . \quad ( 3.64 )$$

And from Eqs ( 3.5 ), ( 3.47 ), and ( 3.48 ),

$$\tilde{W} \sim Pr^{-3/4} W + . . . \quad ( 3.65 )$$

$$\tilde{f} \sim Pr^{-1/4} F + . . . \quad ( 3.66 )$$

$$\tilde{T} \sim T + . . . . \quad ( 3.67 )$$

The scaled variables now show a unique dependency on Ra, Pr, G, and t. Notice also, that Ra/Pr ( in Eqs 3.61 and 3.62 ) is defined as the Grashof number. The energy, vorticity, and stream function equations can now be written as

Energy:

$$Pr \left\{ \hat{G}^2 \frac{\partial T}{\partial \hat{t}} + \hat{G} \left[ \frac{\partial F}{\partial X} \frac{\partial T}{\partial Y} - \frac{\partial F}{\partial Y} \frac{\partial T}{\partial X} \right] \right\} = \frac{\partial^2 T}{\partial X^2} \quad ( 3.68 )$$



Vorticity:

$$\hat{G}^2 \frac{\partial W}{\partial t} + \hat{G} \left\{ \frac{\partial F}{\partial X} \frac{\partial W}{\partial Y} - \frac{\partial W}{\partial X} \frac{\partial F}{\partial Y} \right\} = \hat{G} \frac{\partial T}{\partial X} + \frac{\partial^2 W}{\partial X^2} \quad (3.69)$$

Stream Function:

$$\frac{\partial^2 F}{\partial X^2} = \hat{G}^2 W \quad (3.70)$$

But, in the limit as  $Pr \rightarrow 0$ , the energy equation simplifies to

$$\frac{\partial^2 T}{\partial X^2} = 0 \quad (3.71)$$

which is now completely uncoupled from the vorticity equation.

Eq ( 3.71 ) can be integrated twice to obtain an expression for the temperature distribution as a function of  $X$  .

$$T = C_1 X + C_2 \quad (3.72)$$

By applying the boundary conditions,  $T_i$  and  $T_o$  ,

$$T(X) = 1 - X \quad (3.73)$$

Thus,

$$\frac{\partial T}{\partial X} = -1 \quad (3.74)$$

and

$$\frac{\partial T}{\partial Y} = 0 \quad (3.75)$$

This last expression automatically satisfies the adiabatic boundary condition on the top and bottom horizontal walls.

Using the above results, the vorticity equation reduces to its final form.

$$\begin{aligned} \hat{G}^2 \frac{\partial W}{\partial t} + \hat{G} \left\{ \frac{\partial F}{\partial X} \frac{\partial W}{\partial Y} - \frac{\partial W}{\partial X} \frac{\partial F}{\partial Y} \right\} \\ = - \hat{G} + \frac{\partial^2 W}{\partial X^2} . \end{aligned} \quad ( 3.76 )$$

The boundary conditions for the equations are:

$$F(0,Y) = F(1,Y) = F(X,0) = F(X,1) = 0 \quad ( 3.77 )$$

$$\frac{\partial F}{\partial X} \Big|_{X=0,1} = \frac{\partial F}{\partial Y} \Big|_{Y=0,1} = 0 \quad ( 3.78 )$$

$$T(0,Y) = 1, \quad T(1,Y) = 0 \quad ( 3.79 )$$

$$\frac{\partial T}{\partial Y} \Big|_{Y=0,1} = 0 \quad ( 3.80 )$$

$$\frac{\partial^2 F}{\partial X^2} \Big|_{X=0,1} = \hat{G}^2 W , \quad ( 3.81 )$$

and the initial conditions remain

$$F = W = T = 0 , \quad ( 3.82 )$$

except at the left vertical wall where

$$T = 1 . \quad ( 3.83 )$$

Steady-State Analytical Solution for  $Pr \rightarrow 0$  . Rearranging the stream function equation ( Eq 3.70 ) for the limiting condition of  $Pr \rightarrow 0$  results in the following expression for vorticity:

$$W = \frac{1}{\hat{G}^2} \frac{\partial^2 F}{\partial X^2} . \quad ( 3.84 )$$

Assuming steady-state conditions and substituting Eq ( 3.84 ) into Eq ( 3.76 ) yields

$$\hat{G} \left\{ \frac{\partial F}{\partial X} \frac{\partial^3 F}{\partial X^2 \partial Y} - \frac{\partial^3 F}{\partial X^3} \frac{\partial F}{\partial Y} \right\} = \frac{\partial^4 F}{\partial X^4} - \hat{G}^3 . \quad ( 3.85 )$$

In the limit as  $\hat{G} \rightarrow 0$ , the perturbative solution to this equation can be obtained. The expansion for the stream function is

$$F = \hat{G}^3 F_1 + \hat{G}^7 F_2 + O(\hat{G}^{11}) . \quad ( 3.86 )$$

And, vorticity can be expressed as

$$W = \hat{G} W_1 + \hat{G}^5 W_2 + O(\hat{G}^9) . \quad ( 3.87 )$$

Note that the effects of the convective terms first appear in  $F_2$  and  $W_2$ . Substituting Eq ( 3.86 ) into Eq ( 3.85 ) gives

$$\begin{aligned} & \left\{ \hat{G}^7 \frac{\partial F_1}{\partial X} \frac{\partial^3 F_1}{\partial X^2 \partial Y} + \hat{G}^{11} \frac{\partial F_2}{\partial X} \frac{\partial^3 F_1}{\partial X^2 \partial Y} + \hat{G}^{11} \frac{\partial F_1}{\partial X} \frac{\partial^3 F_2}{\partial X^2 \partial Y} \right. \\ & + \hat{G}^{15} \frac{\partial F_2}{\partial X} \frac{\partial^3 F_2}{\partial X^2 \partial Y} - \hat{G}^7 \frac{\partial^3 F_1}{\partial X^3} \frac{\partial F_1}{\partial Y} - \hat{G}^{11} \frac{\partial^3 F_2}{\partial X^3} \frac{\partial F_1}{\partial Y} \\ & \left. - \hat{G}^{11} \frac{\partial^3 F_1}{\partial X^3} \frac{\partial F_2}{\partial Y} - \hat{G}^{15} \frac{\partial^3 F_2}{\partial X^3} \frac{\partial F_2}{\partial Y} \right\} \\ & = \hat{G}^3 \frac{\partial^4 F_1}{\partial X^4} + \hat{G}^7 \frac{\partial^4 F_2}{\partial X^4} - \hat{G}^3 . \end{aligned} \quad ( 3.88 )$$

By equating terms of like coefficients, the following steady-state results are obtained

$$\hat{G}^3 : \frac{\partial^4 F_1}{\partial X^4} = 1 \quad (3.89)$$

$$\hat{G}^7 : \frac{\partial^4 F_2}{\partial X^4} = \frac{\partial F_1}{\partial X} \frac{\partial^3 F_1}{\partial X^2 \partial Y} - \frac{\partial^3 F_1}{\partial X^3} \frac{\partial F_1}{\partial Y} \quad (3.90)$$

$$\begin{aligned} \hat{G}^{11} : \quad & \frac{\partial F_2}{\partial X} \frac{\partial^3 F_1}{\partial X^2 \partial Y} + \frac{\partial F_1}{\partial X} \frac{\partial^3 F_2}{\partial X^2 \partial Y} \\ & - \frac{\partial^3 F_2}{\partial X^3} \frac{\partial F_1}{\partial Y} - \frac{\partial^3 F_1}{\partial X^3} \frac{\partial F_2}{\partial Y} = 0 \end{aligned} \quad (3.91)$$

$$\hat{G}^{15} : \frac{\partial F_2}{\partial X} \frac{\partial^3 F_2}{\partial X^2 \partial Y} - \frac{\partial^3 F_2}{\partial X^2} \frac{\partial F_2}{\partial X^2} = 0 \quad (3.92)$$

Eq ( 3.89 ) can be integrated four times to obtain an expression for  $F_1(X)$  .

$$F_1(X) = \frac{X^4}{4!} + C_1 \frac{X^3}{3!} + C_2 \frac{X^2}{2} + C_3 X + C_4 \quad (3.93)$$

By applying the boundary conditions ( Eqs 3.77 - 3.78 ), the constants of integration can be determined. The final result for  $F_1(X)$  is

$$F_1(X) = \frac{X^2}{4!} (X - 1)^2 \quad (3.94)$$

An expression for  $W_1$  can now be found by differentiating Eq ( 3.94 ), twice, with respect to  $X$  .

$$W_1 = \frac{\partial^2 F_1}{\partial X^2} = \frac{1}{2} \left\{ X^2 - X + \frac{1}{6} \right\} . \quad ( 3.95 )$$

From Eq ( 3.90 ), and noting that  $\partial F_1 / \partial Y = 0$  from Eq ( 3.94 ), leads to

$$\frac{\partial^4 F_2}{\partial X^4} = 0 . \quad ( 3.96 )$$

Integrating this equation four times gives the result for  $F_2(X)$  .

$$F_2(X) = \frac{C_1}{6} X^3 + \frac{C_2}{2} X^2 + C_3 X + C_4 . \quad ( 3.97 )$$

Applying the boundary conditions, the constants of integration are found to be:

$$C_3 = C_4 = 0 \quad ( 3.98 )$$

$$C_1 = -3 C_2 \quad ( 3.99 )$$

and

$$C_1 = -2 C_2 , \quad ( 3.100 )$$

which can only be true if  $C_1 = C_2 = 0$  . Therefore,

$$F_2(X) = 0 , \quad ( 3.101 )$$

which further implies that  $W_2(X) = 0$  .

With these results, and substituting Eq ( 3.94 ) into ( 3.86 ) and Eq ( 3.95 ) into ( 3.87 ), the final form of the analytical solution for the energy, stream function, and vorticity are:

$$T = 1 - X \quad ( 3.102 )$$

$$F = \hat{G}^3 \frac{x^2}{4!} ( X - 1 )^2 \quad ( 3.103 )$$

$$W = \frac{\hat{G}}{2} ( X^2 - X + \frac{1}{6} ) . \quad ( 3.104 )$$

These one term expansions are good approximations for modeling pre-transitional flow behavior for the limiting condition of  $Pr \rightarrow 0$  . In their present form, however, one could be misled to conclude that they are applicable throughout the entire vertical slot. This is not true because the original partial differential equations ( Eqs 3.68 to 3.70 ), from which these expressions were derived, are not independent of  $Y$  as the analytical solution suggests. Whereas, the analytical solutions are. The best comparison with the numerical solution should occur at half the vertical height (  $Y = 1/2$  ), where the flow stream and vorticity contours for a single cell are, to a good approximation, constant in the  $Y$ -direction.

#### Boundary Layer Equations for High Prandtl Number ( $Pr \geq 10.0$ ).

Using the same reasoning as for the low Prandtl number equations, the dimensionless velocity components, vorticity,

stream function, etc. are:

$$u = Ra^{1/4} \tilde{u} \quad (3.105)$$

$$v = Ra^{1/4} \tilde{v} \quad (3.106)$$

$$W = Ra^{3/4} \tilde{W} \quad (3.107)$$

$$f = Ra^{1/4} \tilde{f} \quad (3.108)$$

$$T = \tilde{T} \quad (3.109)$$

$$t = Ra^{-1/2} \tilde{t} \quad (3.110)$$

$$G = Ra^{1/4} \tilde{G} \quad (3.111)$$

where, again, the tilda over the variable signifies a scaled dimensionless quantity. By substituting Eqs ( 3.105 - 3.111 ) into Eqs ( 2.44 - 2.46 ), and neglecting the terms of order  $\tilde{G}^2/Ra^{1/2}$ ,  $\partial^2/\partial Y^2$ , the governing equations become

Energy:

$$\tilde{G}^2 \frac{\partial \tilde{T}}{\partial \tilde{t}} + \tilde{G} \left\{ \frac{\partial \tilde{f}}{\partial X} \frac{\partial \tilde{T}}{\partial Y} - \frac{\partial \tilde{f}}{\partial Y} \frac{\partial \tilde{T}}{\partial X} \right\} = \frac{\partial^2 \tilde{T}}{\partial X^2} \quad (3.112)$$

Vorticity:

$$\begin{aligned} \tilde{G}^2 \frac{\partial \tilde{W}}{\partial \tilde{t}} + \tilde{G} \left\{ \frac{\partial \tilde{f}}{\partial X} \frac{\partial \tilde{W}}{\partial Y} - \frac{\partial \tilde{W}}{\partial X} \frac{\partial \tilde{f}}{\partial Y} \right\} \\ = Pr \left\{ \tilde{G} \frac{\partial \tilde{T}}{\partial X} + \frac{\partial^2 \tilde{W}}{\partial X^2} \right\} \end{aligned} \quad (3.113)$$

Stream Function:

$$\frac{1}{\tilde{G}^2} \frac{\partial^2 \tilde{f}}{\partial x^2} = \tilde{W} . \quad ( 3.114 )$$

Note that the vorticity equation ( Eq 3.113 ) is now diffusion-dominated for high Prandtl numbers. The boundary and initial conditions remain the same.

Boundary:

$$\tilde{f}(0,Y) = \tilde{f}(1,Y) = \tilde{f}(X,0) = \tilde{f}(X,1) = 0 \quad ( 3.115 )$$

$$\left. \frac{\partial \tilde{f}}{\partial x} \right|_{x=0,1} = \left. \frac{\partial \tilde{f}}{\partial y} \right|_{y=0,1} = 0 \quad ( 3.116 )$$

$$T(0,Y) = 1, \quad T(1,Y) = 0 \quad ( 3.117 )$$

$$\left. \frac{\partial \tilde{T}}{\partial y} \right|_{y=0,1} = 0 \quad ( 3.118 )$$

$$\left. \frac{\partial^2 \tilde{f}}{\partial x^2} \right|_{x=0,1} = \tilde{G}^2 \tilde{W} . \quad ( 3.119 )$$

Initial:

$$\tilde{f} = \tilde{W} = \tilde{T} = 0 , \quad ( 3.120 )$$

except at the left vertical wall where

$$\tilde{T} = 1 . \quad ( 3.121 )$$

Limiting Equations for Infinite Prandtl Number. To make the study complete, one would also like to investigate the



behavior of fluids as the Prandtl number becomes infinite. To accomplish this, the high Prandtl number equations are simplified for the limiting condition of  $Pr \rightarrow \infty$ .

First, let  $Pr \rightarrow \infty$  and assume that temperature remains  $O(1)$ . Now, assume the vorticity and stream functions have the form

$$\tilde{W} = \eta_1 \bar{W}_1 + \dots \quad (3.122)$$

$$\tilde{f} = \eta_2 \bar{f}_1 + \dots \quad (3.123)$$

$$\tilde{T} = \bar{T} + \dots \quad (3.124)$$

Substituting these expressions into Eqs ( 2.44 - 2.46 ), the energy, vorticity, and stream function equations become

Energy:

$$\tilde{G}^2 \frac{\partial \bar{T}}{\partial \tilde{t}} + \eta_2 \tilde{G} \left\{ \frac{\partial \bar{f}}{\partial X} \frac{\partial \bar{T}}{\partial Y} - \frac{\partial \bar{f}}{\partial Y} \frac{\partial \bar{T}}{\partial X} \right\} = \frac{\partial^2 \bar{T}}{\partial X^2} \quad (3.125)$$

Vorticity:

$$\begin{aligned} \tilde{G}^2 \eta_1 \frac{\partial \bar{W}}{\partial \tilde{t}} + \eta_1 \eta_2 \tilde{G} \left\{ \frac{\partial \bar{f}}{\partial X} \frac{\partial \bar{W}}{\partial Y} - \frac{\partial \bar{W}}{\partial X} \frac{\partial \bar{f}}{\partial Y} \right\} \\ = Pr \left\{ \tilde{G} \frac{\partial \bar{T}}{\partial X} + \eta_1 \frac{\partial^2 \bar{W}}{\partial X^2} \right\} \end{aligned} \quad (3.126)$$

Stream Function:

$$\eta_2 \frac{\partial^2 \bar{f}}{\partial X^2} = \eta_1 \tilde{G}^2 \bar{W} \quad (3.127)$$

But, from the stream function equation, Eq ( 3.114 ),

$$\frac{\partial^2 \tilde{f}}{\partial x^2} = \tilde{G}^2 \tilde{w} . \quad ( 3.128 )$$

Therefore, in the limit as  $pr \rightarrow \infty$ ,  $\eta_1 \sim \eta_2 \sim O(1)$ . Also, for this limit, the vorticity equation reduces to the Stokes-like momentum equation. The energy, vorticity, and stream function equations simply become

Energy:

$$\tilde{G}^2 \frac{\partial \tilde{T}}{\partial t} + \tilde{G} \left\{ \frac{\partial \tilde{f}}{\partial x} \frac{\partial \tilde{T}}{\partial y} - \frac{\partial \tilde{f}}{\partial y} \frac{\partial \tilde{T}}{\partial x} \right\} = \frac{\partial^2 \tilde{T}}{\partial x^2} \quad ( 3.129 )$$

Vorticity:

$$\frac{\partial^2 \tilde{w}}{\partial x^2} + \tilde{G} \frac{\partial \tilde{T}}{\partial x} = 0 \quad ( 3.130 )$$

Stream Function:

$$\frac{1}{\tilde{G}^2} \frac{\partial^2 \tilde{f}}{\partial x^2} = \tilde{w} . \quad ( 3.131 )$$

The boundary and initial conditions are similar to those in Eqs ( 3.115 -3.121 ).

Steady-State Analytical Solution for  $Pr \rightarrow \infty$ . Using the same procedure as before, the steady-state perturbation solution for vorticity, stream function, and temperature are found.

Vorticity:

$$\bar{w} = \tilde{G} \bar{w}_1 \quad ( 3.132 )$$

Stream Function:

$$\bar{f} = \tilde{G}^3 \bar{f}_1 \quad ( 3.133 )$$

Temperature:

$$\bar{T} = (1 - x) + \tilde{G}^B (T_2), \quad (3.134)$$

where

$$\bar{w}_1 = \frac{1}{2} \left\{ x^2 - x + \frac{1}{6} \right\} \quad (3.135)$$

$$\bar{f}_1 = \frac{1}{24} x^2 (x - 1)^2 \quad (3.136)$$

$$\bar{T}_2 = \frac{-1}{96} A_1 + \frac{A_2}{34560} \quad (3.137)$$

$$A_1 = \frac{-x^{11}}{415800} + \frac{x^{10}}{75600} + \frac{-x^9}{45360} + \frac{x^6}{10800} \\ + \frac{-x^5}{6900} + \frac{x^4}{15120} + \frac{-x}{387701} \quad (3.138)$$

$$A_2 = \frac{-4}{55} x^{11} + \frac{2}{5} x^{10} + \frac{-5}{6} x^9 + \frac{3}{4} x^8 + \frac{-5}{21} x^7 \\ + \frac{2}{15} x^6 + \frac{-3}{10} x^5 + \frac{x^4}{6} + \frac{-x}{171} \quad (3.139)$$

The boundary-layer equations developed in this chapter for low Prandtl number,  $Pr \rightarrow 0$ , high Prandtl number, and  $Pr \rightarrow \infty$  were solved numerically to obtain stream function, vorticity, and temperature contours for the vertical slot geometry. The numerical techniques employed are discussed in the Chapter IV.

#### IV. Numerical Analysis

There are two topics of discussion in this chapter. The first describes the finite-differencing method used in solving the coupled set of governing partial differential equations. These equations are the 2-D, unsteady, boundary-layer equations developed in Chapter III. The second topic deals with the computational procedure employed to solve the resulting finite-difference equations. Here, the iteration sequence, convergence criterion, and relaxation parameters for the numerical procedure are described.

The basic numerical approach was adopted from Fant ( 1987 ). In this study, however, the geometry was changed from that of an annulus to a vertical slot. The governing equations were converted from polar to Cartesian form.

In computing the streamwise ( Y-direction ) nonlinear convective terms, a corrected, second-order upwind scheme was used for the boundary-layer equations. For the X-coordinate convective terms, a corrected, second-order central-differencing scheme was used. This approach ensures numerical stability when solving highly convective flow problems. The unsteady form of the equations provided the opportunity to capture both steady and unsteady flow behavior when solved in a time accurate fashion.

### Numerical Method

The 2-D, unsteady, boundary-layer equations presented in Eqs ( 2.30 - 2.32 ) and ( 2.44 - 2.46 ) are discretized using finite-differencing techniques. In this form, the governing equations are well suited for solving on a high-speed computer system. The computational domain consists of a rectangular mesh with more nodes in the vertical (  $Y$  ) than in the horizontal (  $X$  ) direction ( Figure 2 ). Non-dimensionalizing the  $\bar{X}$  and  $\bar{Y}$  spacial coordinates with  $L$  and  $l$ , respectively, transforms the geometrical domain into a square box with all sides equal to 1.0. The computer code used to perform the computations had the capability to use variable increments in the computational domain. Although the geometry is symmetrical, vertical and horizontal symmetry were not assumed in the calculations.

Finite-Difference Expressions for Variable Increments. In the governing equations, Taylor series expansions are used to transform the derivatives into finite-difference expressions. Standard forward-, backward-, and central-difference expressions, including formal truncation errors for variable increments, are given in Fant (1987).

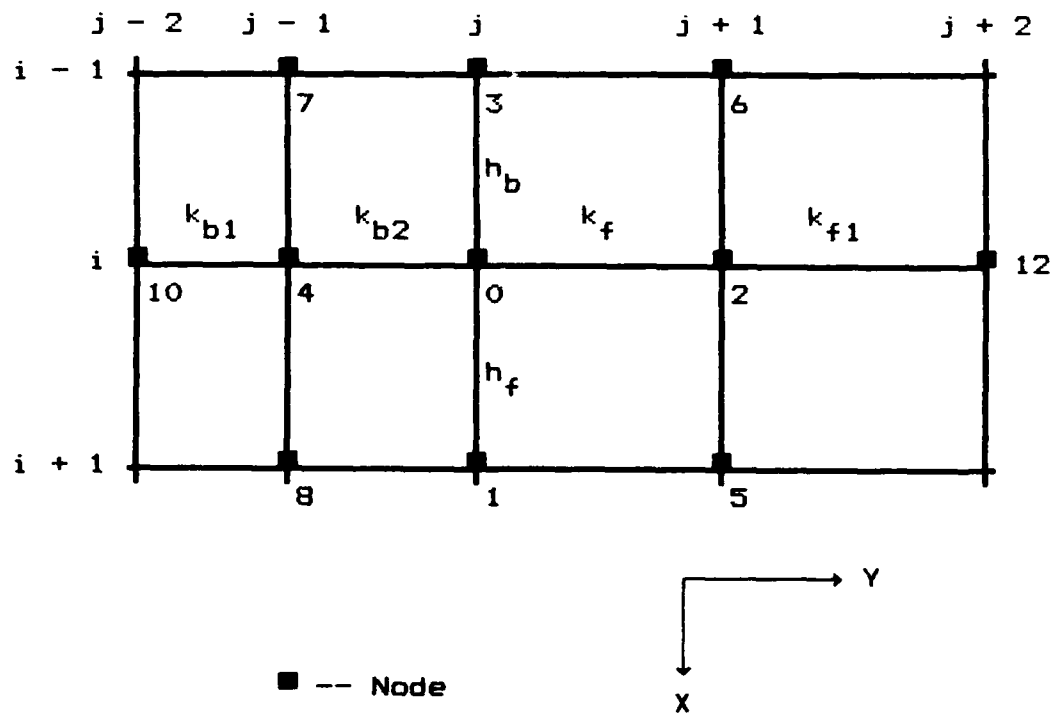


Figure 2. Computational Mesh with Variable Increments.

The unsteady derivatives are approximated with a stable, forward-difference molecule

$$\left. \frac{\partial \phi}{\partial t} \right|_0 = \frac{\phi_0^{n+1} - \phi_0^n}{\Delta t} + O(\Delta t) , \quad ( 4.1 )$$

where  $n$  is the time level at which the variable  $\phi$  is evaluated.

#### Finite-Difference Equations for the Dependent Variables.

All spacial derivatives in the governing equations are second-order, centrally- ( or upwind- ) differenced. This includes the convective terms in the vorticity and energy equations which are represented by a first-order, upwind expression together with a correction term for second-order accuracy. The second-order terms are split in this manner in order to enhance numerical stability when resolving secondary flow behavior. This procedure is explained more fully in Fant ( 1987 ). For the limiting case where Prandtl number goes to zero, the energy equation ( Eq 3.68 ) decouples from the vorticity and stream function equations ( Eqs 3.69 and 3.70 ). Therefore, the energy equation can be solved directly while the other two have to be solved numerically in a coupled manner.

2-D Navier-Stokes Equations. The nonlinear convective terms in the Navier-Stokes equations can be expressed as

$$\begin{aligned}
2 \lambda \left. \frac{\partial \phi}{\partial X} \right|_{X=0} &= (\lambda - |\lambda|) \left\{ \frac{\phi_0 - \phi_3}{h_b} \right. \\
&+ \frac{\phi_1 - H \phi_3 - (1 + H) \phi_0}{h_b + h_f} \Big\} \\
&+ (\lambda + |\lambda|) \left\{ \frac{\phi_1 - \phi_0}{h_f} \right. \\
&+ \frac{\phi_1 / H + \phi_3 - (1 + 1/H) \phi_0}{h_b + h_f} \Big\} \quad (4.2)
\end{aligned}$$

$$\begin{aligned}
2 \mu \left. \frac{\partial \phi}{\partial Y} \right|_{Y=0} &= (\mu - |\mu|) \left\{ \frac{\phi_0 - \phi_4}{k_b} \right. \\
&+ \frac{\phi_2 + k \phi_4 - (1 + k) \phi_0}{k_b + k_f} \Big\} \\
&+ (\mu + |\mu|) \left\{ \frac{\phi_2 - \phi_0}{k_b} \right. \\
&- \frac{\phi_2 / k + \phi_4 - (1 - 1/k) \phi_0}{k_f + k_b} \Big\} , \quad (4.3)
\end{aligned}$$

where  $\phi$  represents the dependent variables  $W$ ,  $f$ , or  $T$ , and

$$H = \frac{h_f}{h_b} \quad \text{and} \quad k = \frac{k_f}{k_b} . \quad (4.4)$$



Eqs ( 4.2 ) and ( 4.3 ) are a combination of first-order, upwind-difference components with the added corrections to bring the differencing up to second-order accuracy. Using this differencing technique, the energy, vorticity, and stream function boundary-layer equations developed in Chapter III can be manipulated into the following general form:

$$\Delta 2 \left\{ - \tilde{\Delta} G^2 \frac{\partial \phi}{\partial t} + \frac{\partial^2 \phi}{\partial x^2} \right\} + 2 \lambda \frac{\partial \phi}{\partial x} + 2 \mu \frac{\partial \phi}{\partial y} + S = 0 . \quad ( 4.5 )$$

The coefficients  $\pm|\lambda|$  and  $\pm|\mu|$  were added to ensure that stable differencing 'into-the-wind' is enforced.  $G$ ,  $t$ ,  $\lambda$ ,  $\mu$ ,  $\Delta 2$ ,  $\phi$ , and  $\tilde{\Delta}$  have different meanings depending upon the application of the boundary-layer equation ( high, low, or limiting  $Pr$  ).

Low Prandtl Number (  $Pr \leq 0.1$  ):

$$G = \tilde{G}, \quad t = \tilde{t} \quad ( 4.6 )$$

$$2 \lambda = \Delta 1 \frac{\partial \tilde{f}}{\partial y} \quad ( 4.7 )$$

$$2 \mu = -\Delta 1 \frac{\partial \tilde{f}}{\partial x} \quad ( 4.8 )$$

$$\Delta 1 = \begin{cases} \text{Pr } \tilde{G}, & \phi = \tilde{T} \\ \text{Pr } \tilde{G}, & \phi = \tilde{W} \\ 0, & \phi = \tilde{f} \end{cases} \quad \Delta 2 = \begin{cases} 1, & \phi = \tilde{T} \\ \text{Pr}, & \phi = \tilde{W} \\ 1/\tilde{G}^2, & \phi = \tilde{f} \end{cases} \quad (4.9)$$

$$\tilde{\Delta} = \begin{cases} \text{Pr}, & \phi = \tilde{T} \\ 1, & \phi = \tilde{W} \\ 0, & \phi = \tilde{f} \end{cases} \quad S = \begin{cases} 0, & \phi = \tilde{T} \\ -\tilde{G} \frac{\partial \tilde{T}}{\partial X}, & \phi = \tilde{W} \\ -\tilde{W}, & \phi = \tilde{f} \end{cases} \quad (4.10)$$

Zero Prandtl Number (  $\text{Pr} \rightarrow 0$  ):

$$G = \hat{G}, \quad t = \hat{t} \quad (4.11)$$

$$2\lambda = \Delta 1 \frac{\partial F}{\partial Y} \quad (4.12)$$

$$2\mu = -\Delta 1 \frac{\partial F}{\partial X} \quad (4.13)$$

$$\Delta 1 = \begin{cases} 0, & \phi = T \\ \hat{G}, & \phi = W \\ 0, & \phi = F \end{cases} \quad \Delta 2 = \begin{cases} 1/\hat{G}^2, & \phi = T \\ 1, & \phi = W \\ 1, & \phi = F \end{cases} \quad (4.14)$$

$$\tilde{\Delta} = \begin{cases} 0, & \phi = T \\ 1, & \phi = W \\ 0, & \phi = F \end{cases} \quad S = \begin{cases} 0, & \phi = T \\ -\hat{G}, & \phi = W \\ -W, & \phi = F \end{cases} \quad (4.15)$$

High Prandtl Number (  $\text{Pr} \geq 10.0$  ):

$$G = \tilde{G}, \quad t = \tilde{t} \quad (4.16)$$

$$2 \lambda = \Delta 1 \frac{\partial \tilde{f}}{\partial Y} \quad (4.17)$$

$$2 \mu = -\Delta 1 \frac{\partial \tilde{f}}{\partial X} \quad (4.18)$$

$$\Delta 1 = \begin{cases} \tilde{G}, & \phi = \tilde{T} \\ \tilde{G}, & \phi = \tilde{W} \\ 0, & \phi = \tilde{f} \end{cases} \quad \Delta 2 = \begin{cases} 1, & \phi = \tilde{T} \\ Pr, & \phi = \tilde{W} \\ 1/\tilde{G}^2, & \phi = \tilde{f} \end{cases} \quad (4.19)$$

$$\tilde{\Delta} = \begin{cases} 1, & \phi = \tilde{T} \\ 1/Pr, & \phi = \tilde{W} \\ 0, & \phi = \tilde{f} \end{cases} \quad S = \begin{cases} 0, & \phi = \tilde{T} \\ \tilde{G} Pr \frac{\partial \tilde{T}}{\partial X}, & \phi = \tilde{W} \\ -\tilde{W}, & \phi = \tilde{f} \end{cases} \quad (4.20)$$

Infinite Prandtl Number (  $Pr \rightarrow \infty$  ):

$$G = \tilde{G}, \quad t = \tilde{t} \quad (4.21)$$

$$2 \lambda = \Delta 1 \frac{\partial \tilde{f}}{\partial Y} \quad (4.22)$$

$$2 \mu = -\Delta 1 \frac{\partial \tilde{f}}{\partial X} \quad (4.23)$$

$$\Delta 1 = \begin{cases} \tilde{G}, & \phi = \tilde{T} \\ 0, & \phi = \tilde{W} \\ 0, & \phi = \tilde{f} \end{cases} \quad \Delta 2 = \begin{cases} 1, & \phi = \tilde{T} \\ 1, & \phi = \tilde{W} \\ 1/G^2, & \phi = \tilde{f} \end{cases} \quad (4.24)$$

$$\tilde{\Delta} = \begin{cases} 1, & \phi = \tilde{T} \\ 0, & \phi = \tilde{W} \\ 0, & \phi = \tilde{f} \end{cases} \quad S = \begin{cases} 0, & \phi = \tilde{T} \\ \tilde{G} \frac{\partial \tilde{T}}{\partial X}, & \phi = \tilde{W} \\ -\tilde{W}, & \phi = \tilde{f} \end{cases} \quad (4.25)$$

With the above results, the boundary-layer equations can be written in the following finite-difference form:

$$C_0 \phi_0^{n+1} = \frac{\Delta 2 \tilde{\Delta} \tilde{G}^2}{\tau} \phi_0 + C_1 \phi_1^{n+1} + C_2 \phi_2^{n+1} + C_3 \phi_3^{n+1} \\ + C_4 \phi_4^{n+1} + E^{n+1} + S^{n+1} \quad (4.26)$$

with the variable  $\phi$  denoting the boundary-layer dependent variables  $T$ ,  $W$ ,  $F$ , and

$$C_0 = \frac{\Delta 2 \tilde{\Delta} \tilde{G}}{\tau} + \frac{2 (\Delta 2)}{h_f h_b} + \Gamma \lambda \left( \frac{1}{h_f} - \frac{1}{h_b} \right) \\ + \Gamma |\lambda| \left( \frac{1}{h_f} + \frac{1}{h_b} \right) + \Gamma \mu \left( \frac{1}{k_f} - \frac{1}{k_b} \right) \\ + \Gamma |\mu| \left( \frac{1}{k_f} + \frac{1}{k_b} \right) \quad (4.27)$$

$$C_1 = 2 (\Delta 2) \left\{ \frac{1}{h_f (h_f + h_b)} \right\} \\ + \Gamma (\lambda + |\lambda|) \frac{1}{h_f} \quad (4.28)$$

$$C_2 = \Gamma (\mu + |\mu|) \frac{1}{k_f} \quad (4.29)$$

$$C_3 = 2 (\Delta 2) \left\{ \frac{1}{h_b (h_f + h_b)} \right\} \\ - \Gamma (\lambda - |\lambda|) \frac{1}{h_b} \quad (4.30)$$

$$C_4 = -\Gamma (\mu - |\mu|) \frac{1}{k_b} \quad (4.31)$$

$$\Gamma = \begin{cases} 1, & \phi = \tilde{T} \\ 1, & \phi = \tilde{W} \\ 0, & \phi = \tilde{f} \end{cases} \quad (4.32)$$

The correction term,  $E^{n+1}$  is defined as

$$\begin{aligned} E^{n+1} = & \Gamma \left( \frac{\lambda}{h_f + h_b} \right) \left\{ \phi_1^{n+1} \left( 1 - \frac{1}{H} \right) + \phi_3^{n+1} (H - 1) \right. \\ & - \left. \phi_0^{n+1} \left( H - \frac{1}{H} \right) \right\} - \Gamma \left( \frac{|\lambda|}{h_f + h_b} \right) \left\{ \phi_1^{n+1} \left( 1 + \frac{1}{H} \right) \right. \\ & + \left. \phi_3^{n+1} (1 + H) - \phi_0^{n+1} \left( 2 + H + \frac{1}{H} \right) \right\} \\ & + \mu \Gamma \left\{ \phi_2^{n+1} \left( \frac{1 + K_f}{B} \right) - \phi_4^{n+1} \left( \frac{1 + K_b}{A} \right) \right. \\ & + \left. \phi_0^{n+1} \left( \frac{1}{A} - \frac{1}{B} \right) + \phi_{10}^{n+1} \left( \frac{K_b}{A} \right) - \phi_{12}^{n+1} \left( \frac{K_f}{B} \right) \right\} \\ & + |\mu| \Gamma \left\{ \phi_2^{n+1} \left( \frac{1 + K_f}{B} \right) + \phi_4^{n+1} \left( \frac{1 + K_b}{A} \right) \right. \\ & - \left. \phi_0^{n+1} \left( \frac{1}{A} + \frac{1}{B} \right) - \phi_{10}^{n+1} \left( \frac{K_b}{A} \right) \right. \\ & \left. - \phi_{12}^{n+1} \left( \frac{K_f}{B} \right) \right\}, \quad (4.33) \end{aligned}$$

where

$$K_f = \frac{k_f}{k_{f1}}, \quad K_b = \frac{k_b}{k_{b1}}, \quad (4.34)$$

and

$$A = k_b + k_{b1}, \quad B = k_f + k_{f1}. \quad (4.35)$$

Boundary Conditions. For the vertical slot, the finite-difference form of the boundary conditions are

Energy:

$$T_{i,j}^{n+1} = 1 \quad \text{and} \quad T_{NR,j}^{n+1} = 0 \quad (4.36)$$

$$\left. \frac{\partial T}{\partial Y} \right|_{i,1} = \left. \frac{\partial T}{\partial Y} \right|_{i,NS} = 0 \quad (4.37)$$

Vorticity:

$$w_{1,j}^{n+1} = \frac{2 F_{2,j}^{n+1}}{(\tilde{G} h_1)^2} \quad (4.38)$$

$$w_{NR,j}^{n+1} = \frac{2 F_{NR-1,j}^{n+1}}{(\tilde{G} h_{NR-1})^2} \quad (4.39)$$

$$w_{i,1}^{n+1} = w_{i,NS}^{n+1} = 0 \quad (4.40)$$

Stream Function:

$$F_{1,j}^{n+1} = F_{NR,j}^{n+1} = F_{i,1}^{n+1} = F_{i,NS}^{n+1} = 0, \quad (4.41)$$

where  $i$  goes from 1 to  $NR$ , and  $j$  from 1 to  $NS$  within the geometric boundaries. Additional nodes exist outside these boundaries ( $i = 0$ ,  $j = 0$ ,  $i = NR + 1$ , and  $j = NS + 1$ ) for computational purposes.

It should be noted that the computer code used to solve the vertical slot problem was originally developed for an annulus. Since an annulus has only two boundaries, inner and outer, a set of finite-difference equations was needed for the adiabatic horizontal walls. As mentioned previously, the finite-difference expressions for the dependent variables are second-order accurate. This suggests the use of a second-order polynomial to represent the adiabatic boundary conditions along the top and bottom horizontal walls. Using a Taylor series expansion, a second-order accurate, finite-difference expression was obtained.

Along the bottom horizontal ( $j = 1$ ) wall,

$$\left. \frac{\partial T}{\partial Y} \right|_{i,1} = \frac{-T_{i,3} + 4T_{i,2} - 3T_{i,1}}{2\Delta Y} = 0 \quad (4.42)$$

from which the temperature is simply

$$T_{i,1} = \frac{4 T_{i,2} - T_{i,3}}{3} . \quad ( 4.43 )$$

For the top horizontal wall (  $j = NS$  )

$$\left. \frac{\partial T}{\partial Y} \right|_{i,NS} = \frac{T_{i,NS-2} - 4 T_{i,NS-1} + 3 T_{i,NS}}{2 \Delta Y} = 0 \quad ( 4.44 )$$

and,

$$T_{i,NS} = \frac{4 T_{i,NS-1} - T_{i,NS-2}}{3} . \quad ( 4.45 )$$

To satisfy the adiabatic constraints, the following conditions also apply:

$$T_{i,2} = T_{i,0} \quad \text{and} \quad T_{i,NS+1} = T_{i,NS-1} . \quad ( 4.46 )$$

The boundary conditions along the left vertical wall were obtained by using a Taylor series expansion and then solving for the second derivative.

$$F_2 = F_1 + \frac{\partial F_1}{\partial X} \Delta X + \frac{\partial^2 F_1}{\partial X^2} \frac{(\Delta X)^2}{2} + O(\Delta X)^3 . \quad ( 4.47 )$$

From the no-slip constraint,  $F_1$  and  $\partial F_1 / \partial X = 0$  . Therefore, with  $\Delta X = h_1$  ,

$$\frac{\partial^2 F_1}{\partial X^2} = \frac{2 F_2}{(h_1)^2} \quad ( 4.48 )$$



and

$$W = \frac{1}{G^2} \frac{\partial^2 F}{\partial X^2} = \frac{2 F_2}{(G h_1)^2} . \quad ( 4.49 )$$

The right vertical wall boundary condition was handled in a similar manner.

The vorticity boundary conditions for the horizontal walls are

$$W_{i,1}^{n+1} = W_{i,NS}^{n+1} = 0 . \quad ( 4.50 )$$

These conditions are a result of the boundary-layer approximation, where

$$W \sim \frac{\partial^2 F}{\partial X^2} \sim \frac{\partial}{\partial X} \left[ \frac{\partial F}{\partial X} \right] . \quad ( 4.51 )$$

But, at the walls, the no-slip constraint requires that  $\frac{\partial F}{\partial X} = 0$ . This implies that  $W$  must also be zero. However, to match the physics of the problem, as well as ensure that  $W = 0$  at the top and bottom walls, requires that

$$W_{i,0}^{n+1} = - W_{i,2}^{n+1} \quad \text{and} \quad W_{i,NS+1}^{n+1} = - W_{NS-1}^{n+1} . \quad ( 4.52 )$$

#### Computational Procedure.

The system of coupled, finite-difference equations described in the preceding section were solved implicitly in time using a point-iterative, Gauss-Siedel scheme with under-relaxation. A computer code was developed for each

Prandtl number range investigated: low Prandtl number,  $Pr \rightarrow 0$ , Prandtl number of order one, and high Prandtl number. In each case, the dependent variables were solved numerically by repeated iterations of the governing equations at a given time level.

At the beginning of each investigation, the initial conditions for temperature, vorticity, and stream function were set to zero everywhere within the slot, except for the isothermal condition along the left vertical wall. In addition, the scaled gap parameter ( $\tilde{G}$  or  $\hat{G}$ ) was set to 1.0 and a node generating program was employed to set-up the computational domain. The output of the initial computer run; consisting of temperature, vorticity, and stream function distributions, was then used as initial conditions for the next run. In this new run, the scaled gap was increased to a slightly higher value and the procedure repeated until transition to multicells occurred.

Iteration Sequence and Convergence Criteria. The finite-difference form of the boundary-layer equations were iterated in the following order:

- i. energy
- ii. vorticity
- iii. stream function

except for the small Prandtl number limiting equations ( $Pr \rightarrow 0$ ), where an analytical expression was obtained for energy.

This sequence was repeated until successive iterations were within a prescribed tolerance. The relative convergence constraint for the maximum modulus of the difference between energy, vorticity, and stream function is defined as

$$\text{Max} \left| \frac{\phi^{m+1,n+1} - \phi^{m,n+1}}{(\phi^{m+1,n+1})_{\text{max}}} \right| < 1 \times 10^{-6} \quad (4.53)$$

where, again,  $\phi$  represents temperature, vorticity, or stream function. When Eq (4.53) was satisfied, the numerical solution was considered converged. In this equation,  $m$  denotes the iteration level and  $n$  denotes the time level.

Relaxation Parameters. To control the rate of convergence, two independent relaxation parameters,  $\Omega_1$  and  $\Omega_2$ , were incorporated into the finite-difference expressions. The parameter,  $\Omega_1$ , was employed in conjunction with the vorticity boundary conditions, namely

$$w_{1,j}^{m+1,n+1} = \Omega_1 \left[ \frac{2F_2^{m,n+1}}{(\tilde{G}h_1)^2} \right] + (1 - \Omega_1) w_{1,j}^{m,n+1} \quad (4.54)$$

along the left vertical wall and

$$w_{NR,j}^{m+1,n+1} = \Omega_1 \left[ \frac{2F_2^{m,n+1}}{(\tilde{G}h_{NR-1})^2} \right] + (1 - \Omega_1) w_{NR-1,j}^{m,n+1} \quad (4.55)$$

along the right wall where  $h$  represents the linear spacing between nodes. The values used to stabilize the numerical computations were generally in the range  $.15 \leq \Omega_1 \leq .3$ . The second parameter,  $\Omega_2$ , was used with the second-order upwind correction terms which were based on the new time level,  $n+1$ . The numerical values for vorticity, at each interior node, were computed according to

$$\begin{aligned}
 w_0^{m+1,n+1} = & \frac{\Delta 2 \tilde{\Delta} \tilde{G}^2}{C_0 \tau} w_0^n + \frac{1}{C_0} \left\{ C_1 w_1^{m,n+1} \right. \\
 & + C_2 w_2^{m,n+1} + C_3 w_3^{m+1,n+1} + C_4 w_4^{m+1,n+1} + S^{m+1,n+1} \left. \right\} \\
 & + \frac{1}{C_0} \left\{ \Omega_2 E^{m+1,n+1} + (1 - \Omega_2) E^{m,n+1} \right\} . \quad (4.56)
 \end{aligned}$$

The correction term,  $E$ , becomes a weighted average of Gauss-Siedel ( at the current level ) and Jacobi ( at the previous level ) iterations for values of  $\Omega_2 < 1.0$ . Values of  $.15 \leq \Omega_2 \leq .3$  were generally employed in the computations. For further details on this procedure, see Fant ( 1987 ).

Numerical Details and Discussion. The majority of the computational runs were made using 31 horizontal and 62 vertical nodes. Because of the large gradients expected near the left and right vertical boundaries, the number of nodes were slightly concentrated in those regions. This helped to improve numerical accuracy.

A few cases were run with a  $31 \times 102$  mesh. This was done for two reasons: first, to determine the influence of mesh size on triggering the onset of cell formation; and second, to concentrate more nodes in the center of the box to resolve the temperature inversions expected for the high Prandtl number investigations.

As explained earlier, each investigation was started by computing the flow field for  $\tilde{G} = 1.0$ . The output from each computational run served as the input for the next with  $\tilde{G}$  incremented to a new value. The procedure was repeated until the formation of multiple cells appeared in the results.

A scaled time step,  $\Delta \tilde{t}$ , was used in each Prandtl number investigation. Since  $\Delta \tilde{t} = (Ra/Pr)^{1/2} \Delta t$ , the actual time step is much smaller. Generally, a  $\Delta \tilde{t}$  of 0.5 was used and the total number of time steps,  $\tau$ , was about 500.

From earlier studies done by Fant (1987) and Bennett (1988), a suitable range of values for  $\tilde{G}$ , where cell formation might occur, was surmized. Initially,  $\tilde{G}$  was incremented by as large a value as possible for each succeeding run. This increment generally ranged from  $1.0 < \tilde{G} < 3.0$ . Once cell formation developed,  $\tilde{G}$  was reset to the previous value where a single cell was still present. The results from the previous (single cell) computational run were then used as input, but

with the increment for  $\tilde{G}$  reduced (  $\Delta\tilde{G} \sim .1, .2, \text{etc.}$  ). Additional runs were then accomplished until multicellular formation occurred again, with the value for  $\tilde{G}$  now more accurately determined.

Prior to the onset of multiple cell formation, the CPU time required to obtain the results for each run was usually on the order of 30 minutes to an hour. However, when the flow began to transition, the number of iterations for convergence and the CPU time increased significantly. This was particularly true for the high Prandtl number cases where CPU time was approximately 24 hours per run for  $Pr = 1000$  .

The validity of this last statement is suspect, however, since major modifications were made to the VAX computer system which may have slowed the processing speed considerably. These modifications were done while the study was in progress. Prior to this, the computational runs proceeded at a fairly rapid pace ( several accomplished each day ). But, after that, things slowed down dramatically. One run required over 90 hours elapsed ( 24 hours CPU ) time to complete. Thus, the amount of studies accomplished for the high Prandtl number regime were reduced.

## V. Results and Discussion

In this chapter, the various flow fields computed for the low, high, and limiting Prandtl number regimes are examined. This includes temperature, vorticity, and stream function distributions throughout the vertical slot. In each case, the hot, isothermal wall appears on the left, while the right vertical wall is maintained at zero. To establish validity in the numerical procedure, the results are compared to analytical solutions obtained for steady-state conditions.

### Zero Prandtl Number.

Needless to say, a fluid with a Prandtl number equal to zero does not exist in the real physical world. It is a hypothetical fluid whose thermal diffusivity approaches infinity. In this case, the energy equation reduces to the simple steady-state conduction equation. For the vertical slot, this is just a linear temperature distribution across the width of the slot for the boundary conditions imposed.

Since the thermal diffusivity is infinite, thermal perturbations cannot exist because they are instantaneously diffused throughout the slot. Thus, any instabilities generated are purely hydrodynamic in nature. The way in which the flow develops for increasing  $\hat{G}$  is shown in the stream function plots, Figure 3 ( a - e ).

Figure 3a shows the streamlines for the steady-state condition where  $\hat{G} = 3.0$ . The motion of the fluid is always in a clockwise manner throughout the slot. Notice that even when the flow is stable, weak convective cells have formed at the extreme top and bottom of the cavity. Cells form in this region first because the boundaries force the fluid to turn. Since momentum diffusivity is so low, the motion does not dissipate quickly enough causing some of the fluid particles to continue in a circular path. Lee and Korpela ( 1983 ) obtained a similar one cell result using the complete Navier-Stokes equations. However, as mentioned by the authors, their plot did not show the weak cells at the top and bottom because of insufficient resolution. As  $\hat{G}$  increases, these cells become stronger ( Figure 3b and c ) where forced turning of the fluid by the physical boundary continues to contribute to their development.

Finally, at  $\hat{G} = 4.0$  ( Figure 3d ), transition begins to take place and multiple cells begin to form. Cell formation takes place near the top and bottom, first, and then toward the center. Only a moderate increase in  $\hat{G}$ , from 4.0 to 4.2, was needed to trigger complete multicellular formation ( Figure 3e ). A total of nine cells are present with the strongest cells appearing near the horizontal walls and the weaker ones in the center. Figure 3 also shows that the entire fluid flow is slightly skewed toward the upper right cold wall and toward the



lower left hot wall, respectively.

Figures 4 and 5 show the comparison of the numerical results with the analytical solution ( Eq 3.103 ) obtained for the stream function, at the horizontal centerline, for the steady-state condition of  $\hat{G} = 3.0$  . The agreement between numerical and analytical results is excellent. Figure 5 is more revealing in that it shows that the largest relative error (  $\sim 5\%$  ) between the numerical and analytical solutions occurs very close to the vertical boundaries. This is acceptable, because it represents the difference between two numbers very close to zero (  $\sim 10^{-4}$  ).

Equally as interesting, is the development of vorticity throughout the cavity. This is shown in Figures 6 ( a - e ), which are contour plots of constant vorticity. Vorticity is in the counter-clockwise direction ( positive ) along the vertical walls, and clockwise ( negative ) in the central region of the slot

Note how the vorticity contours arrange themselves into a pattern similar to that for the stream function. Notice, also, that the vorticity tends to concentrate in specific nodal regions along the vertical walls ( Figure 6e ). These concentrations form near the ends of the walls, first, and then towards the center ( Figure 6c, d, and e ). Also, the

concentrations along the left wall do not align with their counterparts on the right. This may be a result of the skewed fluid motion mentioned earlier. Lastly, the contours that intersect the horizontal walls represent zero vorticity. This is the point where vorticity changes direction, from counter-clockwise to clockwise or vice-versa.

It is interesting to note that there are no vorticity concentrations along the horizontal walls. This may be due to the boundary-layer approximation to the Navier-Stokes equations as  $Ra \rightarrow \infty$  and  $G \rightarrow 0$  where

$$\frac{G^2}{Ra^{1/2}} \frac{\partial^2 w}{\partial Y^2}$$

and the associated boundary conditions are neglected.

Comparisons between analytical ( Eq 3.104 ) and numerical results at the horizontal centerline are shown in Figures 7 and 8 . Again, the comparison is quite good. However, this time the maximum error occurs not near the vertical wall, but at the region where the vorticity changes direction ( Figure 8 ). Again, the error is small (  $\sim 3.0\%$  ) and represents the error between two numbers very close to zero.

As expected for the zero Prandtl number case, the isotherm contours were simply straight vertical lines and are of no interest. Therefore, they are omitted from this study.

### Low Prandtl Number.

Liquid Metals (  $Pr \sim 0.02$  ). When the Prandtl number of the fluid is increased to that of liquid mercury, very little changes. Figure 9 shows the stream function contours for a fluid of  $Pr = 0.02$ . The same pattern of cell development as that for  $Pr = 0$  was observed with cell formation occurring near the horizontal walls, first, and then in the central region.

Figure 9a shows the fluid flow for  $\tilde{G} = 1.0$ . Even for this low value, the single cell shows a definite necking down region near the horizontal walls where weak convective cells are beginning to form. For  $\tilde{G} = 1.5$ , multicellular development is well in progress ( Figure 9b ) and is complete when  $\tilde{G} = 1.6$  ( Figure 9c ).

Recalling that  $\tilde{G} = \hat{G} Pr^{1/4}$ , and substituting the value for  $\hat{G}$  at which multicellular formation occurred for the zero Prandtl number case (  $\sim 4.2$  ), leads to  $\tilde{G} = 1.57$  which is in good agreement with the actual value obtained. Further increases in  $\tilde{G}$  did not cause an increase in the number cells that formed, but only increased their strength. As a result, steady-state conditions were maintained over the range of  $\tilde{G}$  that was studied. Notice, also, that nine cells formed with the strongest cells near the horizontal boundaries; just as in the case for  $Pr = 0$ .

Figures 10 and 11 show the comparison between numerical and analytical ( Eq 3.40 ) results. Again, the comparisons are good and show similar trends.

Vorticity also developed in the same manner. This is shown in Figure 12. Figure 12e clearly illustrates the tendency for vorticity to concentrate in specific regions along the vertical walls and has trends similar to the  $Pr = 0$  case. And as before, the analytical ( Eq 3.41 ) and numerical comparisons for vorticity were very good ( Figures 13 and 14 ).

Temperature contours, however, were no longer vertical straight lines ( Figure 15 ). For  $\tilde{G} = 1.8$  ( Figure 15e ), the contours showed a distinct oscillation in regions where cell formation took place. This is because, with a finite Prandtl number, thermal diffusion is no longer instantaneous. Therefore, the temperature distribution is slightly influenced by the convective motion of the fluid. Similar results were reported by Lee and Korpela ( 1983 ).

As expected, the analytical ( Eq 3.42 ) and numerical solutions for the single cell, steady-state condition compared very well ( Figures 16 and 17 ).

### Prandtl Number of Order One.

Air (  $Pr \sim 0.70$  ). With air, an interesting phenomenon was observed. For  $\tilde{G} = 3.9$ , two tiny cells formed in the center of the vertical slot ( Figure 18b ). Increasing  $\tilde{G}$  to 4.0 ( Figure 18c ) caused an immediate formation of multiple cells, with the stronger cells occurring in the center of the slot. This is in direct contrast to the very low Prandtl numbers, where the cells formed near the horizontal boundaries, first.

For air, momentum diffusivity is higher. Therefore, fluid motion dissipates more quickly and forced turning of the fluid by the boundaries no longer has the same effect. As a result, cells no longer form adjacent to the horizontal boundaries, reducing the total number of cells from nine to seven. Furthermore, cells form in the center of the slot, first, due to shearing caused by the opposing movement of adjacent fluid layers.

A total of seven distinct cells are visible in Figure 18c. However, as  $\tilde{G}$  was further increased, the lower cell disappeared while the remaining ones became stronger ( Figures 18d and e ). Again, these results are very similar to that obtained by Lee and Korpela ( 1983 ) using the complete Navier-Stokes equations. In their study, they reported that as the cells became stronger, the distance between them increased. The same happened in this study, causing the cell at the bottom to be absorbed. Notice that this time however, the strongest cells are not in the

regions near the horizontal boundaries, as was the case for  $Pr = 0$  and  $Pr = 0.02$ , but are located in the center of the vertical slot where shearing of the fluid is strongest.

Figure 19 shows the vorticity distribution for air. It is interesting to note that the contours of constant vorticity verify that the distance between cells is increasing. Figure 19c clearly shows a line of constant vorticity surrounding the seven convection cells, shown in Figure 18c ( stream function ). Figure 19d indicates that regions of constant vorticity have formed between the top, center, and bottom cell groups. The only way for this to happen is for the cells to be spacially separating.

Constant temperature ( Figure 20 ) contours obtained for air were very similar to those reported by Lee and Korpela ( 1983 ). Temperature contours tend to bend toward the cold wall along the upper horizontal surface, away from it along the lower wall, and also oscillate in the region where convective cells form ( Figure 20c, d, and e ). The only notable difference was in the slight temperature reversal, near the horizontal boundaries, that they obtained.

As has been the case so far, analytical ( Eqs 3.40 - 3.42 ) and numerical comparisons for the stream function, vorticity, and temperature at the centerline are quite good and also show

the same trends as before ( Figures 22 - 26 ).

In Chapter III, it was mentioned that because the analytical equations are a function of  $X$  only, one could be misled to conclude that they are valid throughout the vertical slot. To verify this statement, the analytical solution was compared to the numerical solution at other locations a distance of 20 percent from the top and bottom, respectively. This corresponds to nodes  $i, 12$  and  $i, 50$ . Figures ( 36 - 53 ), in appendix A, show that the analytical solutions for temperature, vorticity, and stream function are still a very good approximation for distances up to 20 percent from the horizontal walls.

Generally, the difference between the numerical and analytical solutions for stream function and temperature was less than ten percent. Vorticity, however, was the exception with an error of 20 percent. Notice that in the lower portion of the vertical slot, the maximum error occurs near the left boundary; and then shifts to the right side near the top of the slot ( Figures 36 - 53 ). The reason for this can be seen from the stream function, vorticity, and temperature contours ( Figures 18 - 20 ). The analytical solution is only valid at the horizontal centerline of the slot while the contours for stream function, vorticity, and temperature bend toward the lower left and upper right vertical walls, respectively.

### High Prandtl Number.

Oils ( Pr ~ 1000 ). For high Prandtl numbers, the flow is momentum-diffusion dominated and instabilities that result are more thermal in nature. Bas.-flow heat transfer is convection dominated to such an extent that distinct boundary layers form on each wall in a vertical slot. de Vahl Davis and Mallinson ( 1975 ) and Lee and Korpela ( 1983 ) both performed numerical studies using the complete Navier-Stokes equations. An attempt was made, in this study, to duplicate those results using the boundary-layer equations.

Figure 27 shows the stream function contours for a fluid of Pr = 1000. de Vahl Davis and Mallinson ( 1975 ) reported multiple cell formation at a Rayleigh number between  $2.4 \times 10^5$  and  $5.0 \times 10^5$ . They based their Rayleigh number on the width of the vertical slot ( L ). The Rayleigh number used in the boundary-layer formulation was based on height ( l ). An estimate for the value of  $\tilde{G}$  where transition should occur was made by converting their Rayleigh number in the following manner:

$$Ra_L = \Delta T \beta L^3 \frac{g}{\nu \alpha}$$

$$Ra_l = \Delta T \beta l^3 \frac{g}{\nu \alpha}$$

$$G = L/l .$$



By rearranging the last equation and substituting for  $L$ ,

$$Ra_L = \Delta T \beta G^3 l^3 \frac{g}{\nu \alpha} = Ra_1 G^3 .$$

Now, recalling that

$$\tilde{G} = G Ra_1^{1/4} ,$$

gives the final result for the transformation,

$$\tilde{G} = ( G Ra_L )^{1/4} .$$

By substituting the values of  $Ra_L = 2.4 \times 10^5$  and  $5.0 \times 10^5$ , and  $G = 0.1$ , transition was expected to occur between

$$12.5 < \tilde{G} < 15.0 .$$

Indeed, multiple cells did form at a value of  $\tilde{G} = 12.5$  ( Figure 27d ).

Prior to transition, the stream function plots agree very well with the results obtained by de Vahl Davis and Mallinson and Lee and Korpela ( Figures 27a, b, and c ). However, once the cells formed, the arrangement of the cell patterns generated by the boundary-layer program ( Figures 27d and e ) differed from the ones that they obtained. The cell patterns that they generated showed a large single cell in the center of the box with weaker ones just above and below. As the Rayleigh number increased, the cells became stronger and weaker cells began to form between them, as well as above and below.

The boundary-layer equations generated two cells of approximately the same strength ( Figure 27d ) , simultaneously. As  $\tilde{G}$  increased, these cells became stronger and began to split apart to form other cells. Weaker cells also formed above and below.

The reason for the differing results may be due to the boundary-layer approximation where the streamwise viscous terms and related boundary conditions were neglected. For finite Rayleigh numbers and high Prandtl numbers, these terms are no longer negligible but need to be included. However, even without these terms, multiple cells do form; but in a different manner, which indicates a fairly weak dependency. And, in contrast to the low Prandtl number fluids, the fluid motion is now slightly skewed in the opposite direction. This also agrees with the results obtained by de Vahl Davis and Mallinson as well as Lee and Korpela. Finally, it should also be noted that the solutions obtained for the high Prandtl number fluids are unsteady in nature.

Figure 28 shows the vorticity distribution within the slot. Notice that for high Prandtl number fluids the vorticity no longer concentrates in distinct nodal regions along the vertical walls as it did for low Prandtl numbers; but instead, concentrates almost uniformly along the entire length. In addition, the vorticity distribution becomes antisymmetrical

within the left and right regions ( Figures 28c, d, and e ) and no longer seems to be influenced by the number of convective cells that form or their location ( see Figures 6, 12, and 19 ).

Temperature distributions ( Figure 29 ) obtained from the boundary layer program also agree well with the results reported by de Vahl Davis and Mallinson and Lee and Korpela, up to the point of transition. Notice the sinusoidal appearance of the temperature contours prior to multiple cell formation ( Figures 29b and c ), in contrast to the nearly vertical contours obtained for the low Prandtl number fluids. Notice also the slight temperature inversions that exist where cells have formed ( Figures 29d and e ). Although the boundary-layer program captured these temperature inversions, it did not do so completely. It failed to capture the temperature inversion at the center of the slot because no cell formed in that region.

And finally, analytical ( Eqs 3.132 - 3.134 ) and numerical comparisons for stream function, vorticity, and temperature are shown in Figures ( 30 - 35 ). Once again, the comparisons are very good.

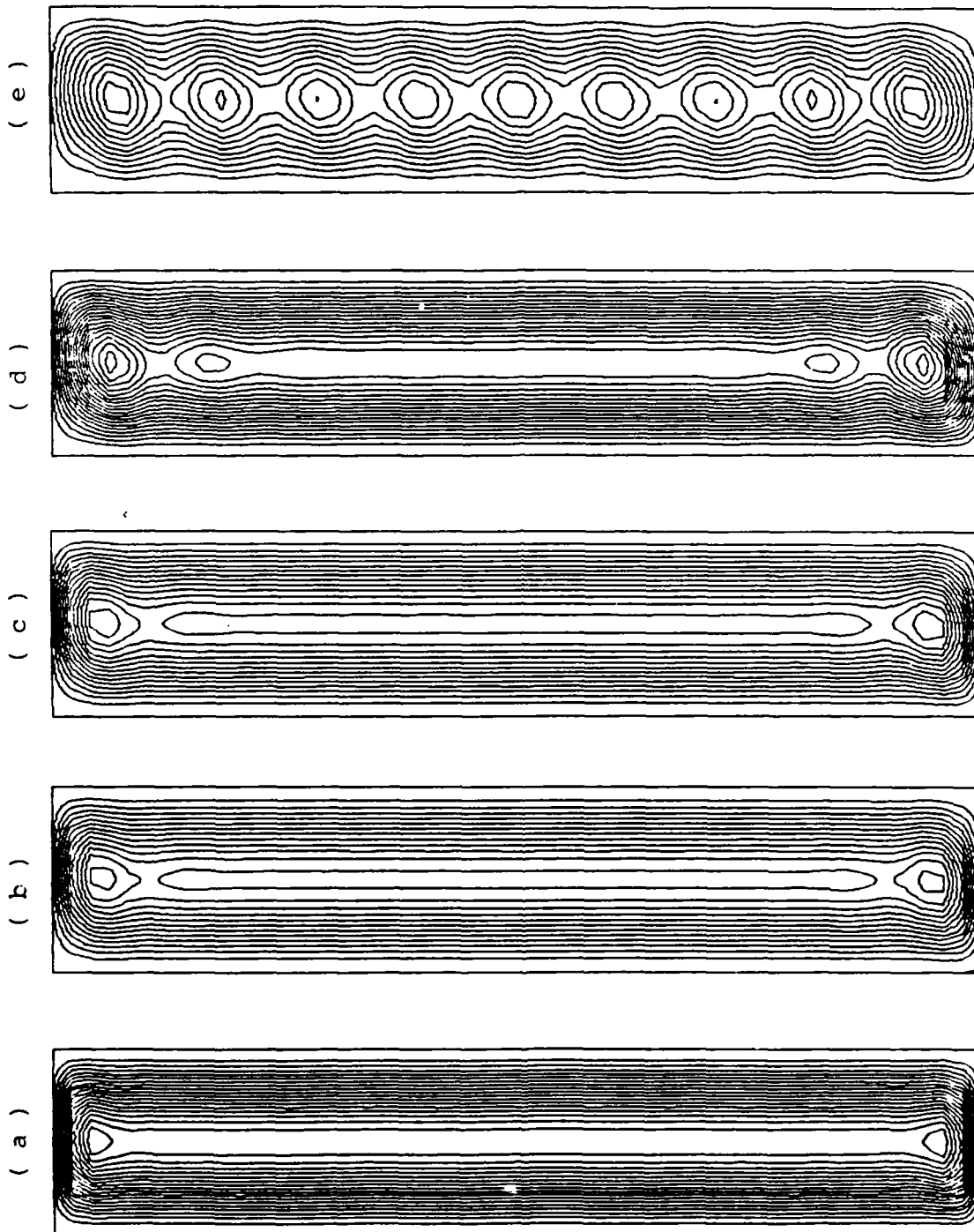


Figure 3. Stream Function contours for  $Pr = 0$ .

a)  $\hat{G} = 3.0$ , b)  $\hat{G} = 3.6$ , c)  $\hat{G} = 3.7$ , d)  $\hat{G} = 4.0$ , e)  $\hat{G} = 4.2$ ,

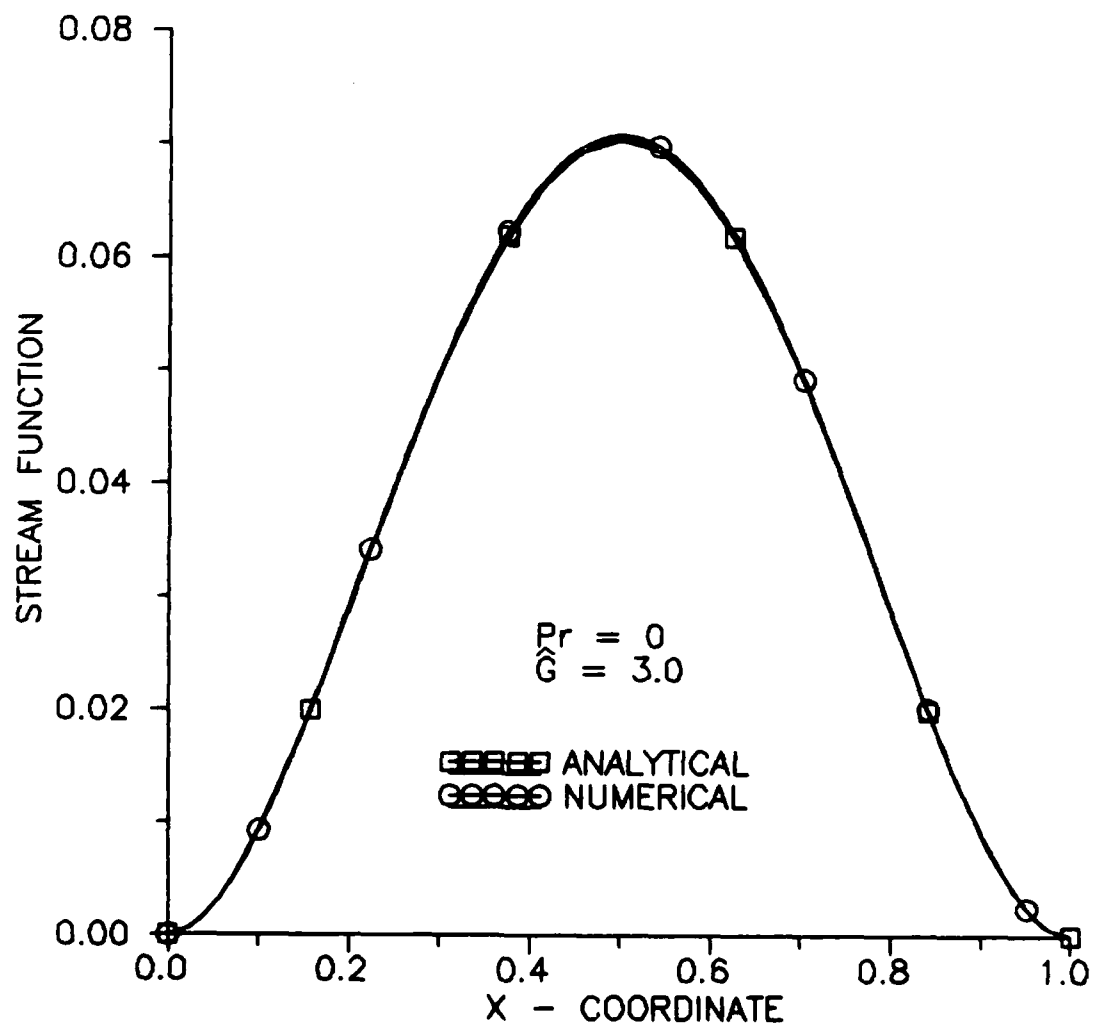


Figure 4. Stream function variation at the horizontal centerline

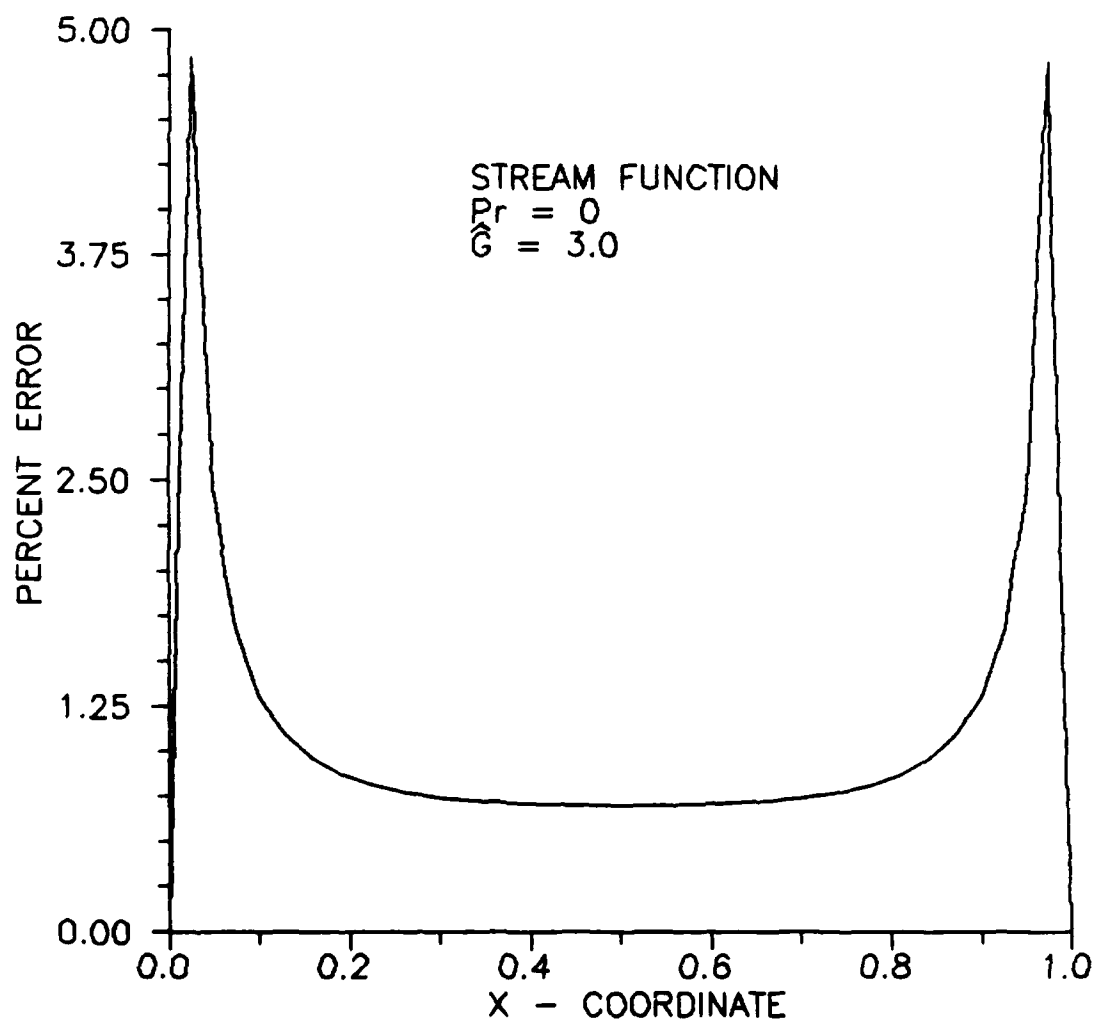


Figure 5. Stream function relative error.

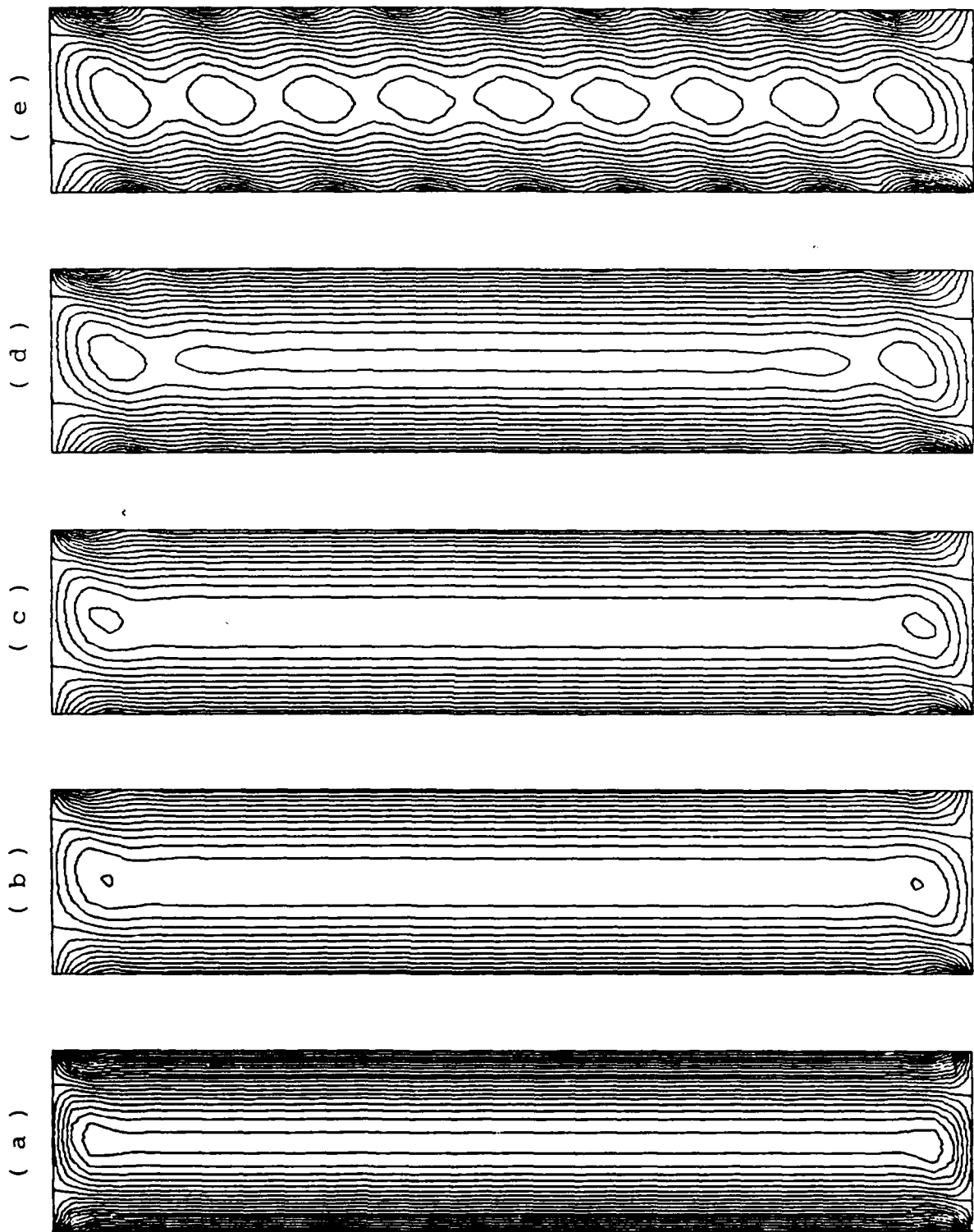


Figure 6. Vorticity Contours for  $Pr = 0$ .

a)  $\hat{G} = 3.0$ , b)  $\hat{G} = 3.6$ , c)  $\hat{G} = 3.7$ , d)  $\hat{G} = 4.0$ , e)  $\hat{G} = 4.2$ ,

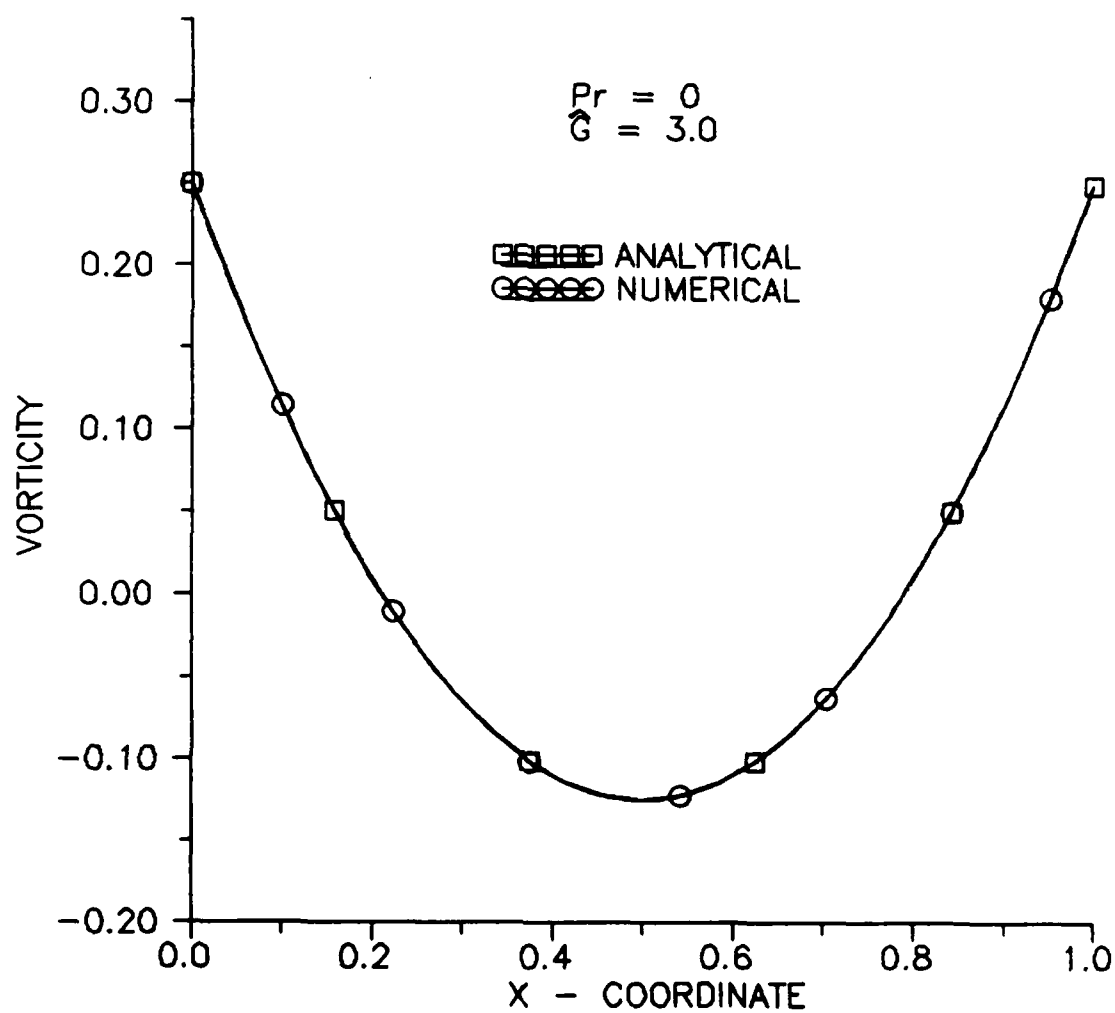


Figure 7. Vorticity variation at the horizontal centerline



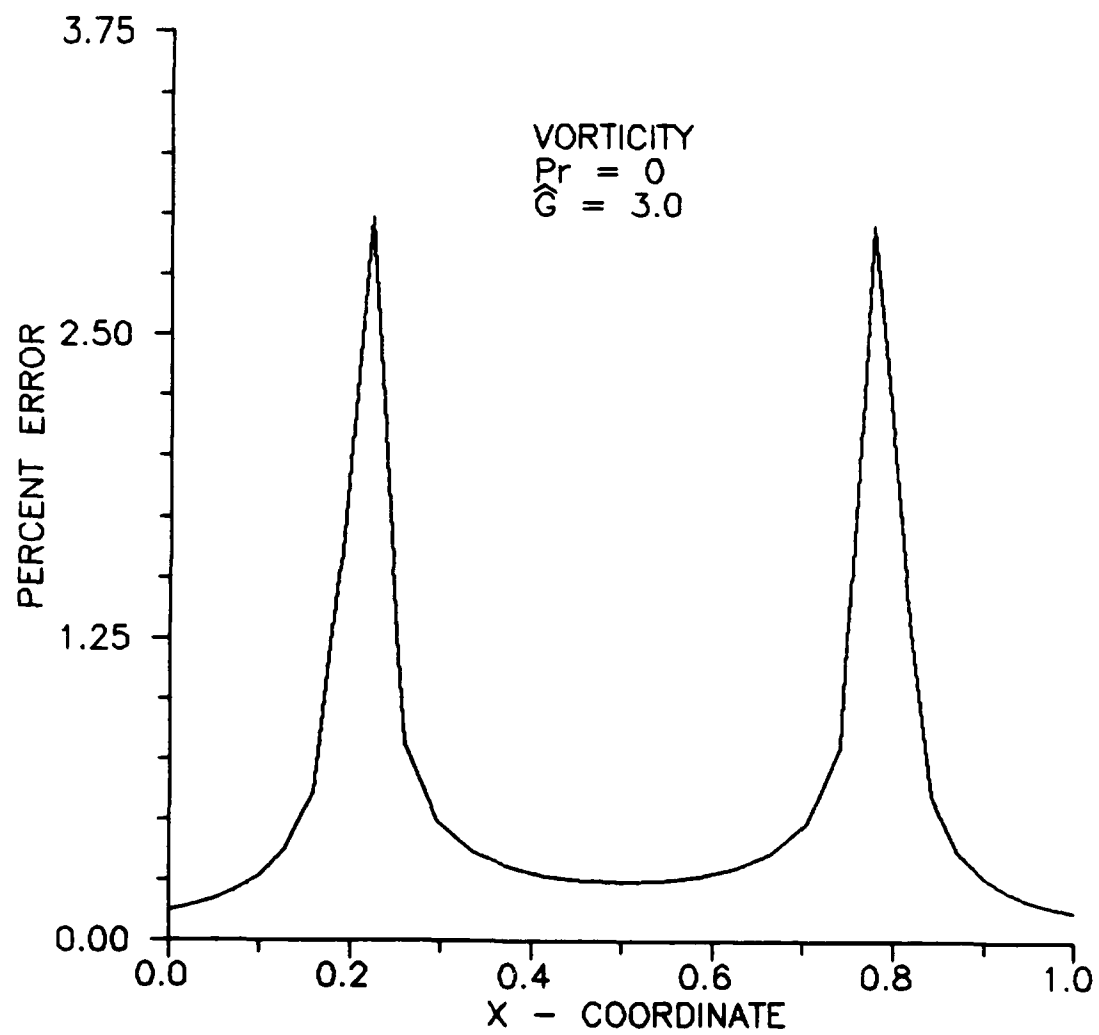


Figure 8. Vorticity relative error.

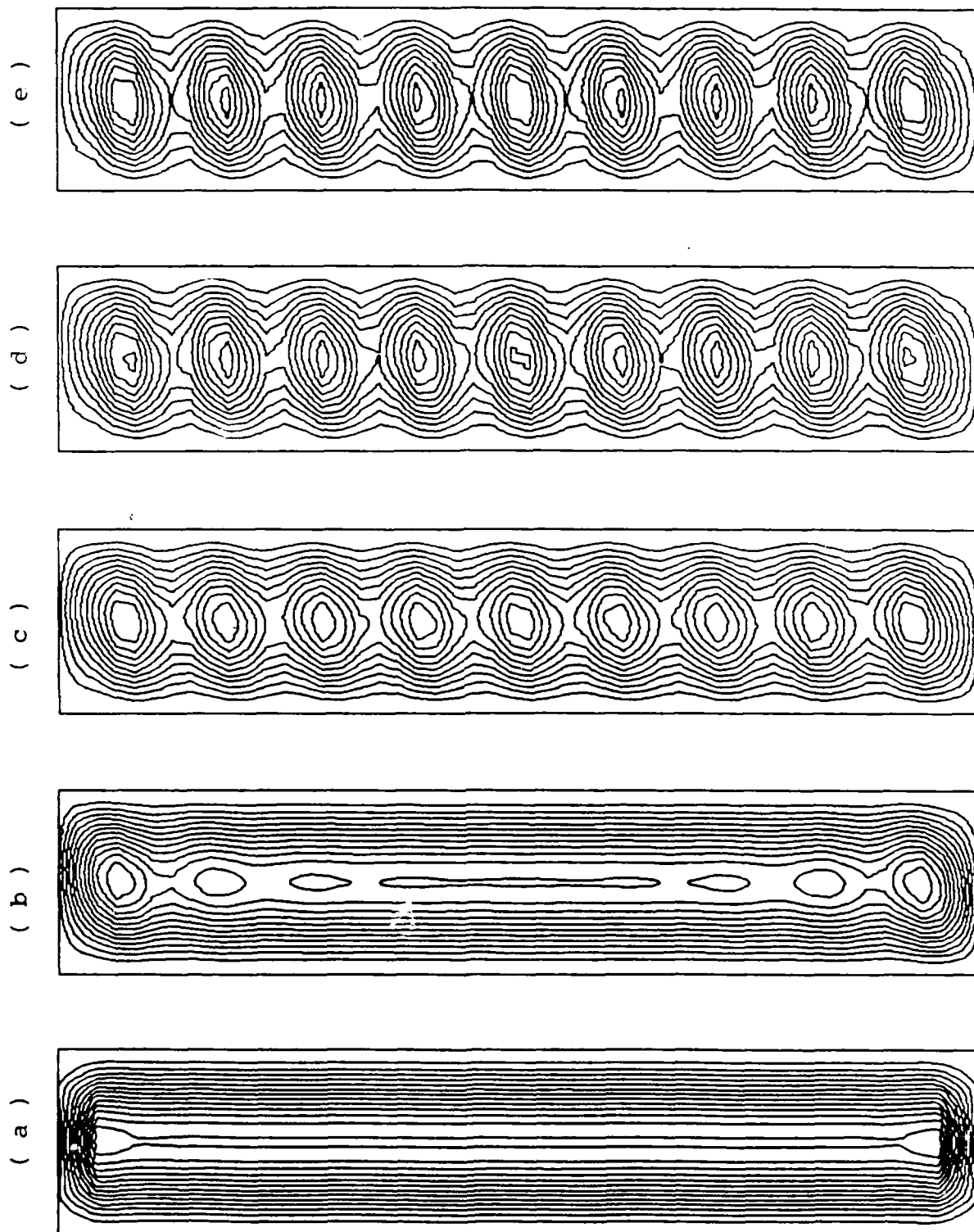


Figure 9. Stream Function contours for  $Pr = 0.02$  .

a)  $\tilde{G} = 1.0$ , b)  $\tilde{G} = 1.5$ , c)  $\tilde{G} = 1.6$ , d)  $\tilde{G} = 1.7$ , e)  $\tilde{G} = 1.8$

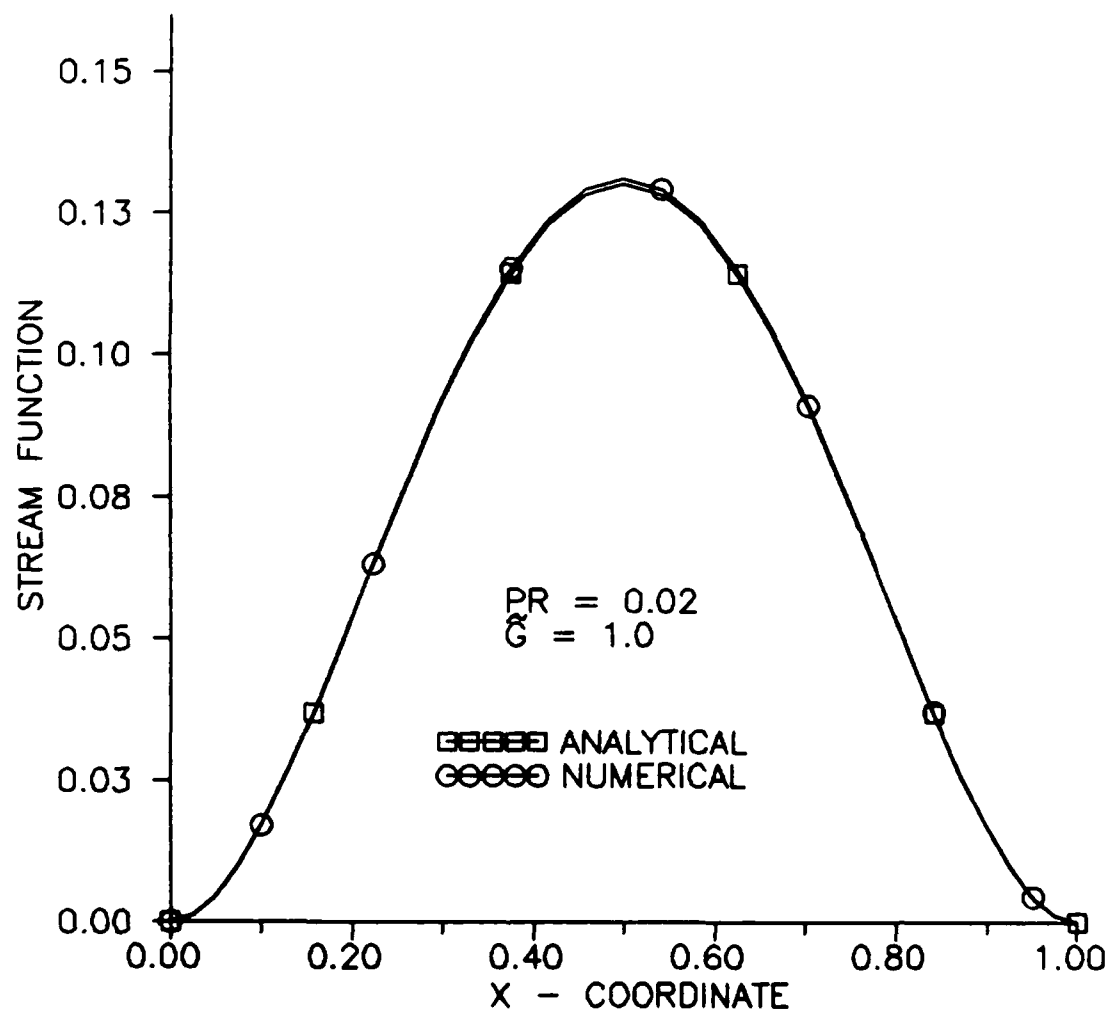


Figure 10. Stream function variation at the horizontal centerline.

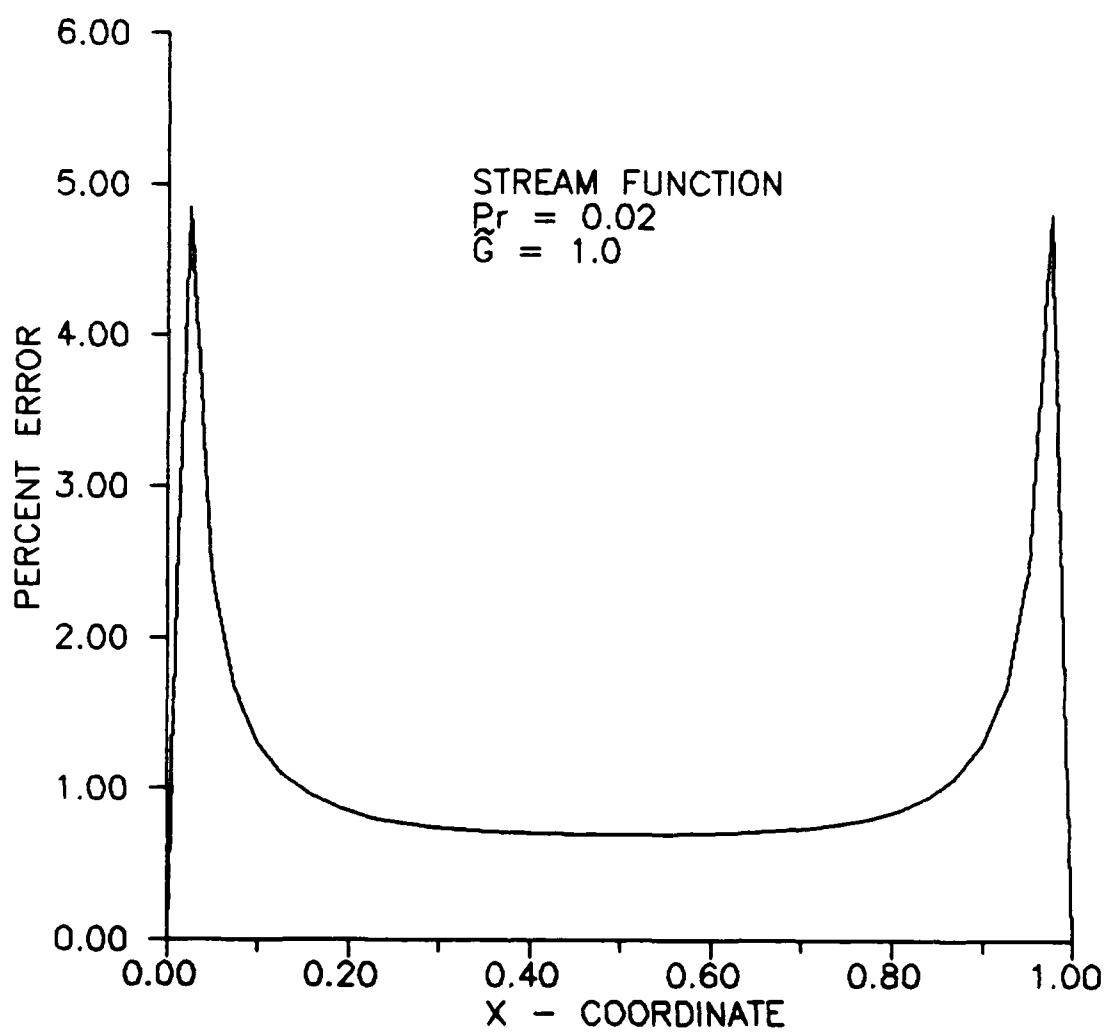


Figure 11. Stream function relative error

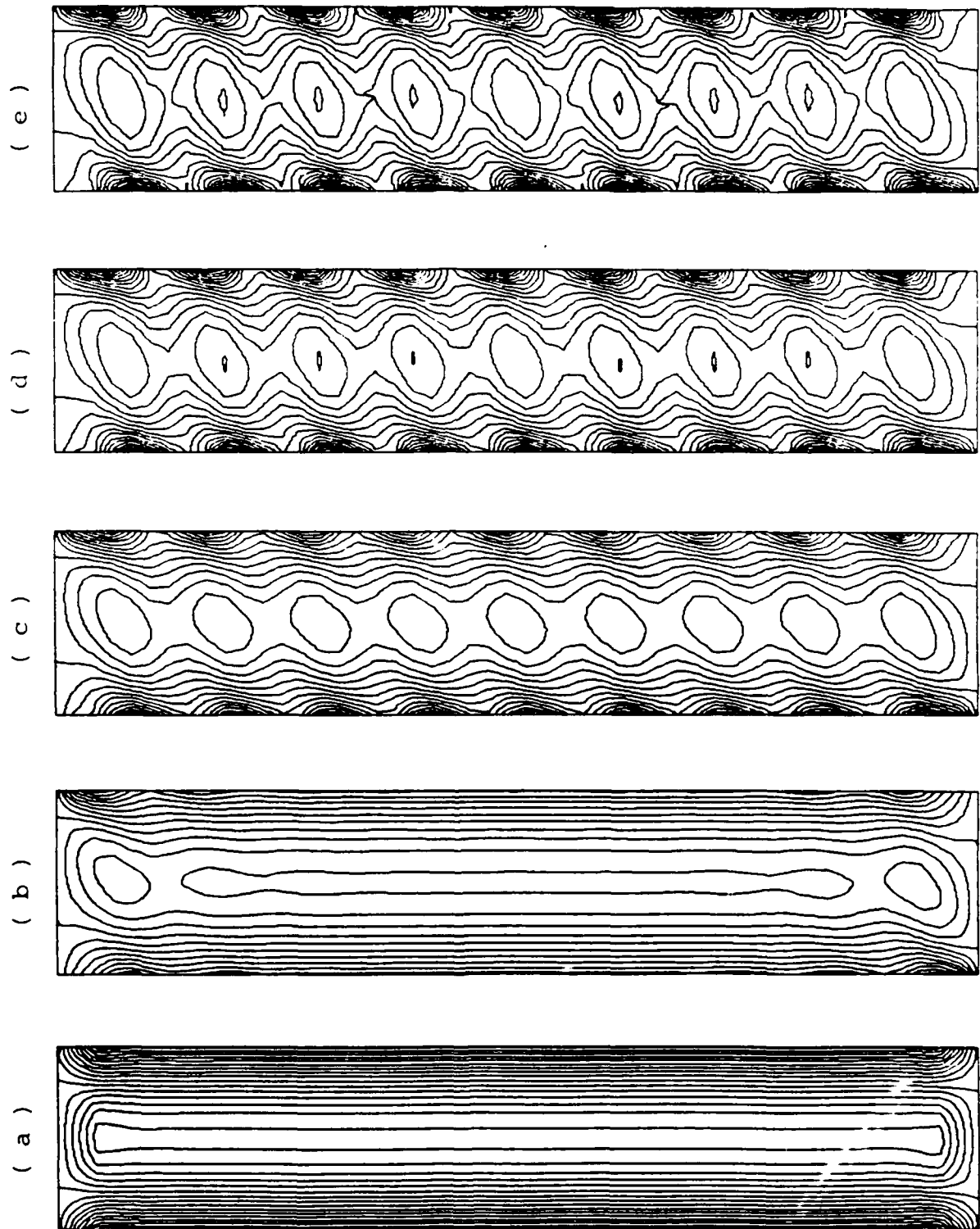


Figure 12. Vorticity Contours for  $Pr = 0.02$  .

a)  $\tilde{G} = 1.0$ , b)  $\tilde{G} = 1.5$ , c)  $\tilde{G} = 1.6$ , d)  $\tilde{G} = 1.7$ , e)  $\tilde{G} = 1.8$

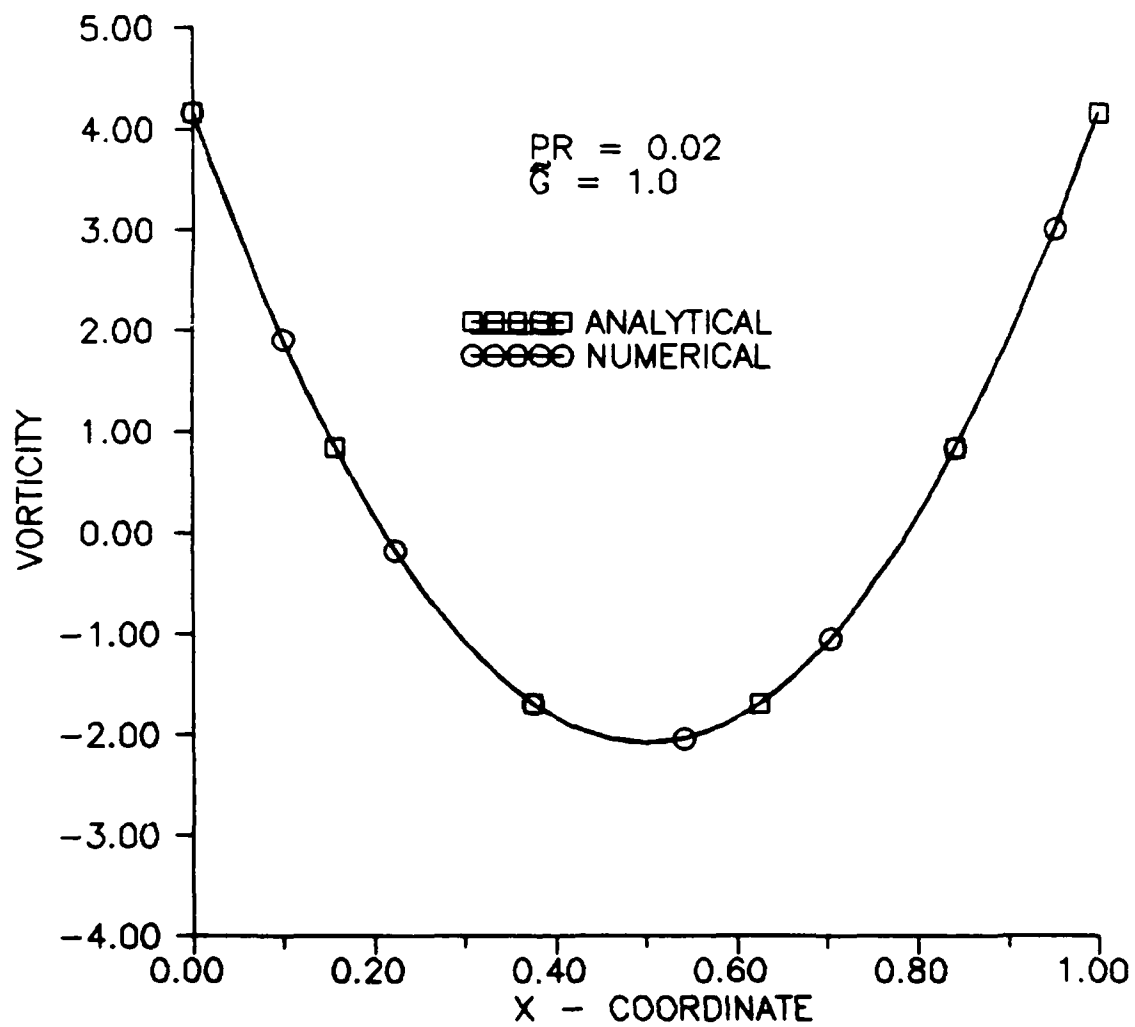


Figure 13. Vorticity variation at the horizontal centerline.

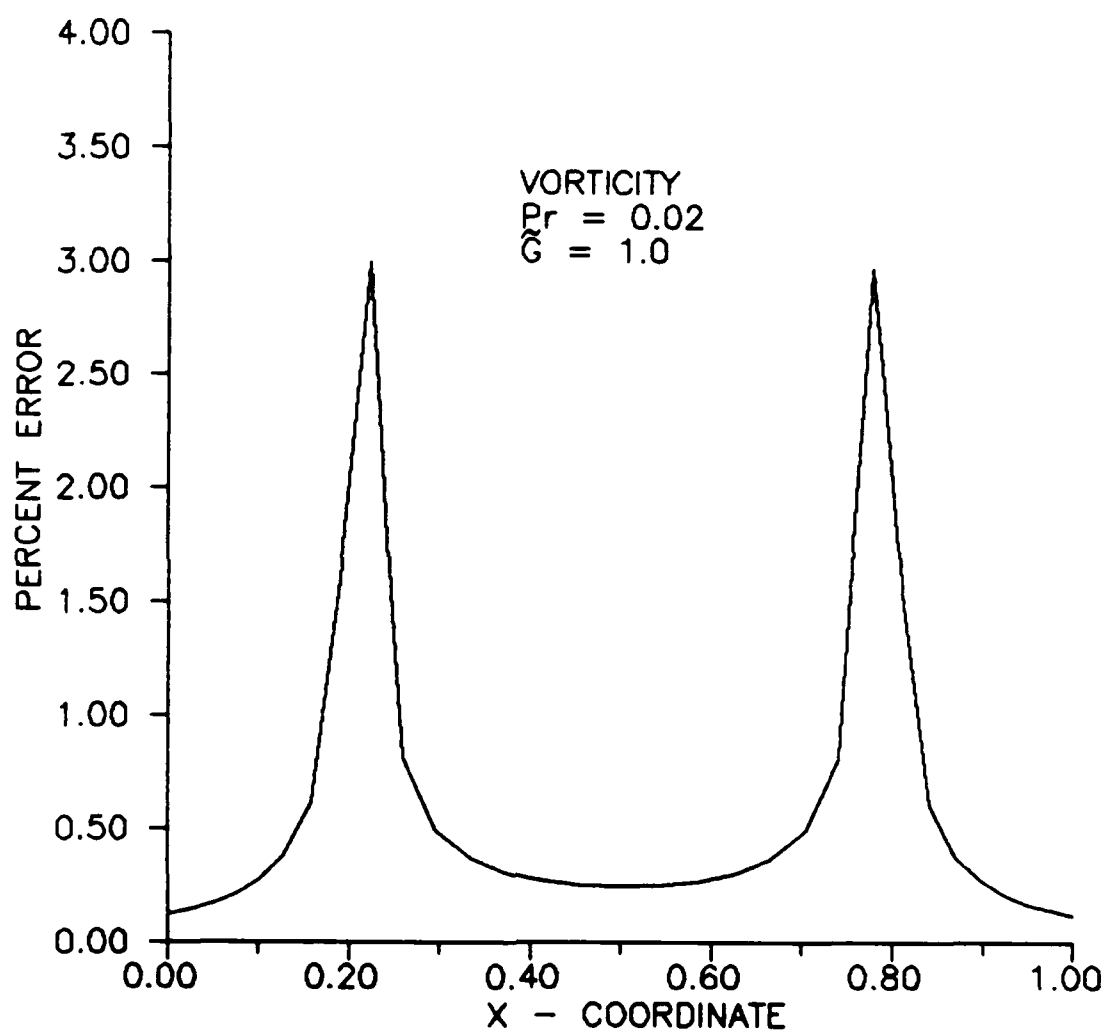


Figure 14. Vorticity relative error.

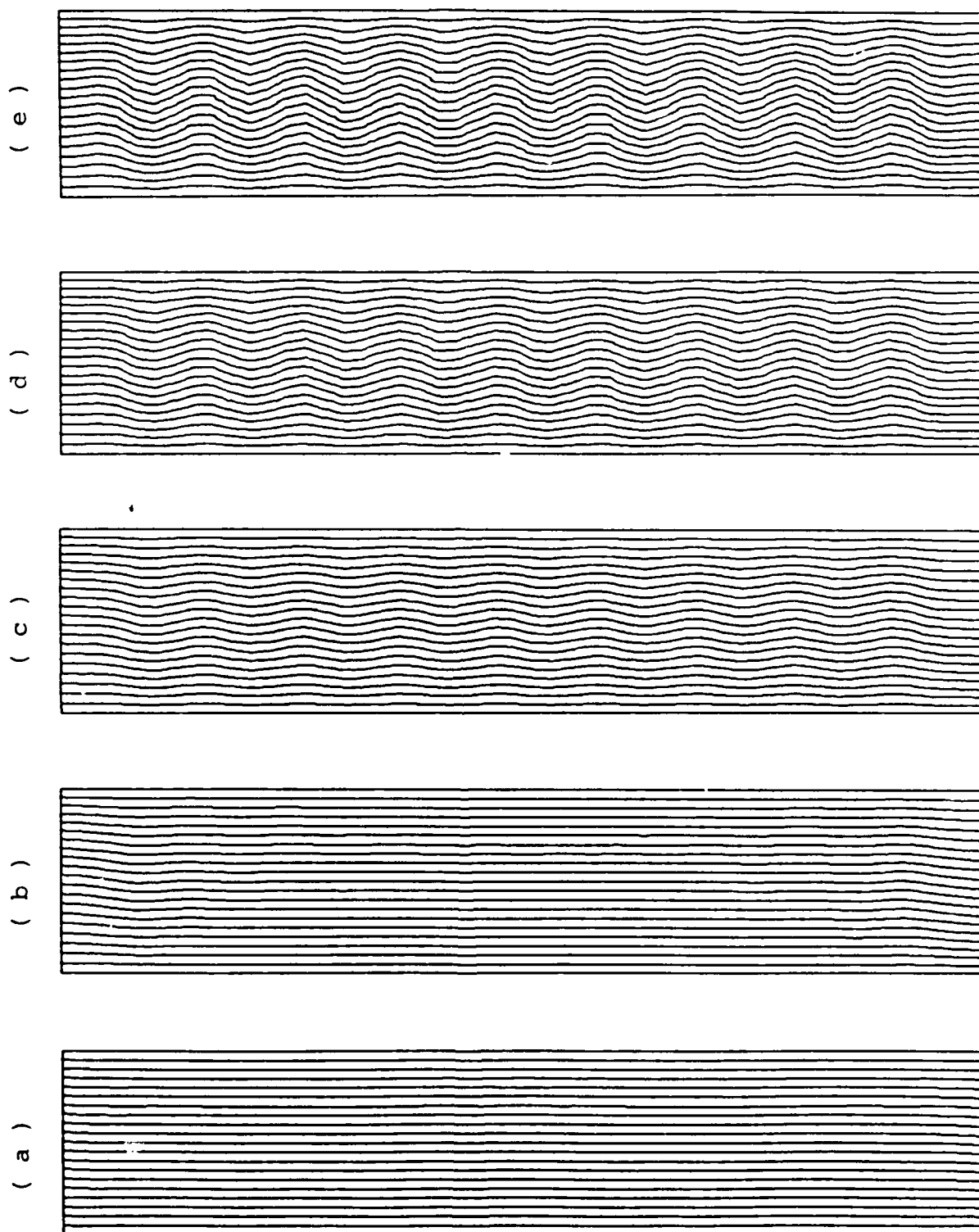


Figure 15. Temperature Contours for  $Pr = 0.02$  .

a)  $\tilde{G} = 1.0$ , b)  $\tilde{G} = 1.5$ , c)  $\tilde{G} = 1.6$ , d)  $\tilde{G} = 1.7$ , e)  $\tilde{G} = 1.8$



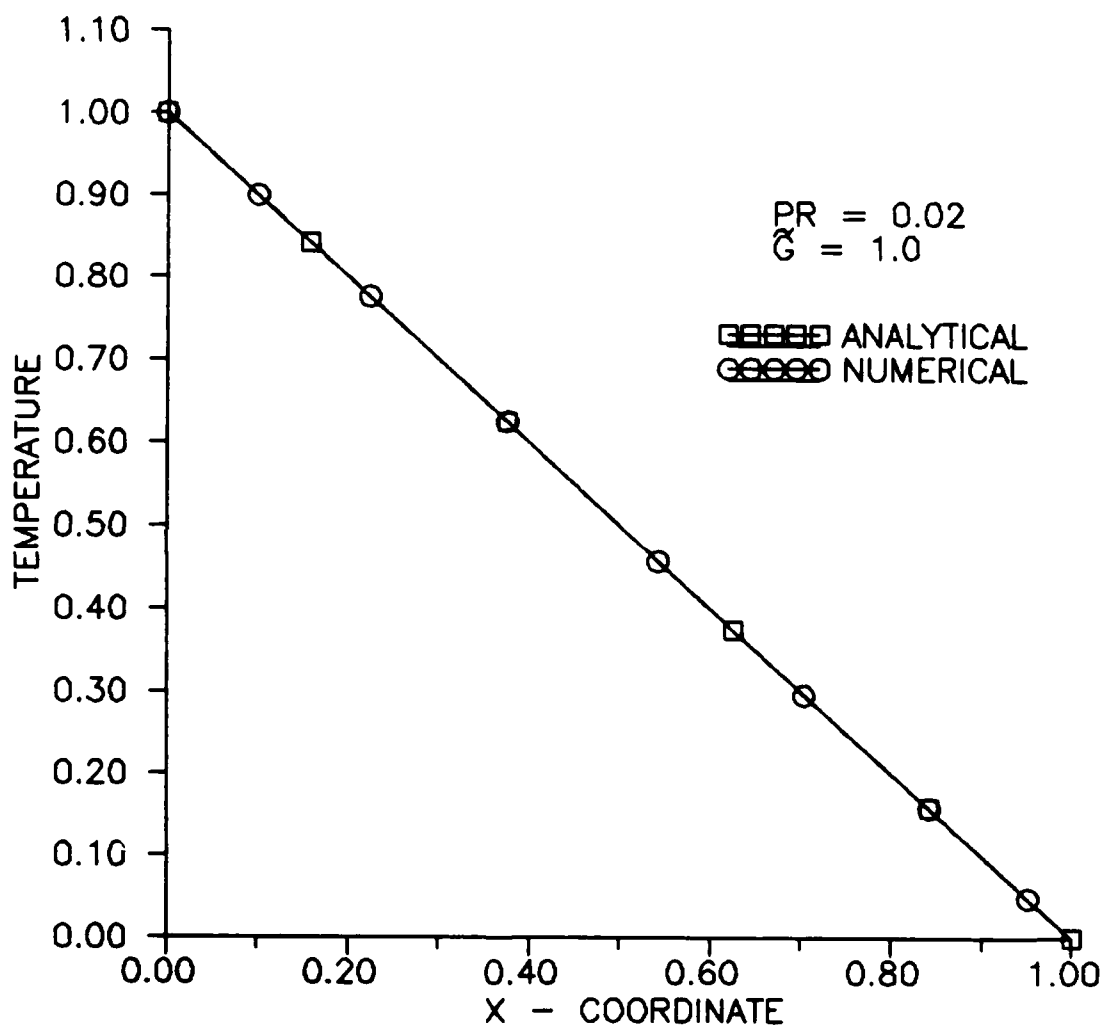


Figure 16. Temperature variation at the horizontal centerline.

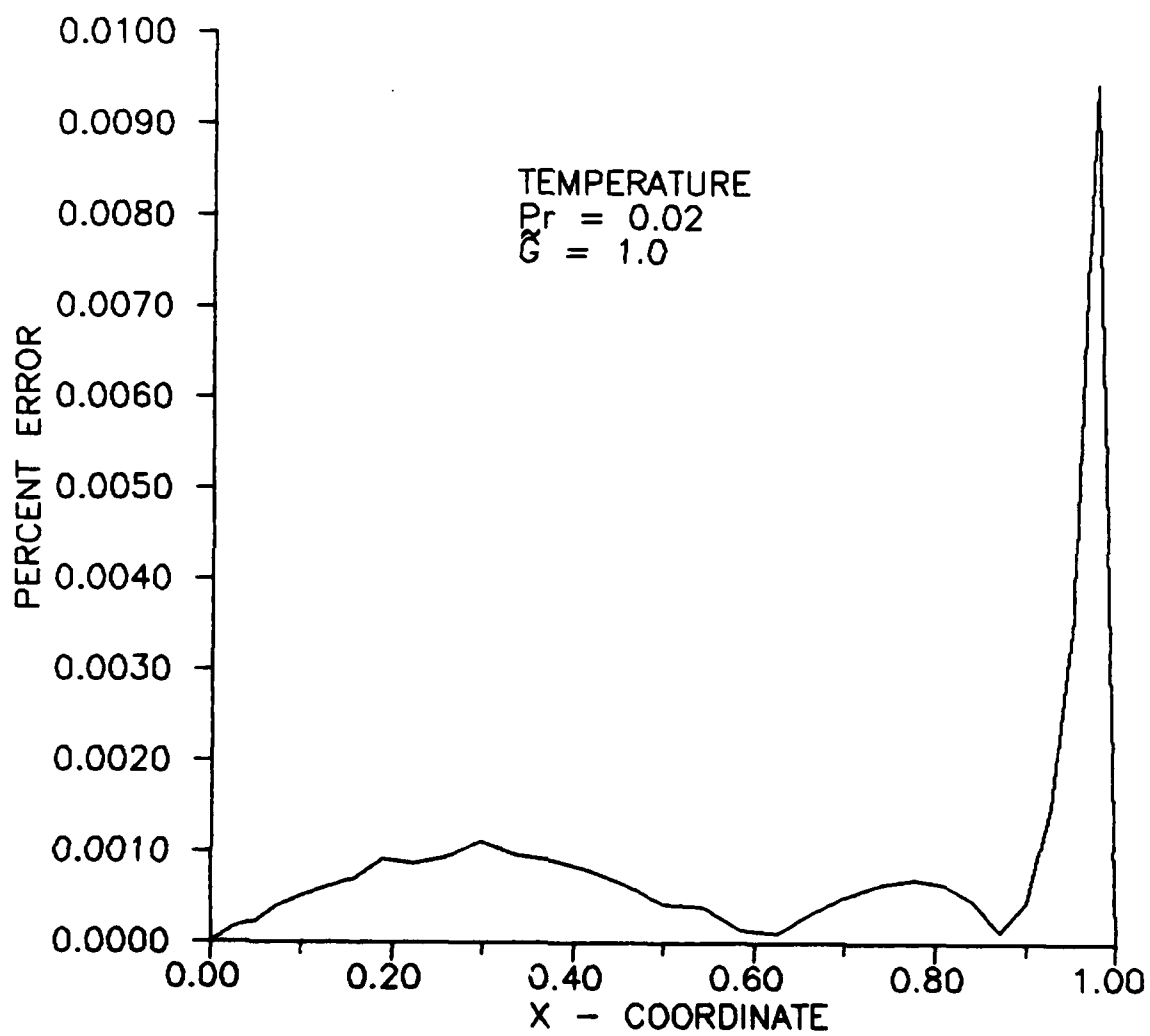


Figure 17. Temperature relative error.

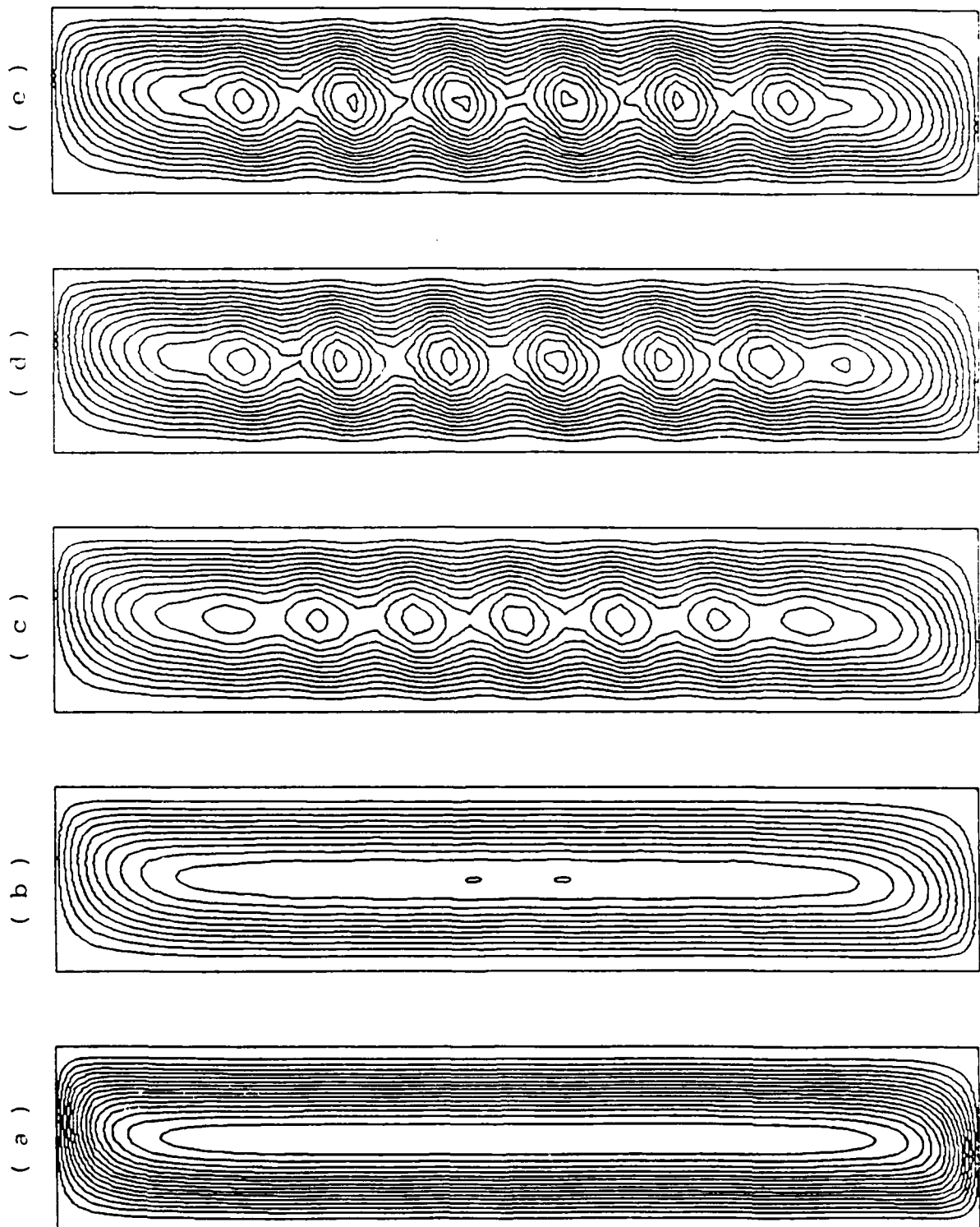


Figure 18. Stream Function contours for  $Pr = 0.706$  .  
a)  $\tilde{G} = 3.5$ , b)  $\tilde{G} = 3.9$ , c)  $\tilde{G} = 4.0$ , d)  $\tilde{G} = 4.2$ , e)  $\tilde{G} = 4.3$

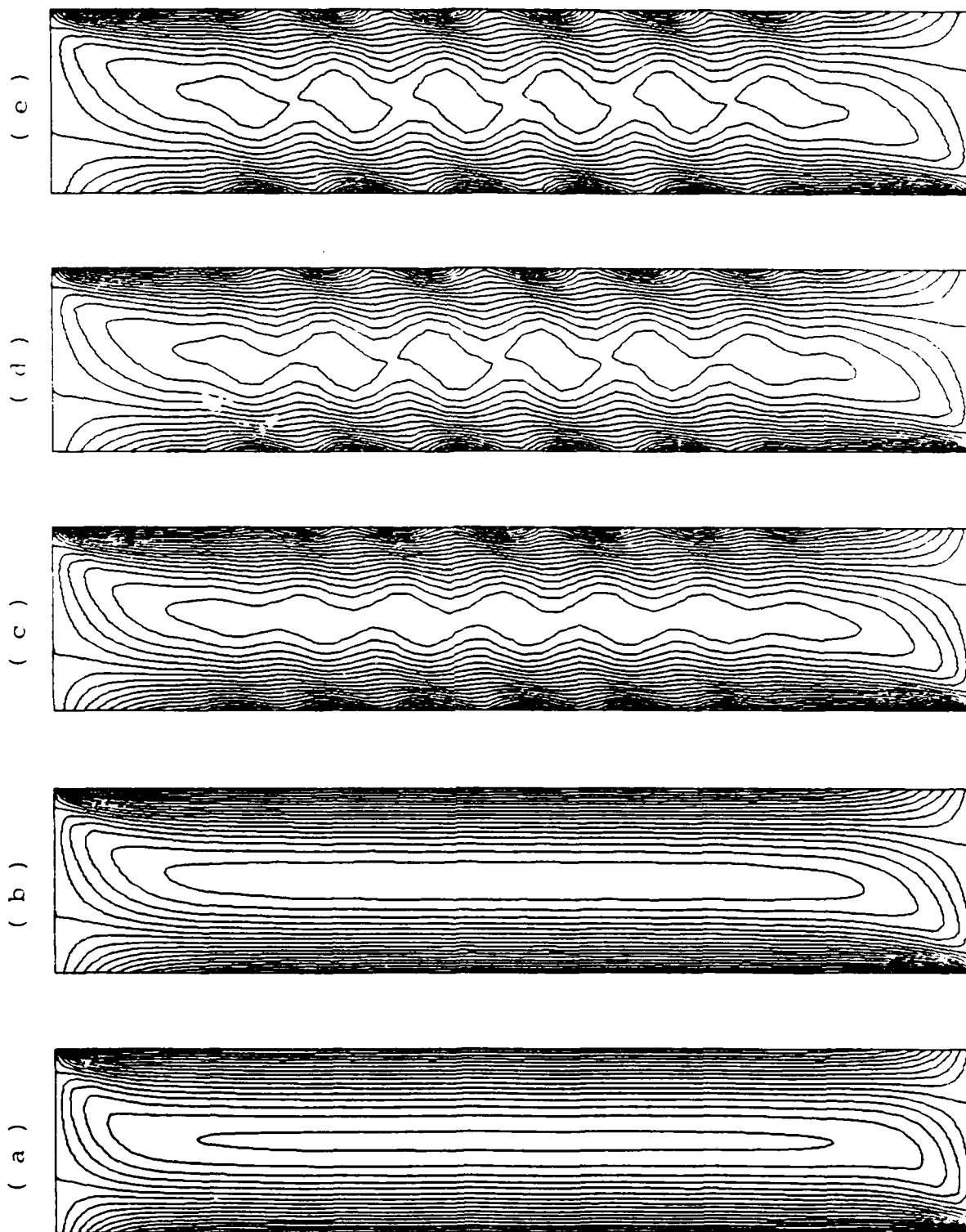


Figure 19. Vorticity Contours for  $Pr = 0.706$  .

a)  $\tilde{G} = 3.5$ , b)  $\tilde{G} = 3.9$ , c)  $\tilde{G} = 4.0$ , d)  $\tilde{G} = 4.2$ , e)  $\tilde{G} = 4.3$

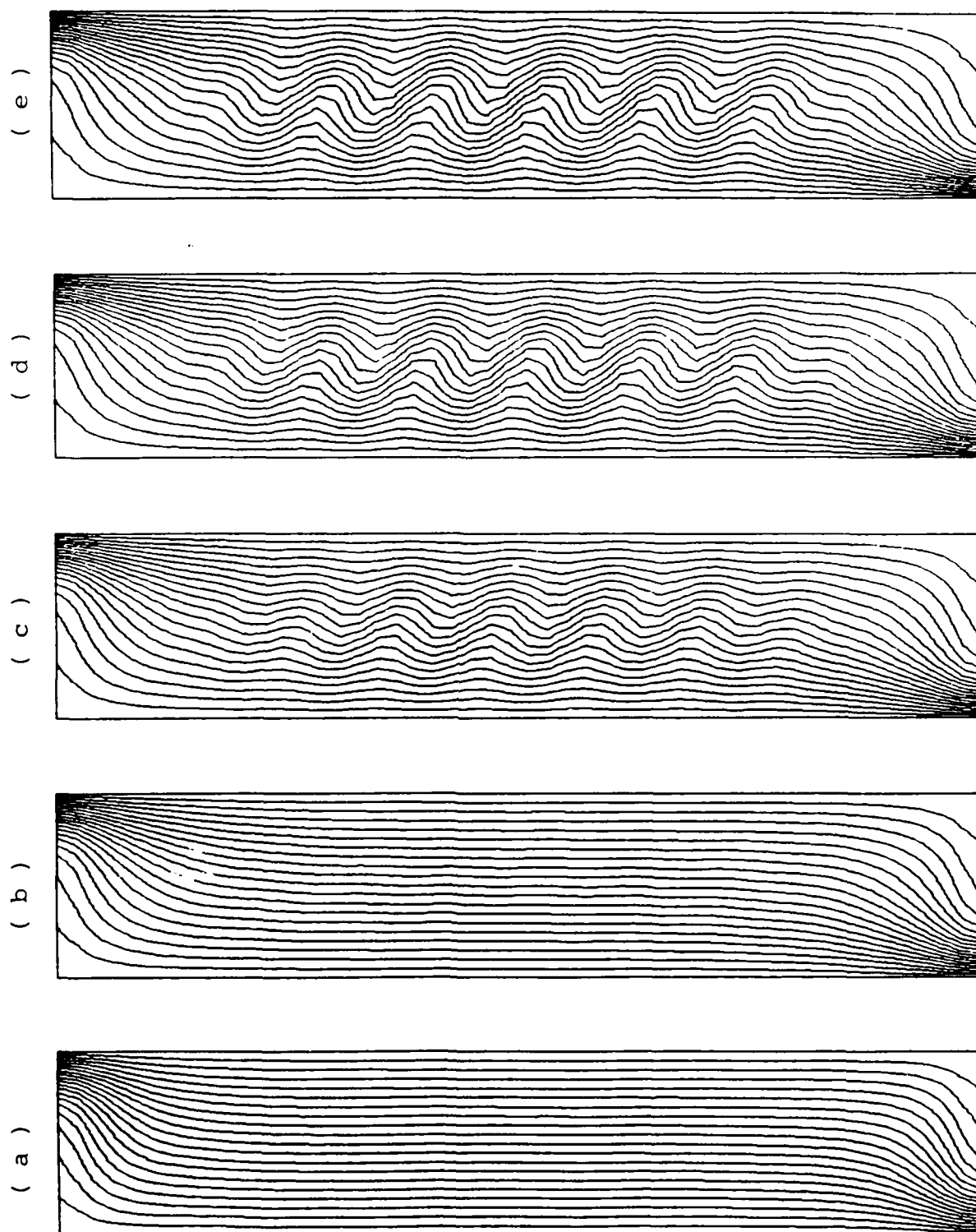


Figure 20. Temperature Contours for  $Pr = 0.706$  .

a)  $\tilde{G} = 3.5$ , b)  $\tilde{G} = 3.9$ , c)  $\tilde{G} = 4.0$ , d)  $\tilde{G} = 4.2$ , e)  $\tilde{G} = 4.3$

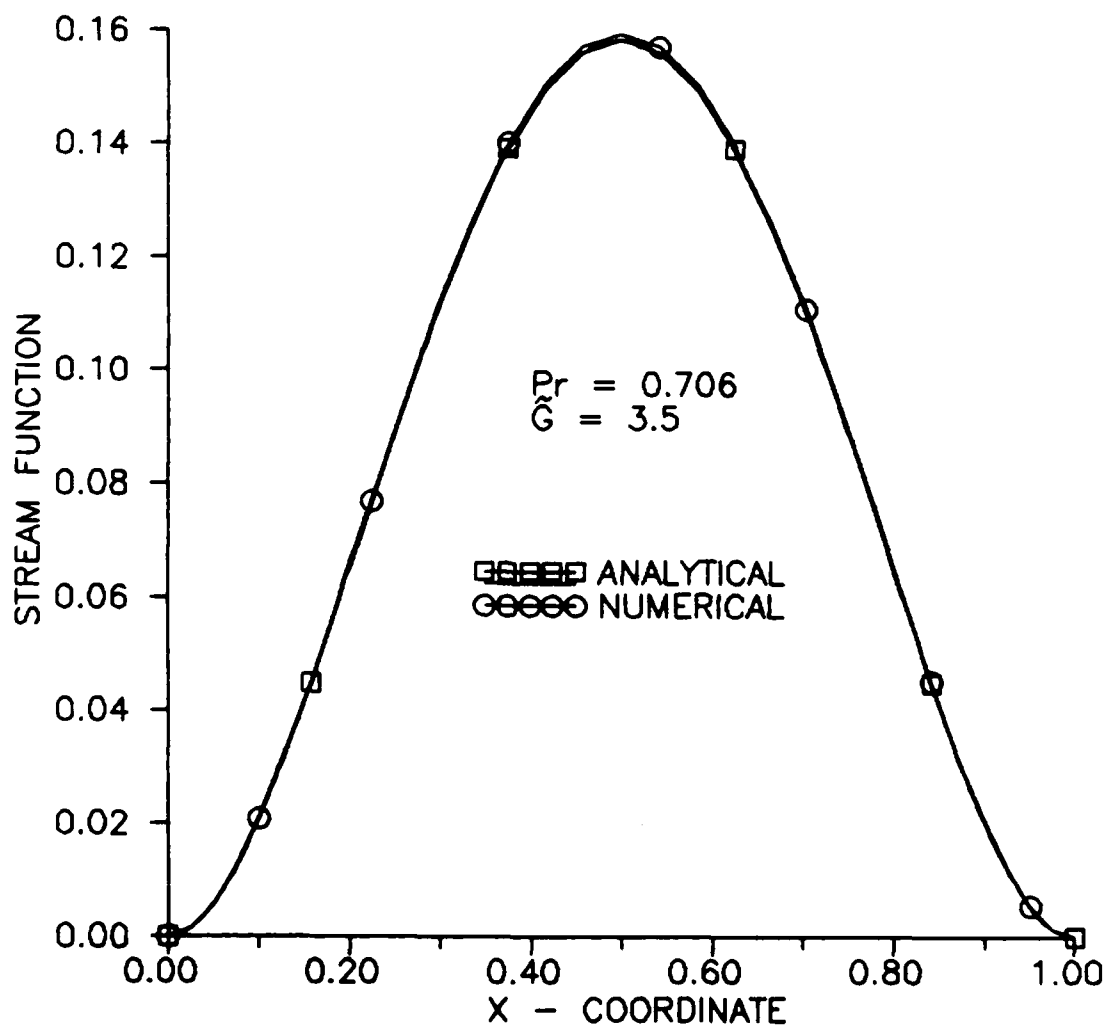


Figure 21. Stream function variation at the horizontal centerline

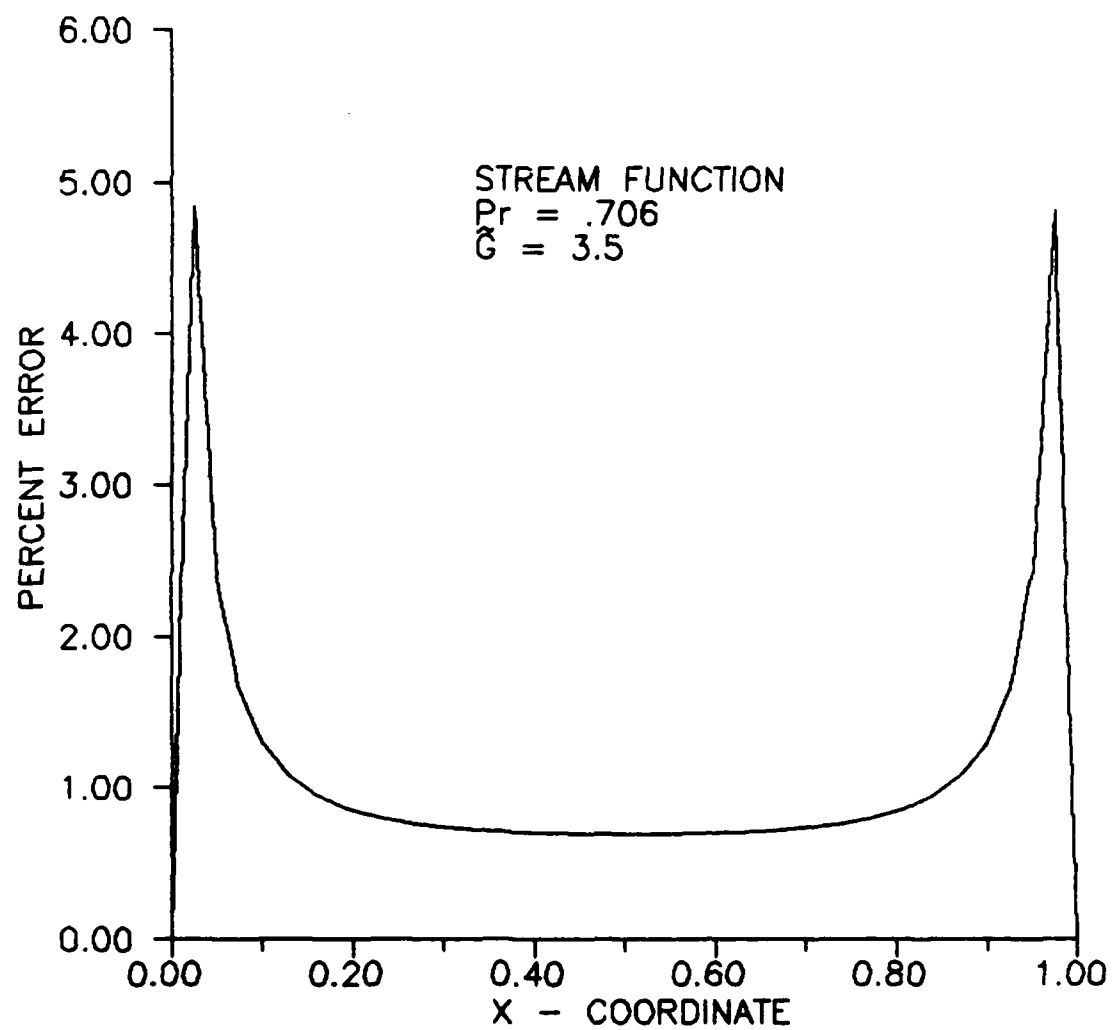


Figure 22. Stream function relative error

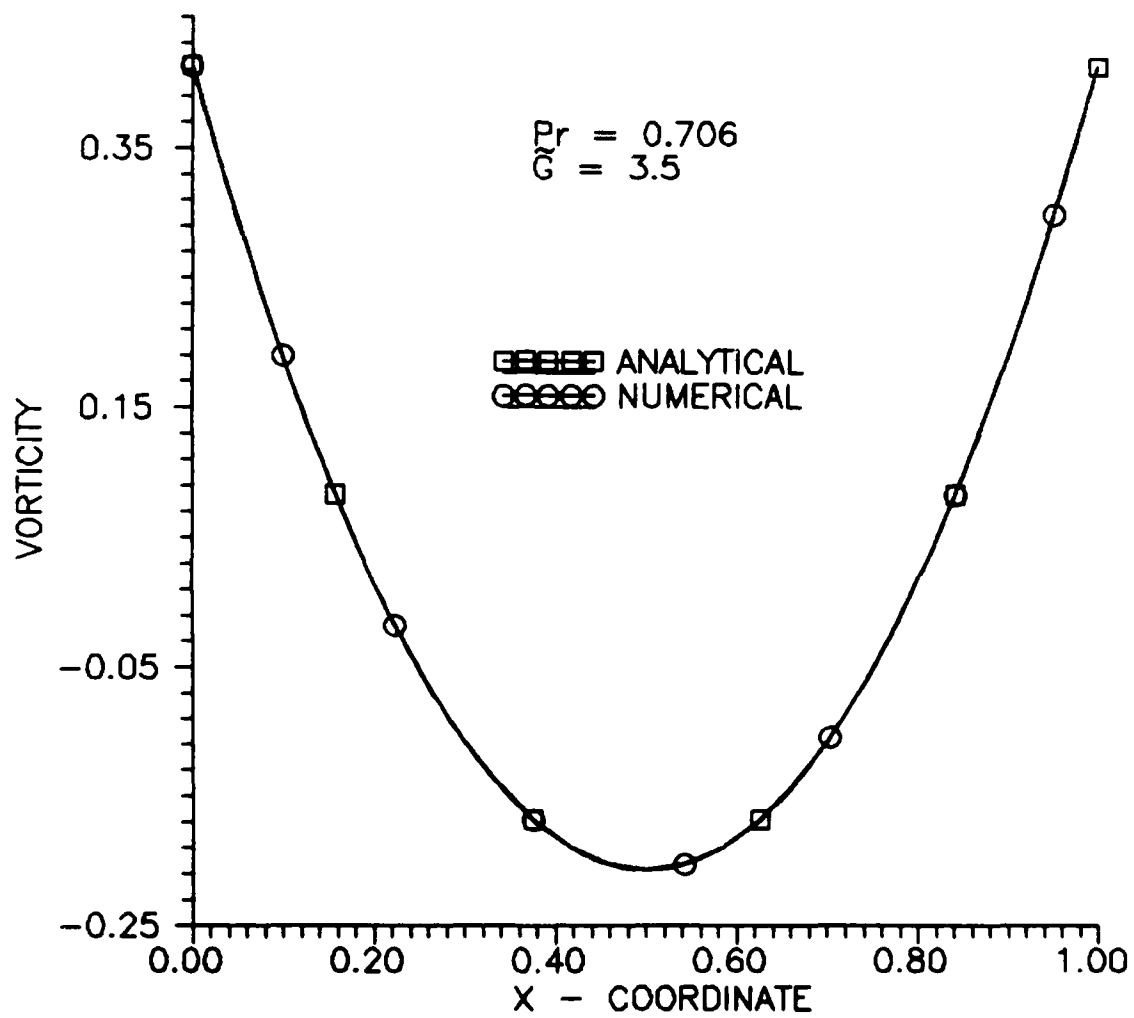


Figure 23. Vorticity variation at the horizontal centerline.



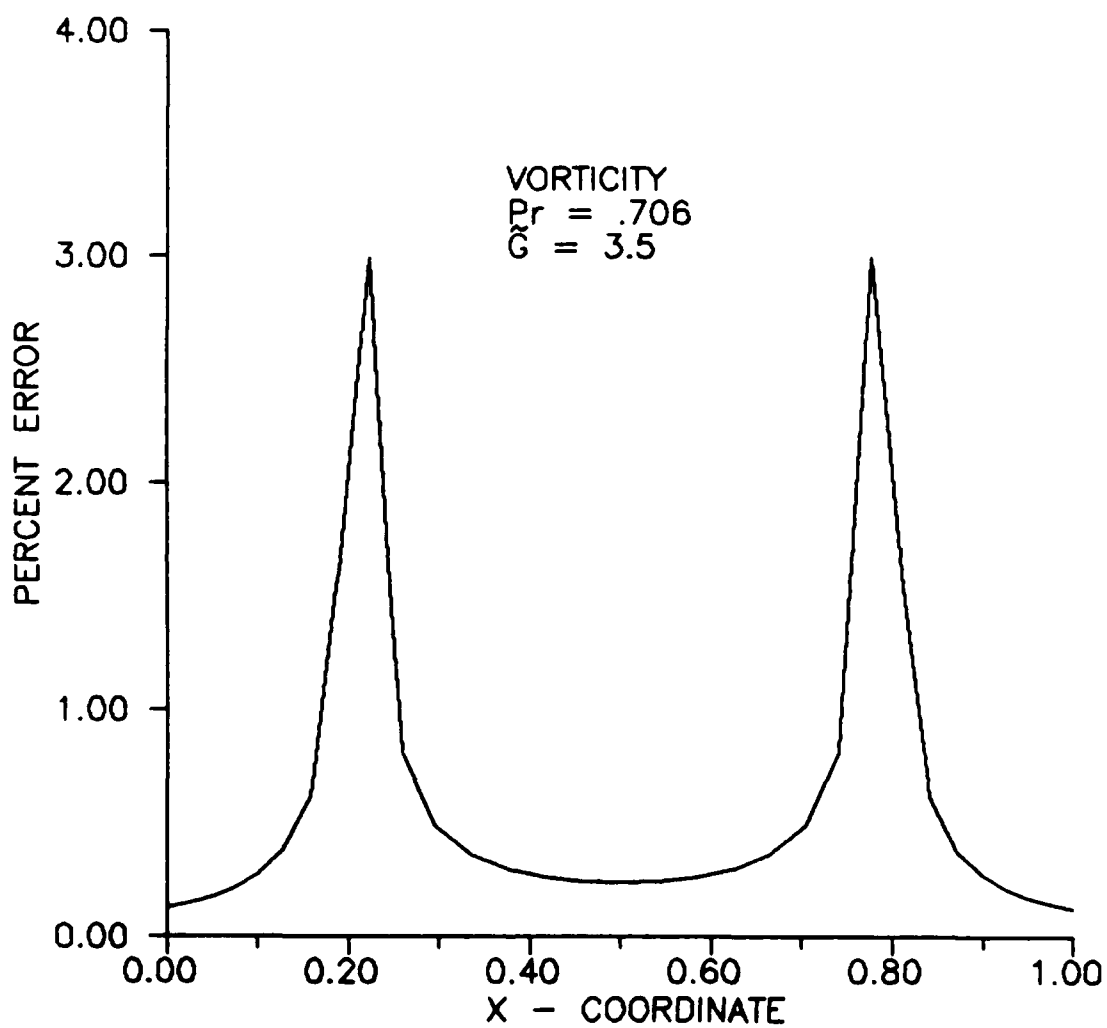


Figure 24. Vorticity relative error.

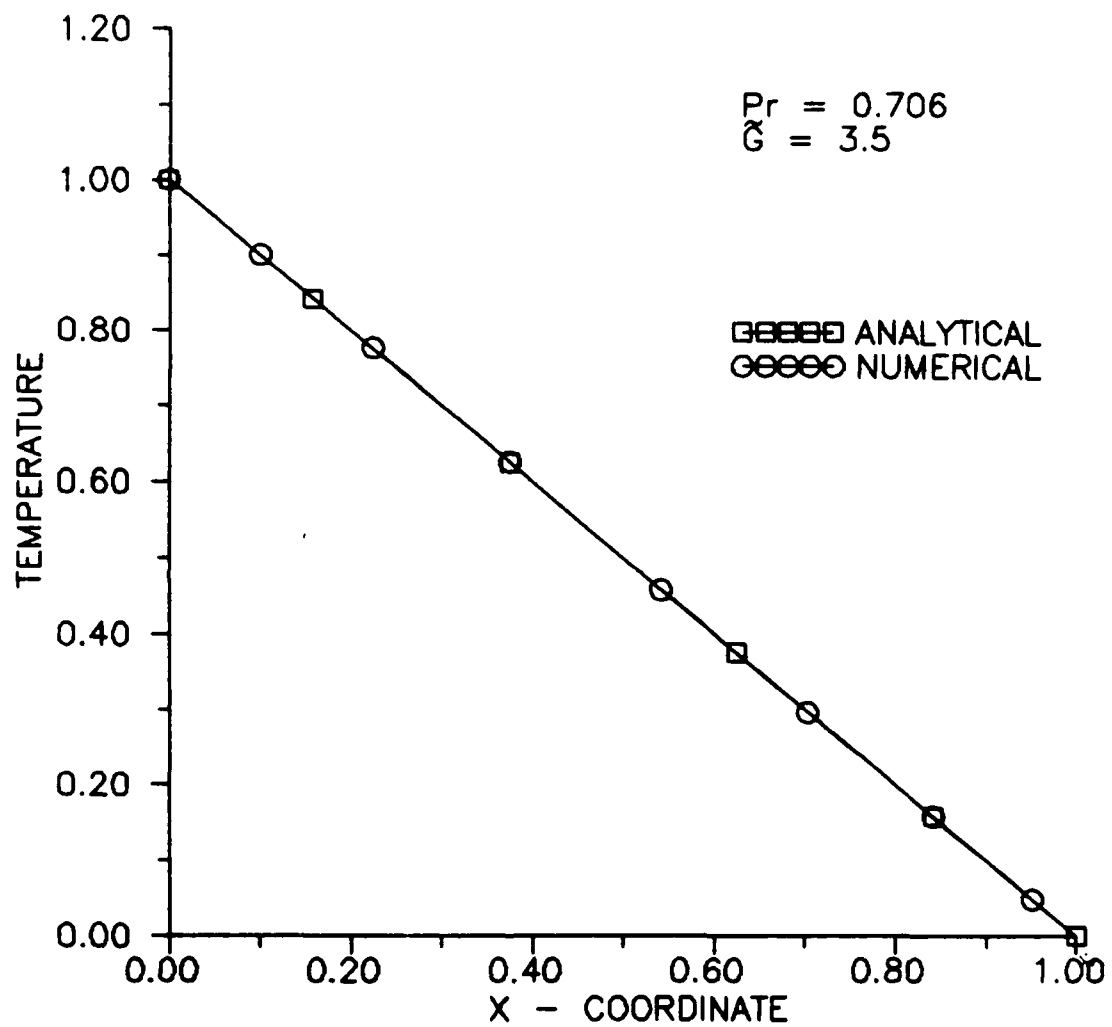


Figure 25. Temperature variation at the horizontal centerline

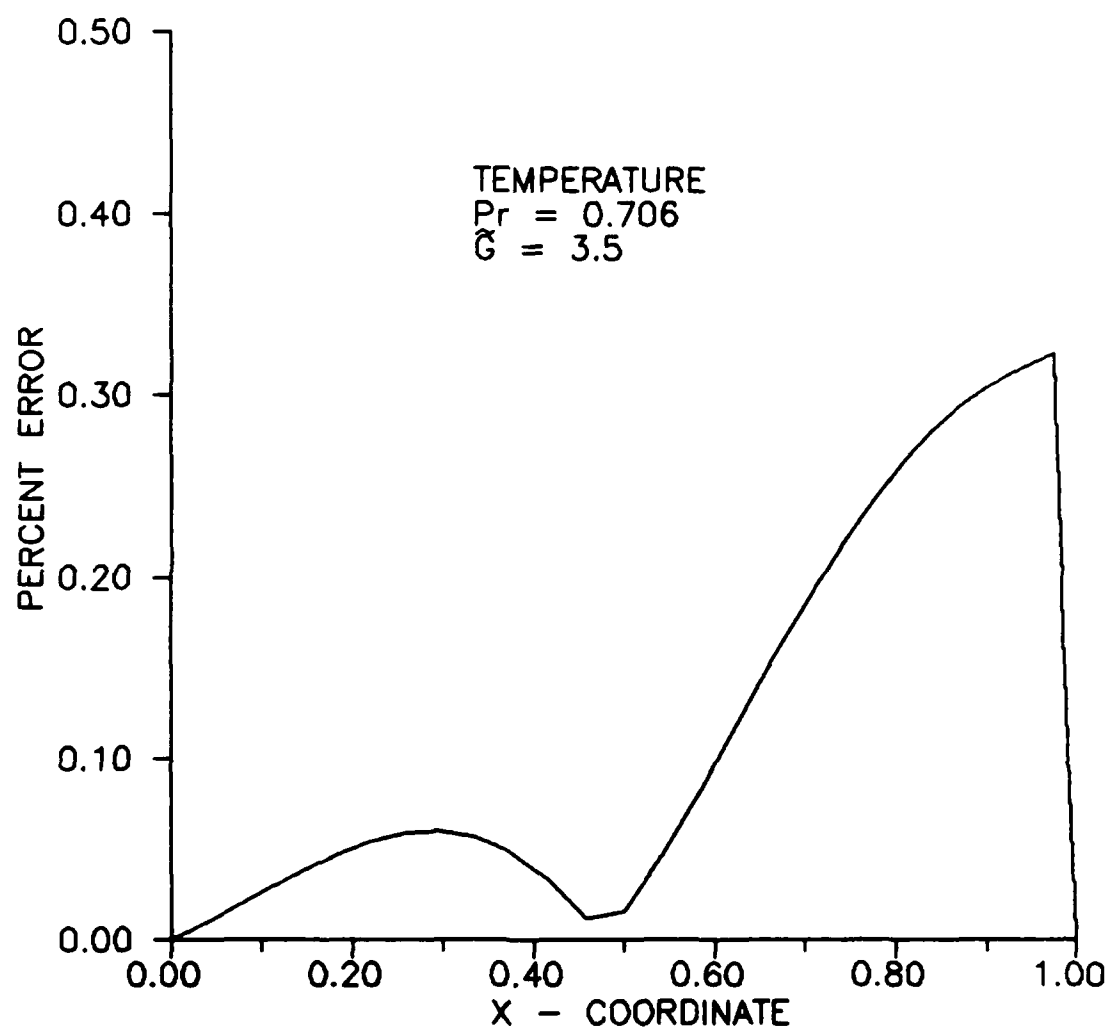


Figure 26. Temperature relative error.

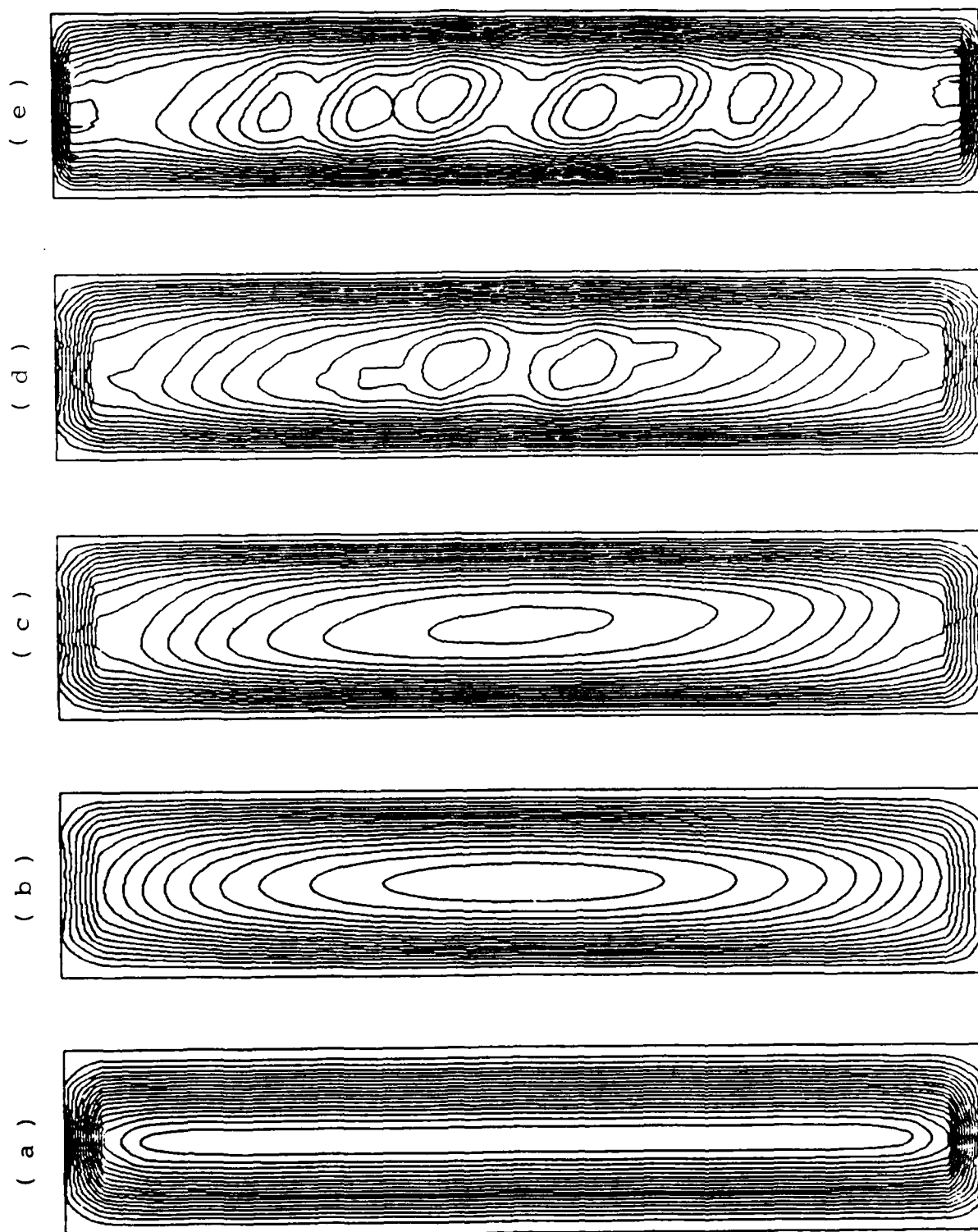


Figure 27. Stream Function contours for  $Pr = 1000$  .

a)  $\tilde{G} = 3.0$ , b)  $\tilde{G} = 10.0$ , c)  $\tilde{G} = 12.0$ , d)  $\tilde{G} = 12.5$ , e)  $\tilde{G} = 13.0$

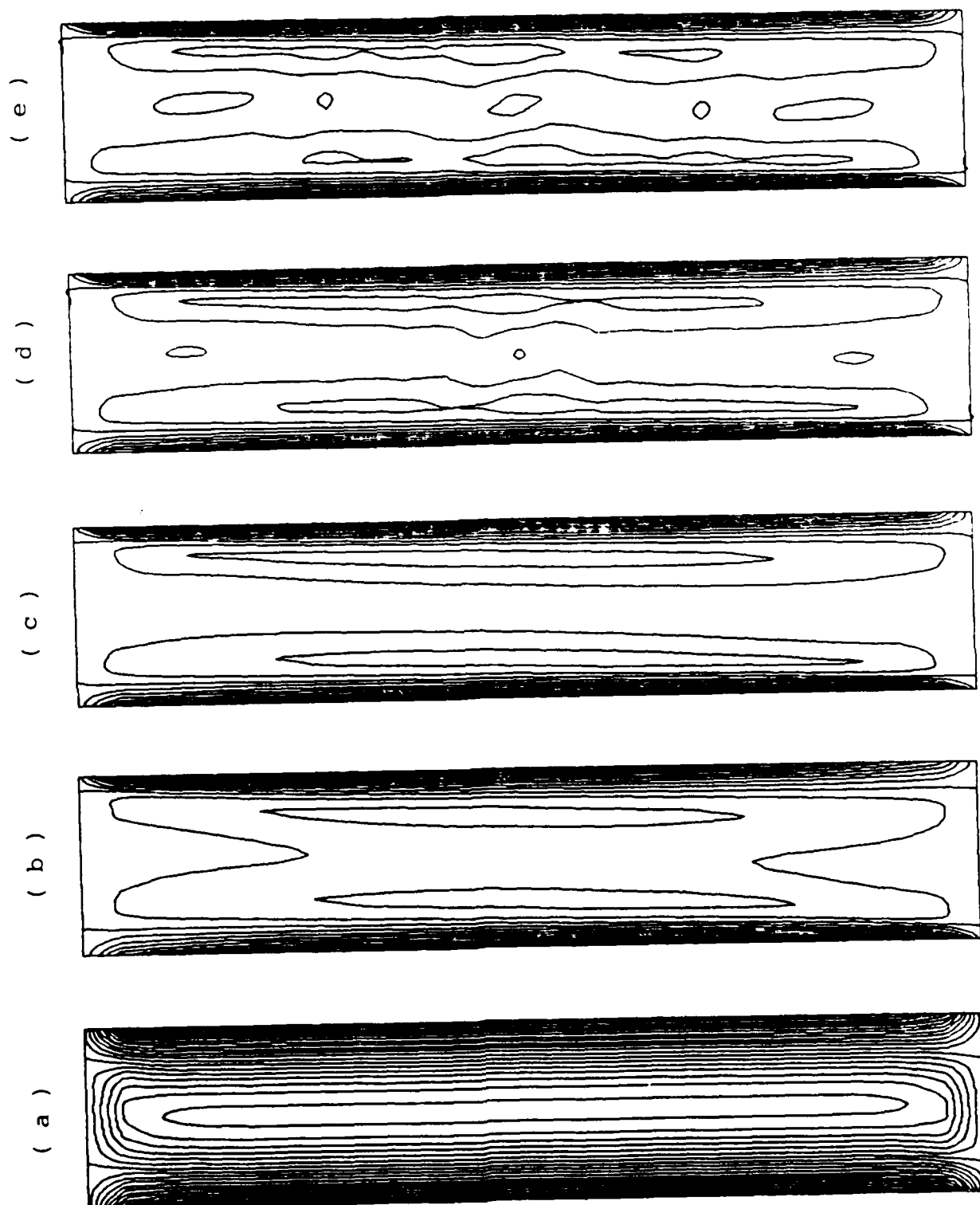


Figure 28. Vorticity Contours for  $Pr = 1000$ .

a)  $\tilde{G} = 3.0$ , b)  $\tilde{G} = 10.0$ , c)  $\tilde{G} = 12.0$ , d)  $\tilde{G} = 12.5$ , e)  $\tilde{G} = 13.0$

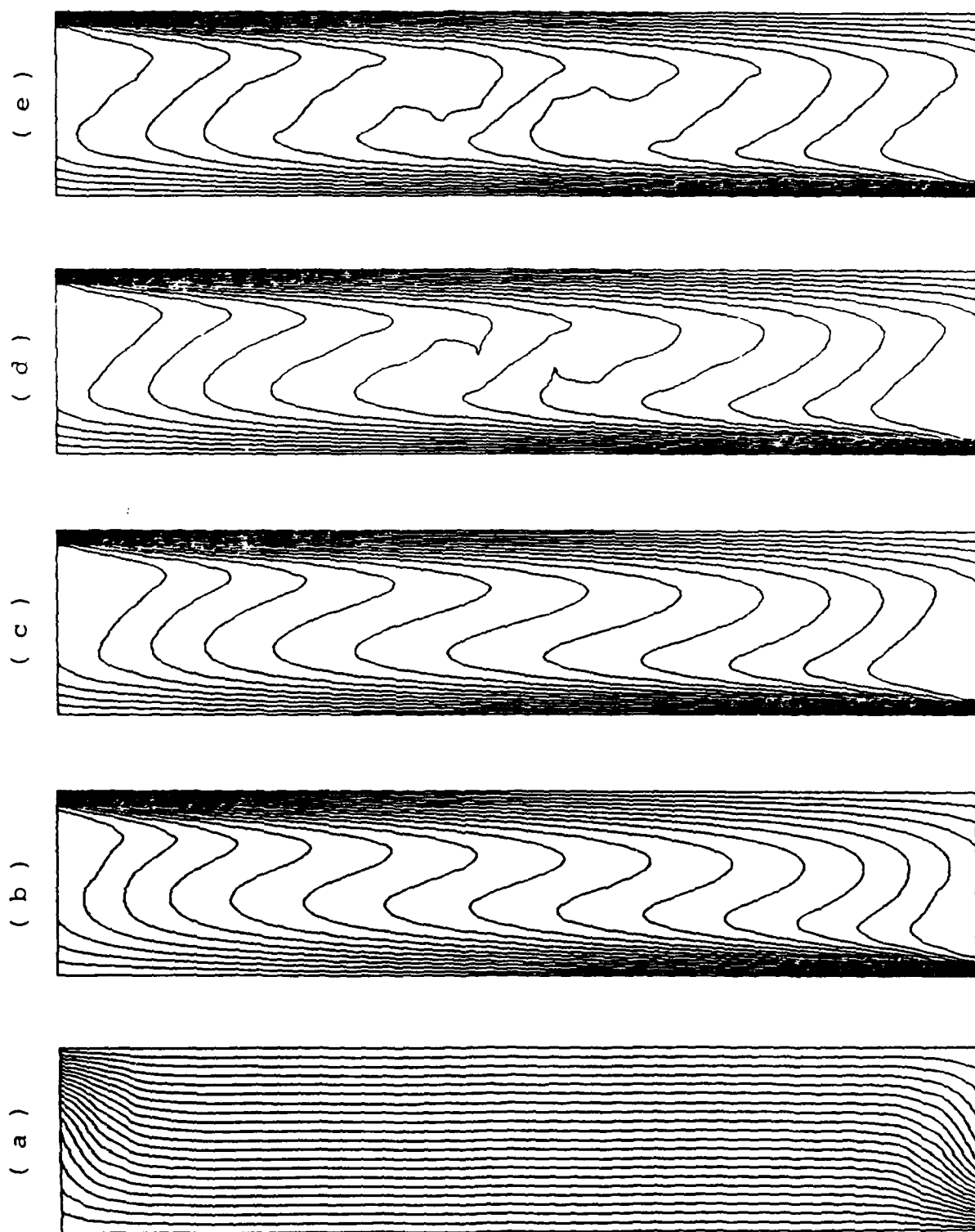


Figure 29. Temperature Contours for  $Pr = 1000$  .

a)  $\tilde{G} = 3.0$ , b)  $\tilde{G} = 10.0$ , c)  $\tilde{G} = 12.0$ , d)  $\tilde{G} = 12.5$ , e)  $\tilde{G} = 13.0$

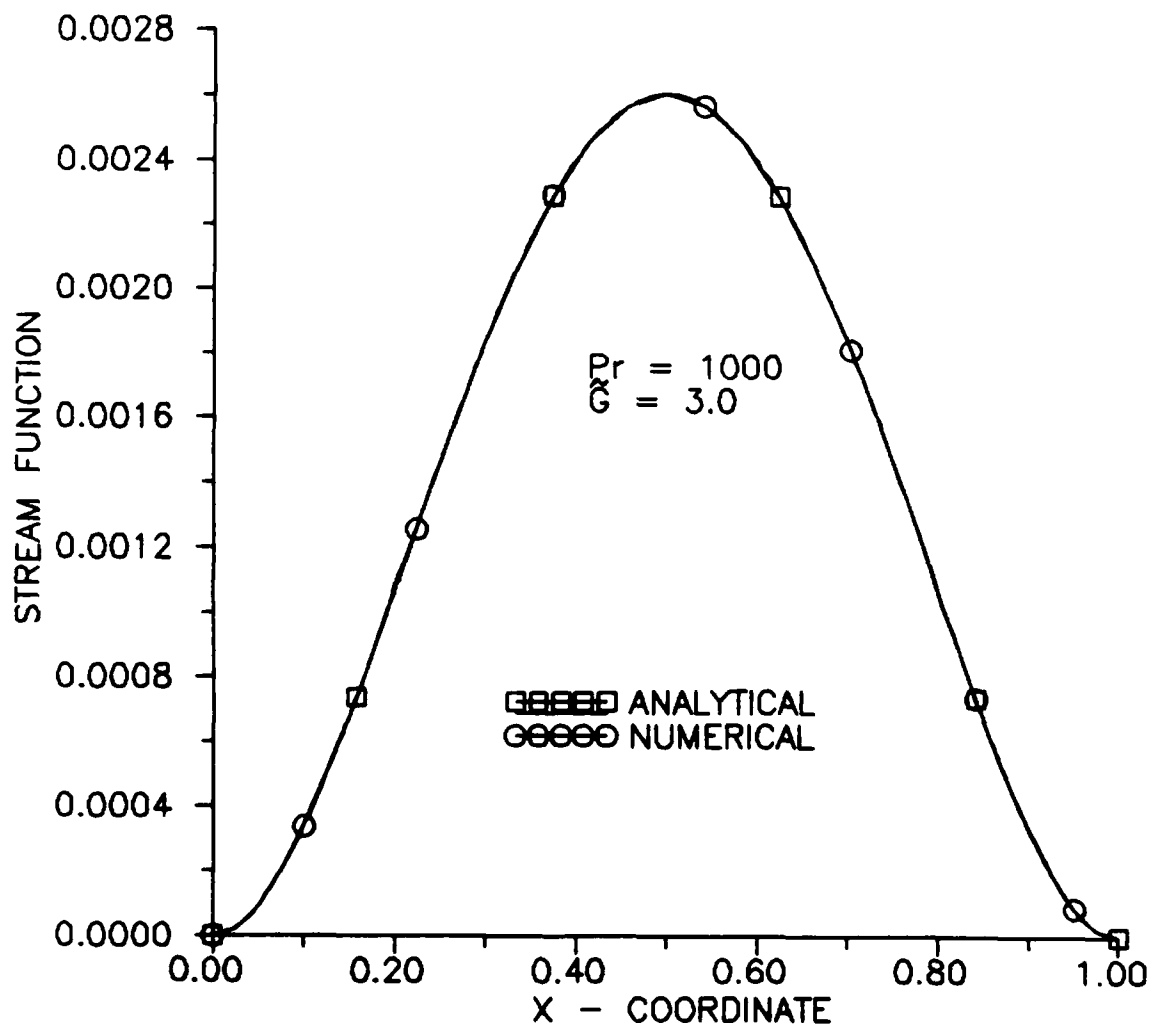


Figure 30. Stream function variation at the horizontal centerline.

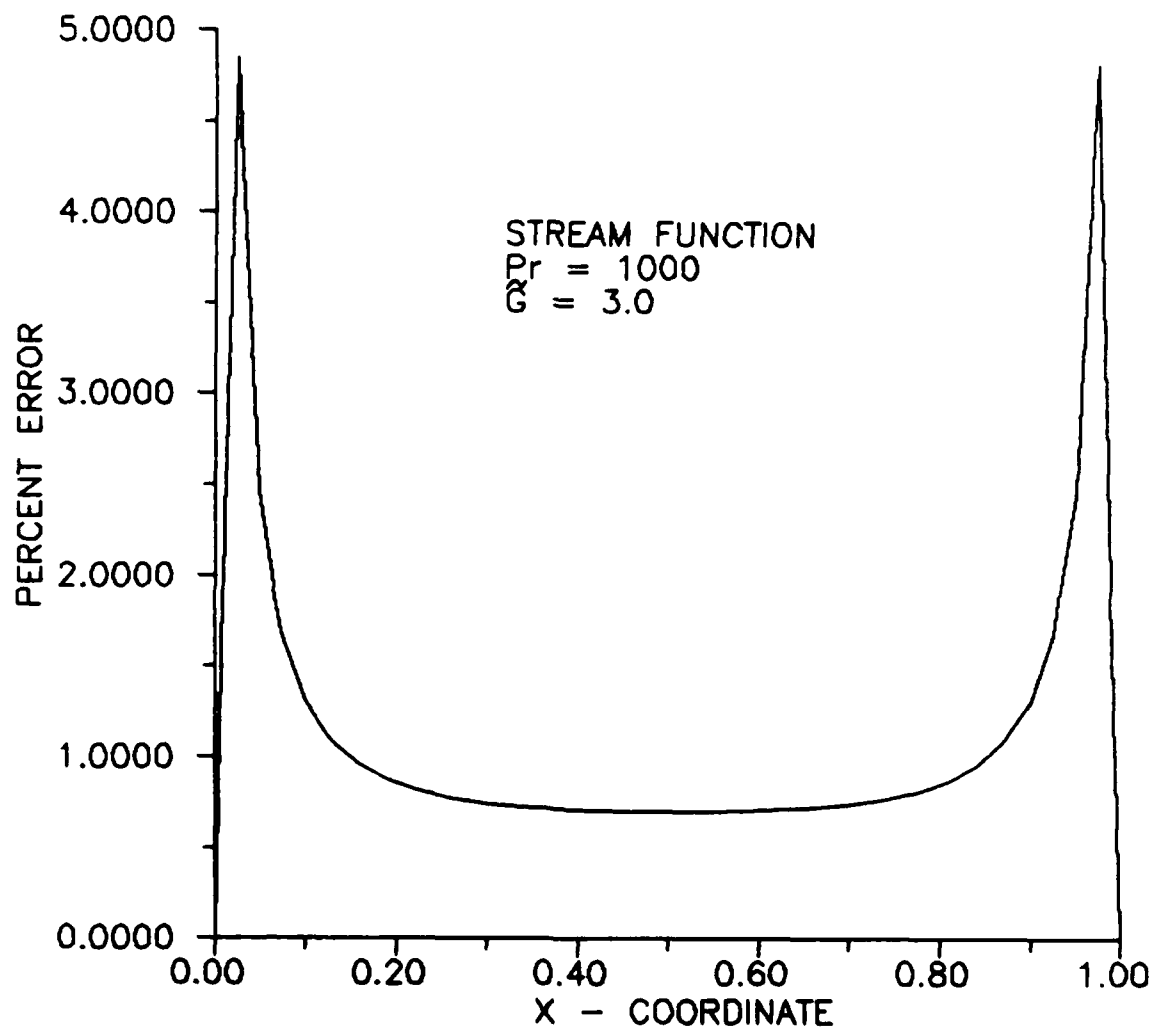


Figure 31. Stream function relative error



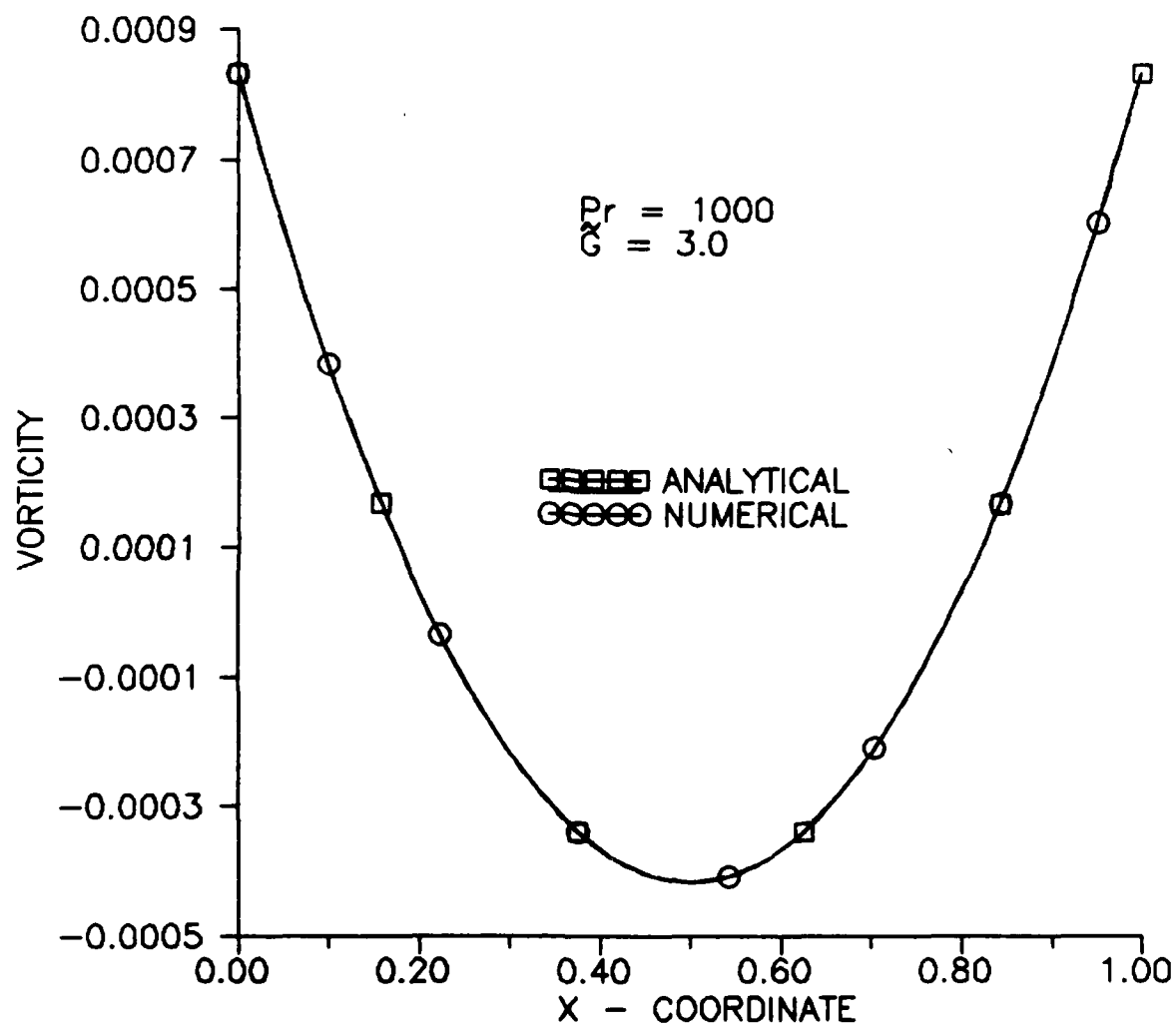


Figure 32. Vorticity variation at the horizontal centerline.

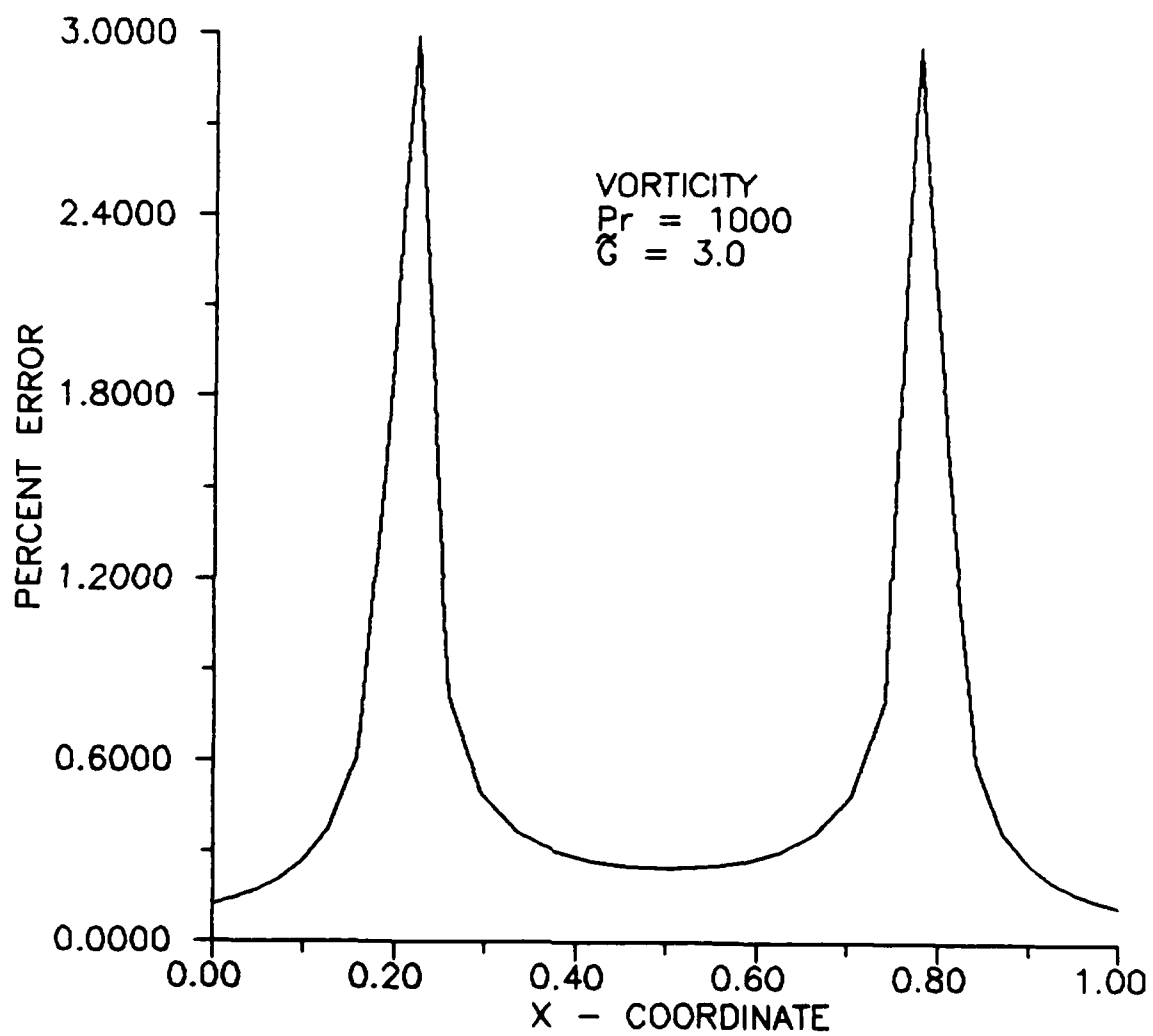


Figure 33. Vorticity relative error.

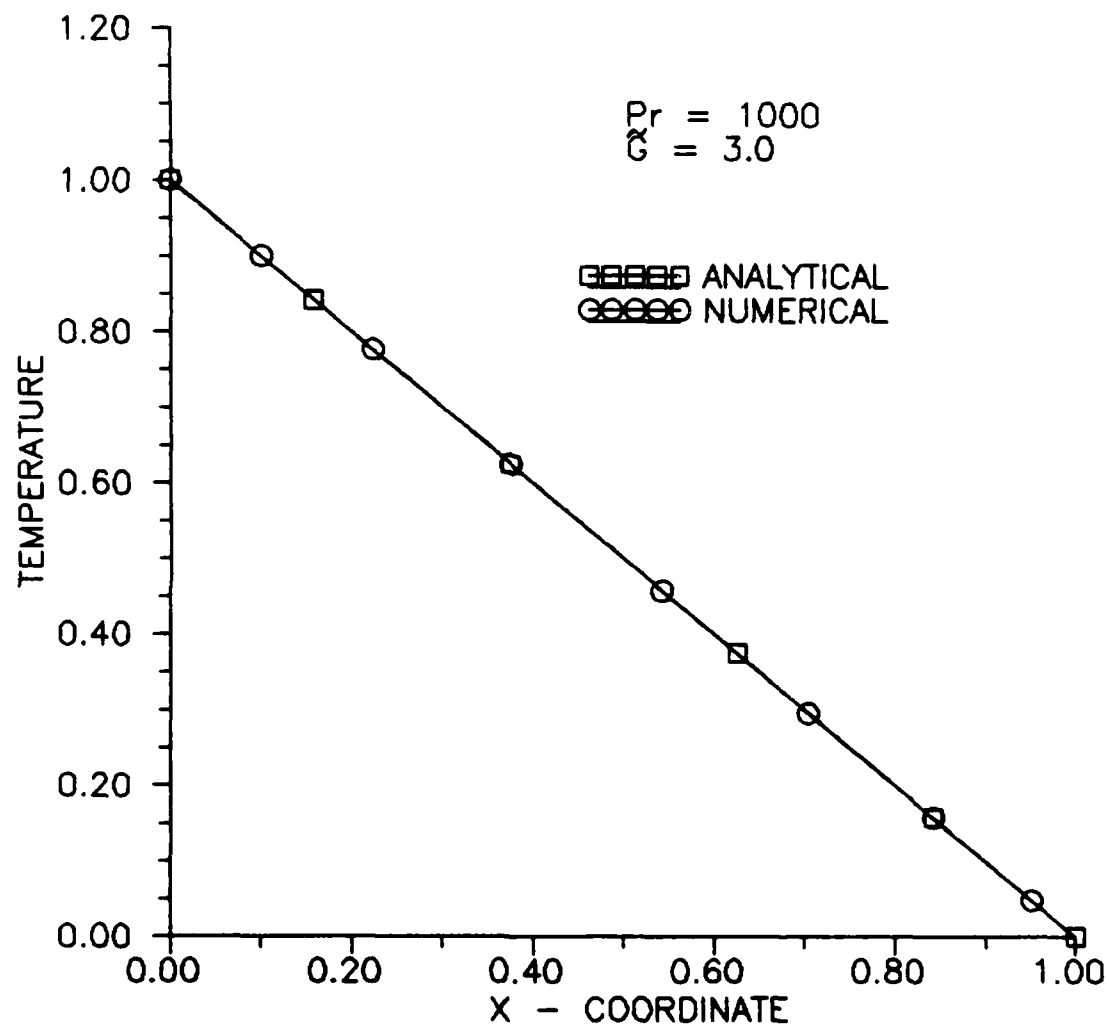


Figure 34. Temperature variation at the horizontal centerline.

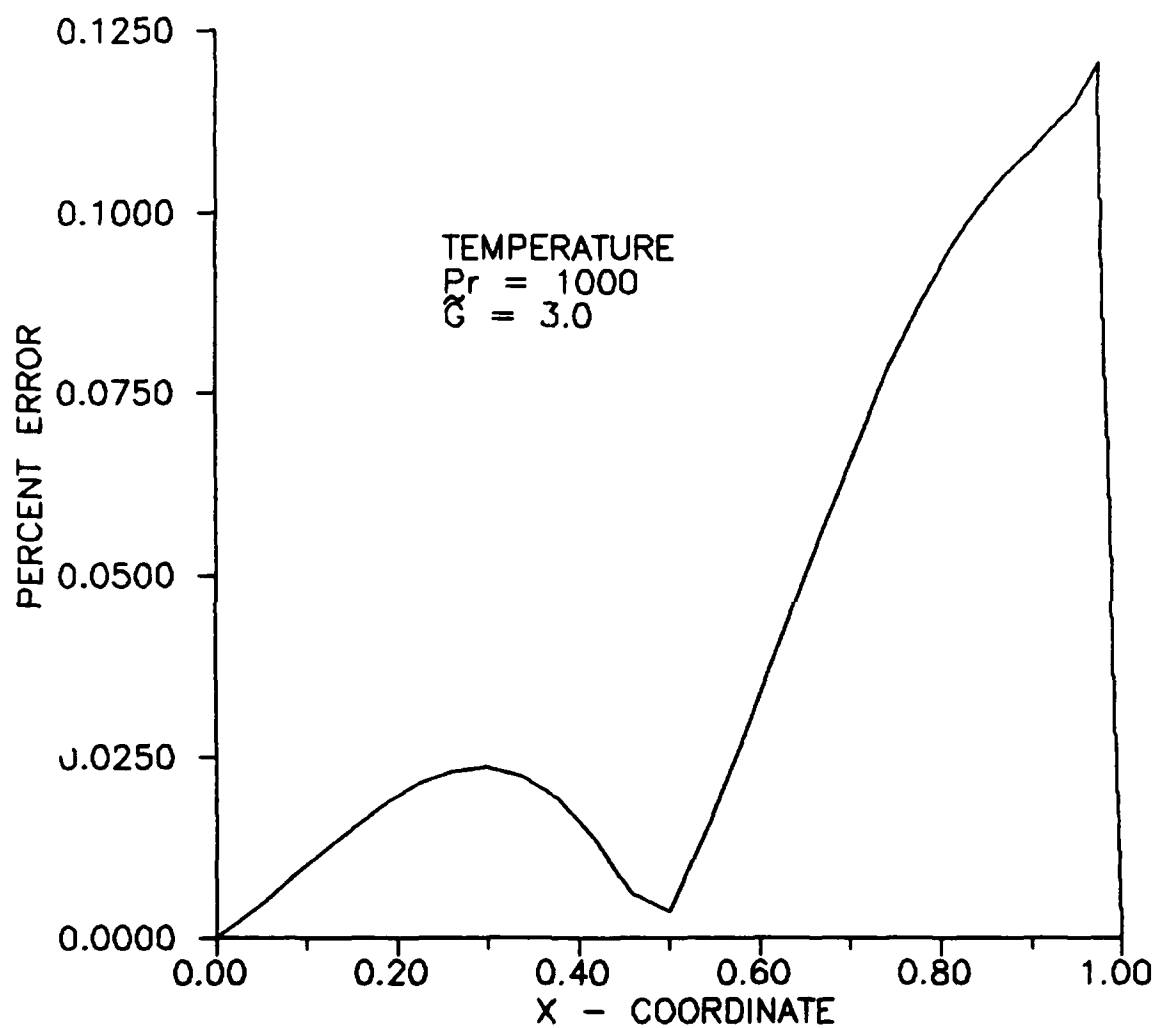


Figure 35. Temperature relative error.

## VI. Conclusions and Recommendations

### Conclusions.

In the course of this study, it was found that there are two distinct classes of fluid behavior. Fluids with low Prandtl numbers displayed patterns of cell formation, vorticity, and temperature profiles similar to each other, but different from those with high Prandtl numbers. Below  $Pr = 0.1$ , thermal diffusion dominates and the instabilities are hydrodynamic in nature. Above  $Pr = 10.0$ , momentum diffusion dominates and the instabilities become thermal in nature.

The 2-D boundary-layer form of the Navier-Stokes equations were able to capture all of the important physics of multicellular flow in the vertical slot for low Prandtl numbers and Prandtl number of order one. Excellent qualitative agreement with results obtained by other researchers, using different methods, was achieved with this approach. Cells formed, gained in strength, and distributed themselves throughout the vertical slot, in a like manner.

For very low Prandtl numbers ( $\sim 0.02$  and lower), convective cells formed near the horizontal boundaries first, and gained in strength as  $\hat{G}$  ( or  $\tilde{G}$ , as the case may be ) increased. The weakest cells formed in the center of the slot.

The opposite was true for air (  $Pr = 0.71$  ). For air, the cells formed in the central region first, and were strongest there, while weaker cells formed near the horizontal walls.

For low Prandtl numbers, vorticity was found to have a tendency to concentrate in nodal regions along the left and right vertical boundaries. Within the slot, the distribution of vorticity seemed to be influenced by the number of convective cells that formed and their location. The direction of vorticity changed from counter-clockwise at the left and right vertical walls, to clockwise in the center of the slot.

Temperature profiles obtained for air (  $Pr \sim 0.7$  ) and mercury (  $Pr \sim 0.02$  ) with the boundary-layer approach also showed similar trends and behavior to that obtained by others. Distinct, oscillatory isotherms were present in the multicellular regions.

In all cases, analytical results were in excellent agreement with the numerical results obtained for steady-state conditions.

High Prandtl number fluids behaved in a different manner. The boundary-layer approach was not able to completely duplicate the results obtained by other researchers. This is most likely because the streamwise viscous terms, neglected under the assumptions employed in the boundary-layer technique, have a

more pronounced effect on cell formation and distribution for high Prandtl numbers as opposed to the low Prandtl number cases. None-the-less, the boundary-layer approach was able to capture single and multiple convective cell formation as well as certain other physical properties of the flow. Most notable among these is the way in which vorticity and temperature develop within the slot.

For high Prandtl number fluids (  $Pr \sim 1000$  ), vorticity no longer concentrated in nodal regions; but was fairly uniform along the vertical boundaries, which is most likely a ramification of large momentum diffusivities. In addition, the vorticity contours appeared to be antisymmetrically distributed within the slot and no longer influenced by the number of cells that formed or their location.

Temperature profiles were highly oscillatory in nature, even before multiple cells formed. This suggests that the instability is thermal in nature. When multiple cells did form, the temperature profiles showed slight inversions present in the center of the cells. This is in agreement with that observed by other researchers. However, the inversions obtained by the boundary-layer method were not as pronounced.

Overall, the boundary-layer approach works quite well for fluids whose Prandtl number is of order one and lower in a

narrow vertical slot. It does have difficulty modeling convective cell formation at high Prandtl numbers; however, the approach captures some of the important physical properties. Although quantitative experimental comparisons are lacking in this study, comparisons with analytical results, as well as the numerical results of other researchers, lends validity to this method.

#### Recommendations.

Additional analytical and numerical research is recommended with the high Prandtl number fluids. The boundary-layer program can be modified to include the streamwise viscous terms neglected in this study. Incorporating these terms would also change the boundary conditions along the horizontal walls. The results obtained should be in better agreement with those obtained in previous numerical studies. By doing this, one can demonstrate the importance of retaining the streamwise viscous terms for large Prandtl number fluids. In addition, studies could be done with other boundary conditions such as conducting horizontal walls or horizontal walls with constant heat flux.

Due to insufficient time, the  $Pr \rightarrow \infty$  case was not investigated. This study could be done also. The analytical and numerical expressions for the limiting case of  $Pr \rightarrow \infty$  are included in Chapters III and IV.



Another interesting study would be to analyze the parallel, vertical ( or horizontal ) flat plate problem using the boundary-layer assumptions employed in this study.

The entropy distribution within the vertical slot could also be determined and plotted. This could be accomplished for the entire range of Prandtl numbers (  $0 \leq Pr \leq \infty$  ) and would help shed more light on the multicellular phenomenon.

And finally, a numerical study of the vertical slot with discrete heat sources at the left wall could be performed. As mentioned in the literature search ( Chapter I ), experimental data exists which can be compared to.

Appendix A

**Supplementary Analytical Results**

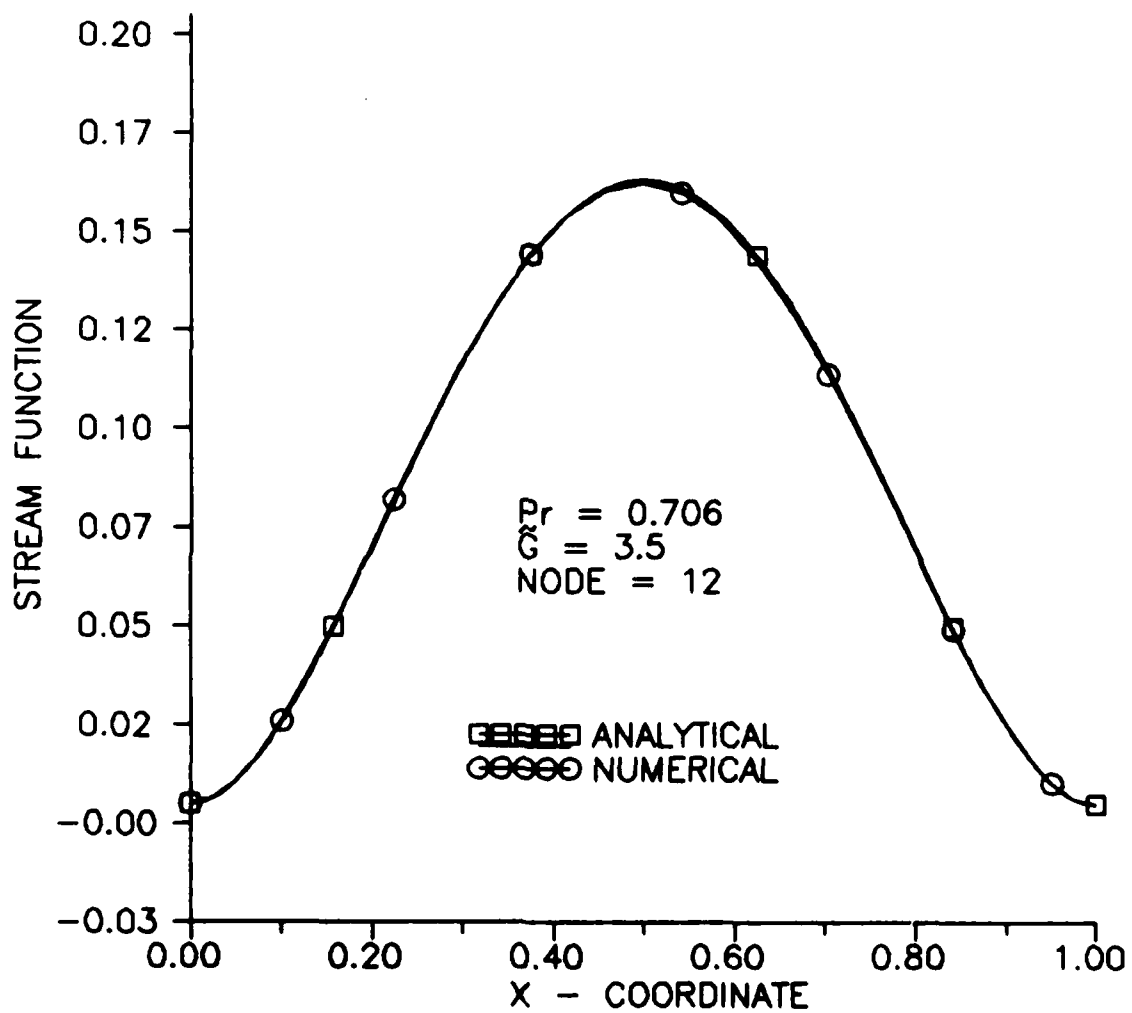


Figure 36. Stream function variation at node 12.

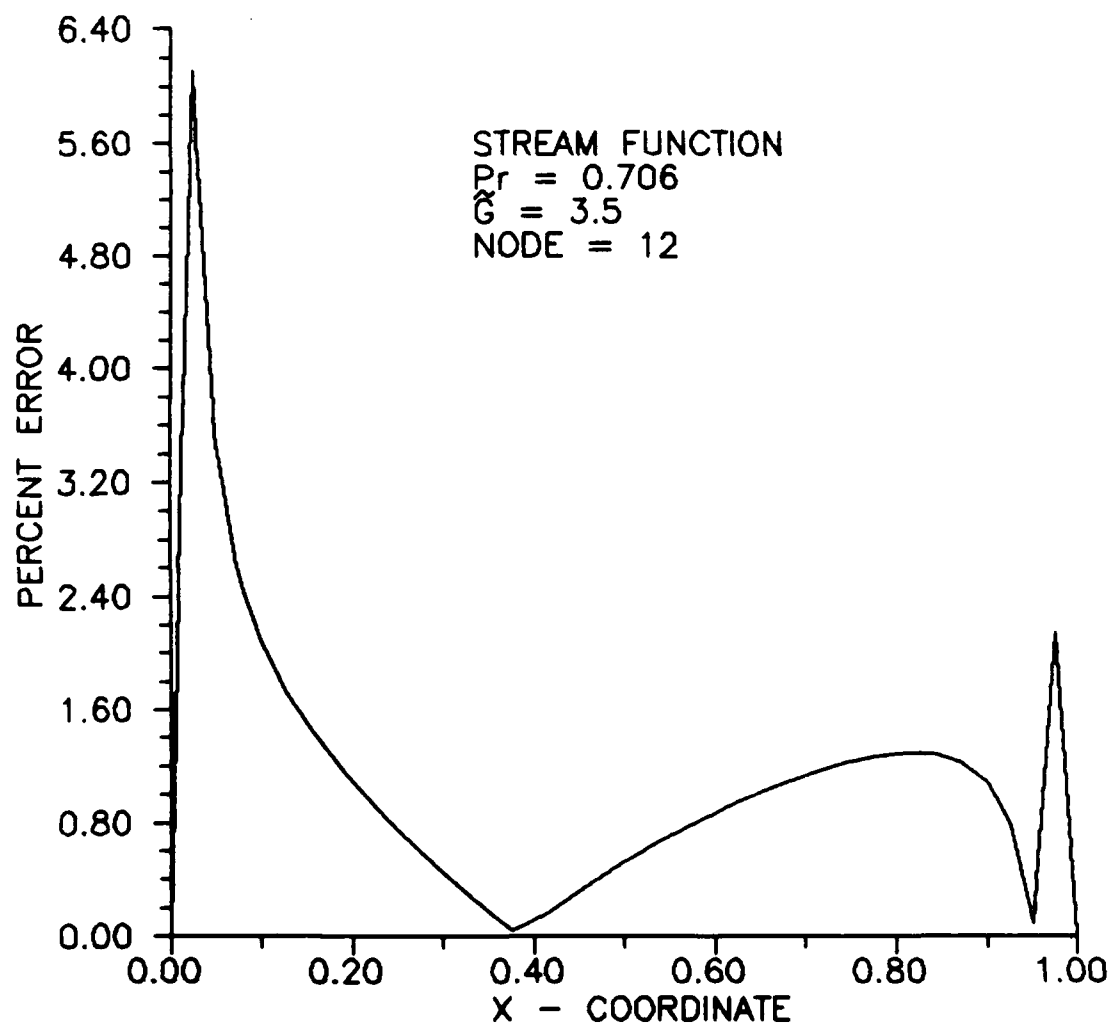


Figure 37. Stream function relative error.

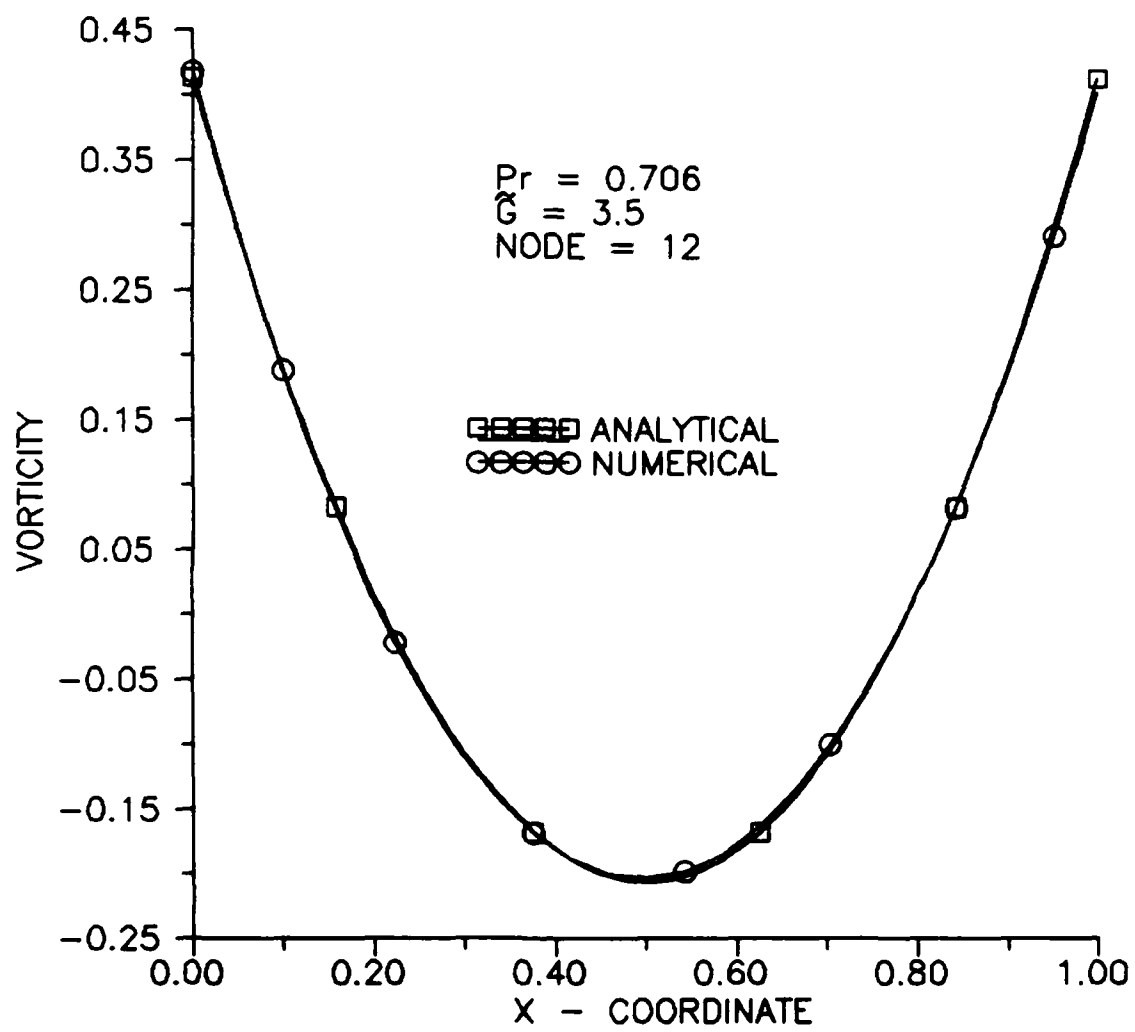


Figure 38. Vorticity variation at node 12.

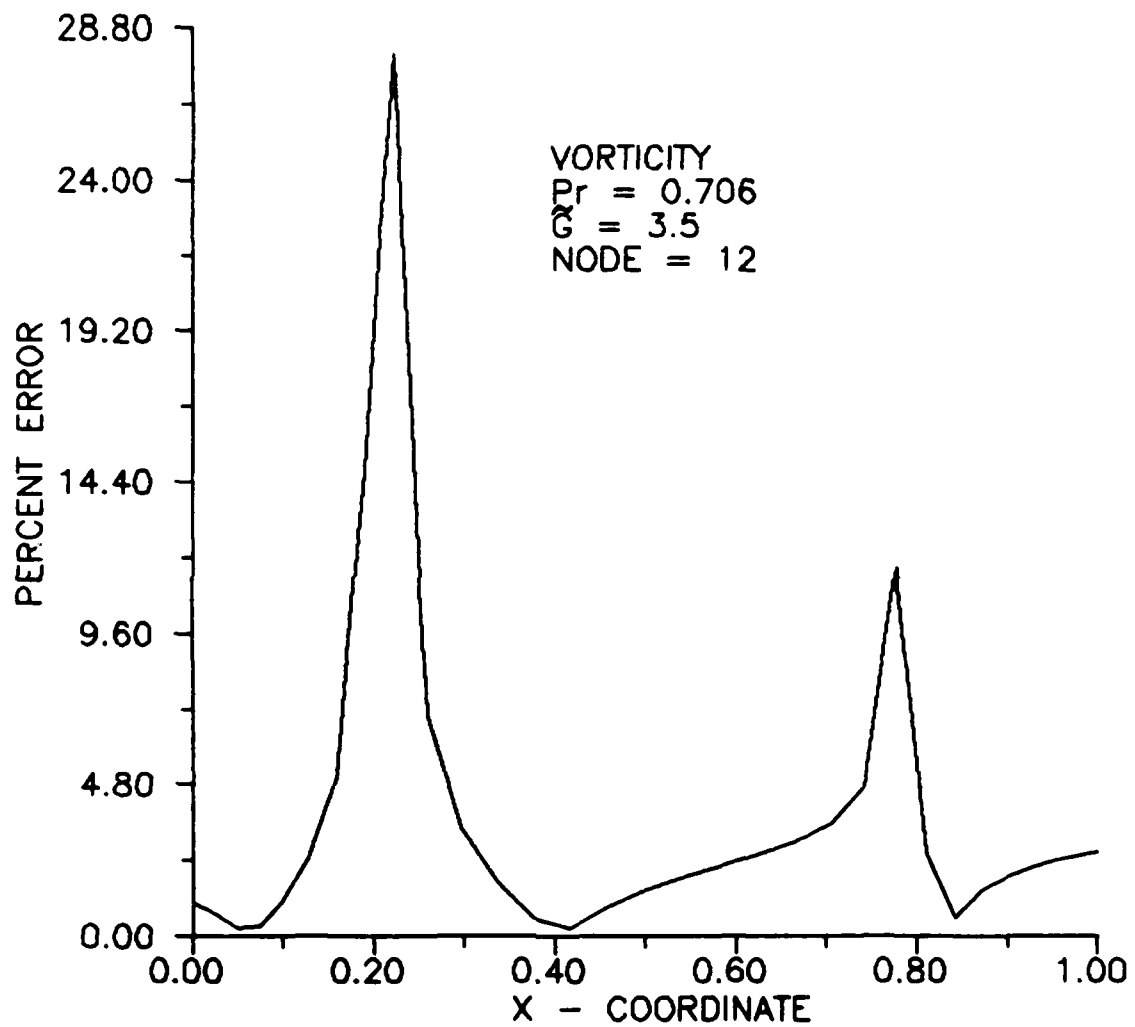


Figure 39. Vorticity relative error.

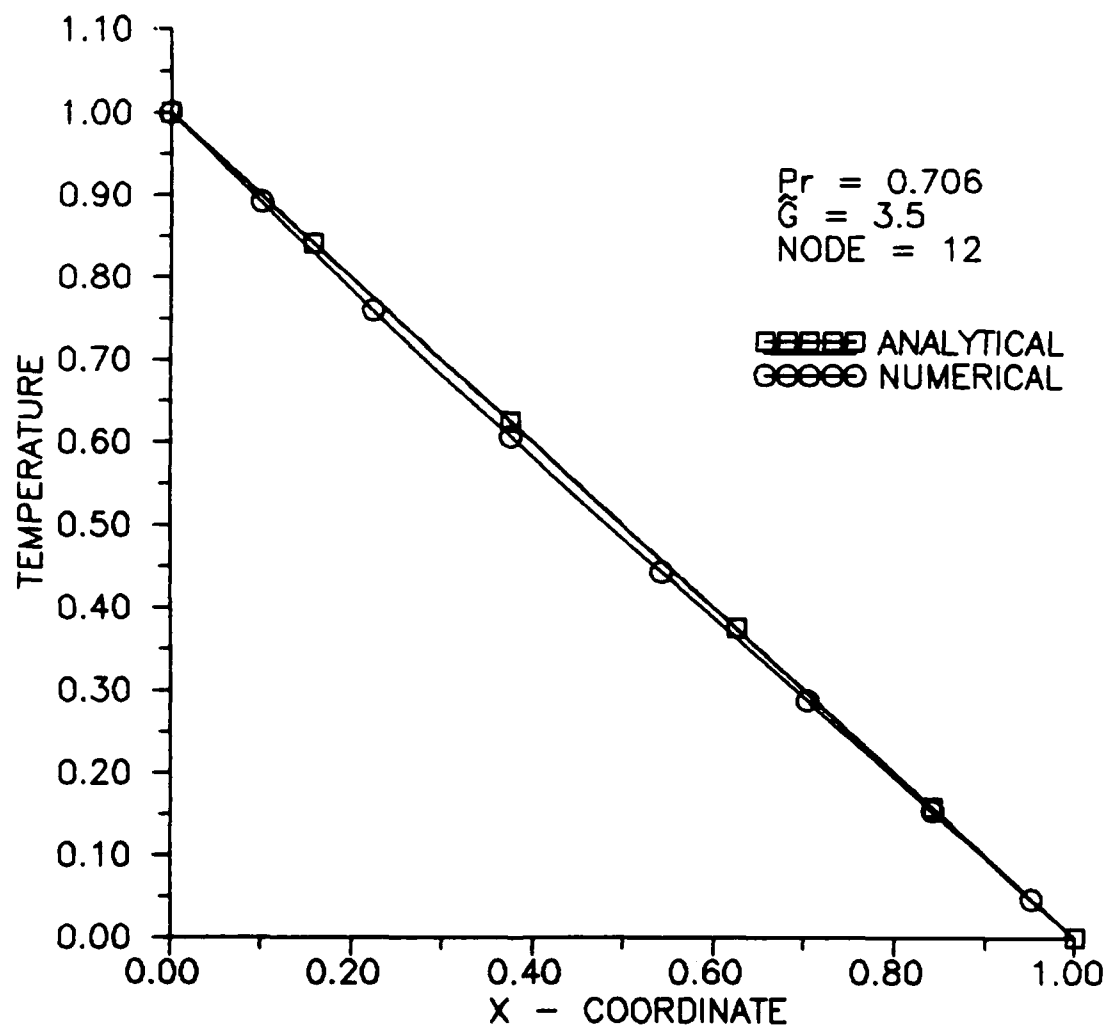


Figure 40. Temperature variation at node 12.

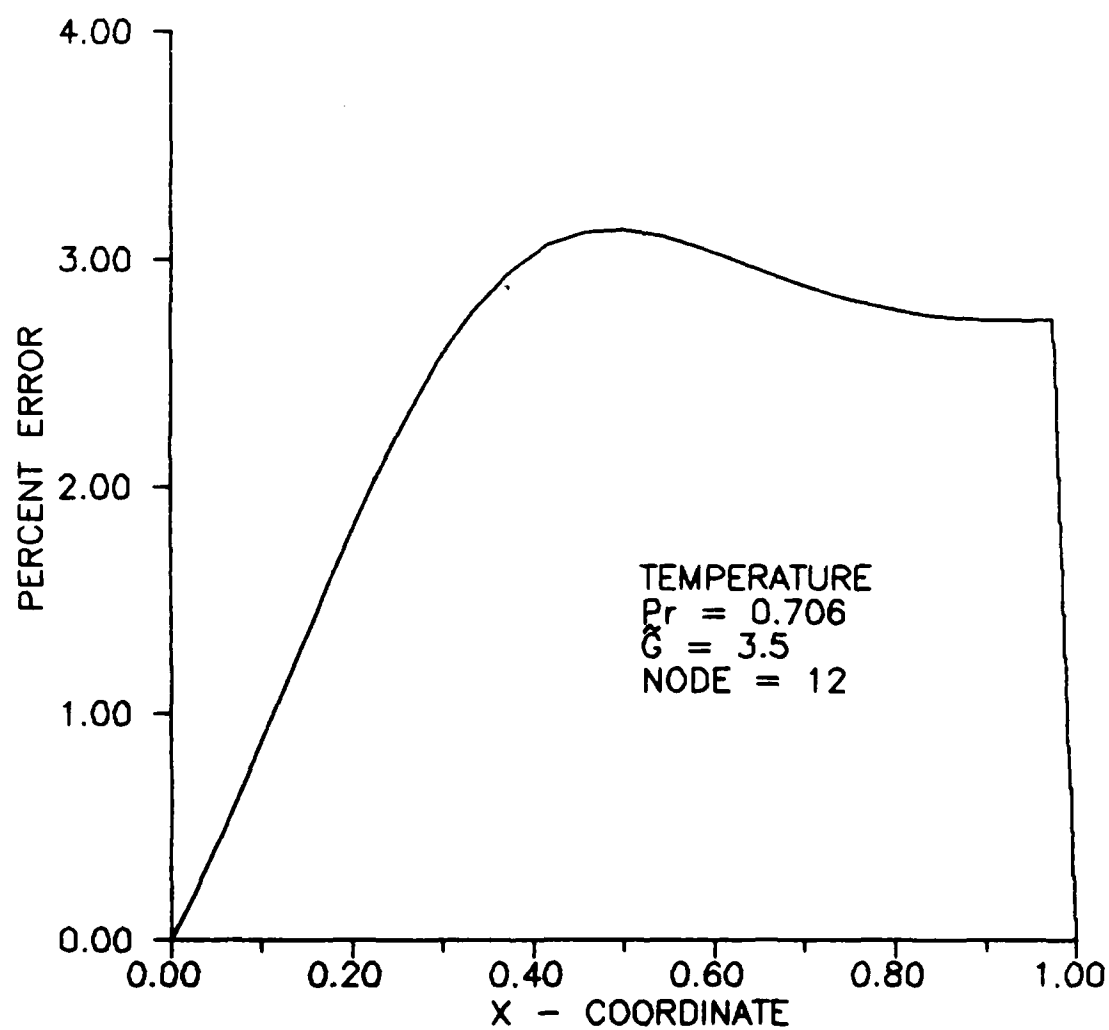


Figure 41. Temperature relative error.



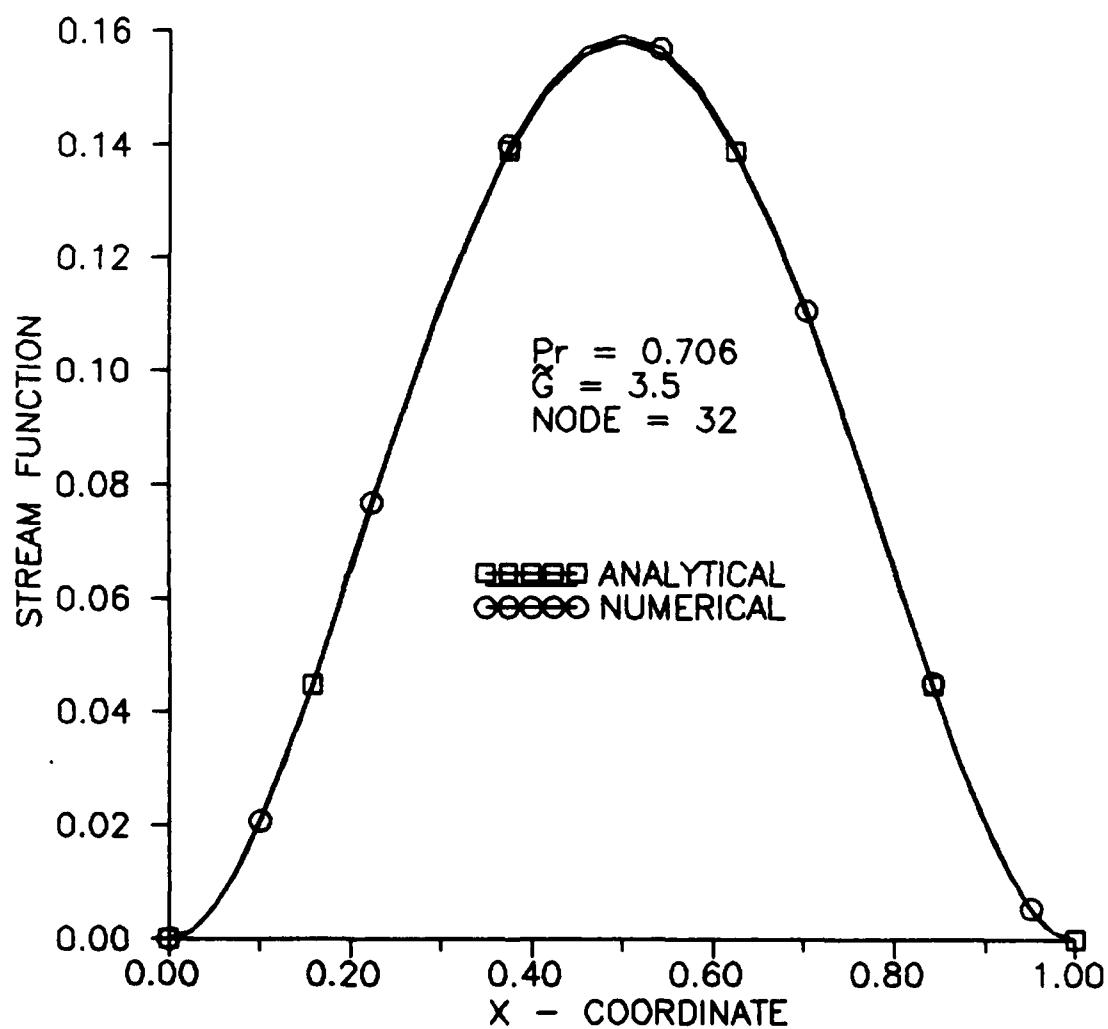


Figure 42. Stream function variation at node 32.

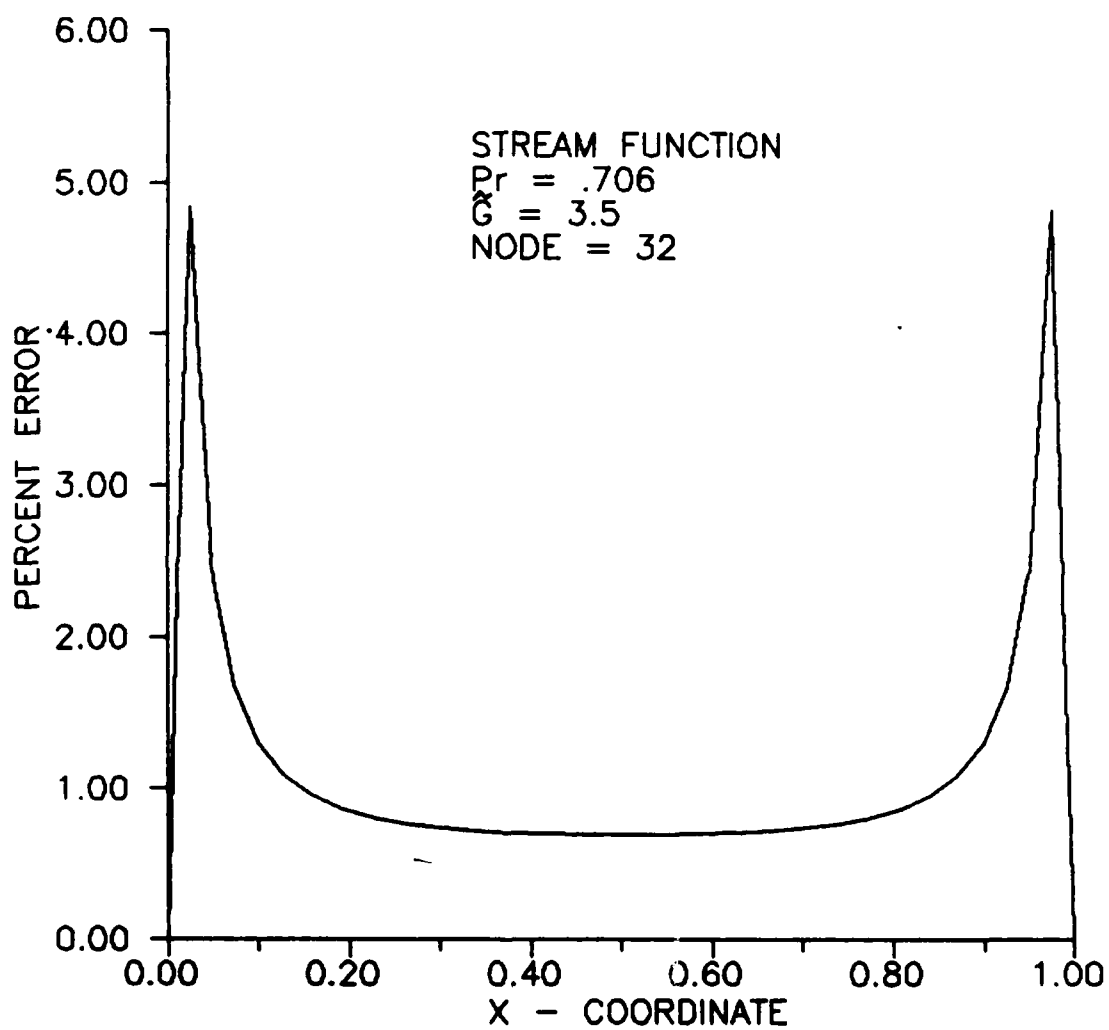


Figure 43. Stream function relative error

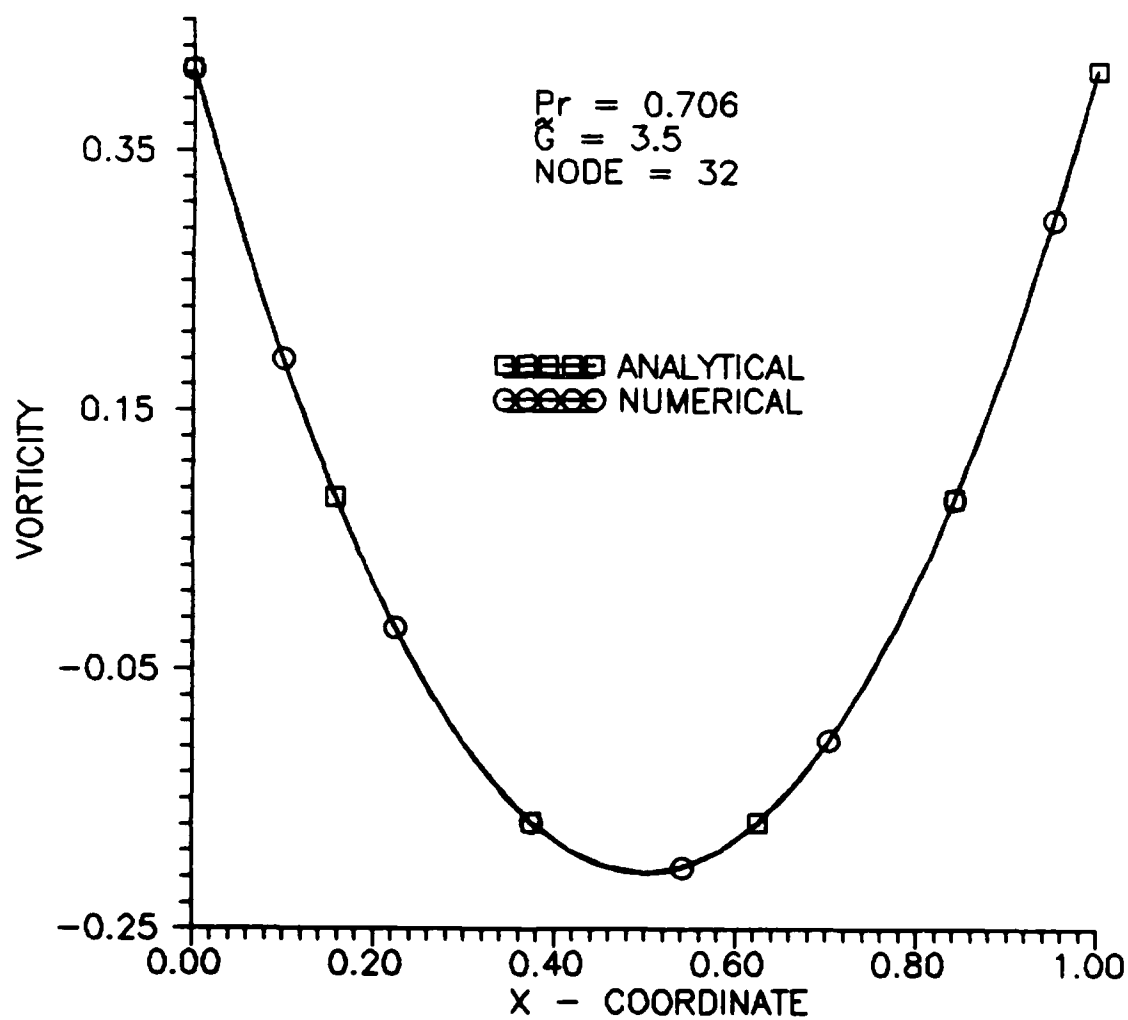


Figure 44. Vorticity variation at node 32.

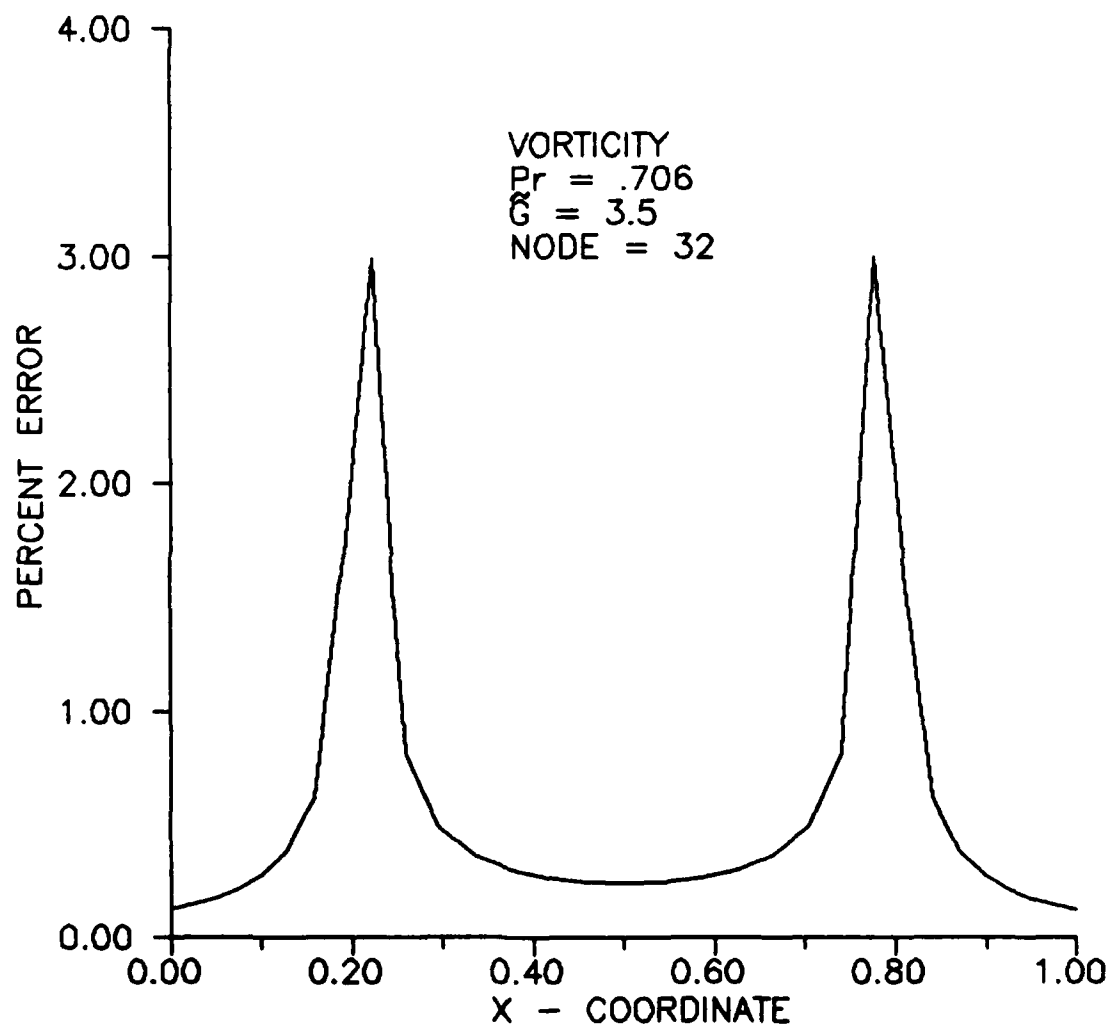


Figure 45. Vorticity relative error.

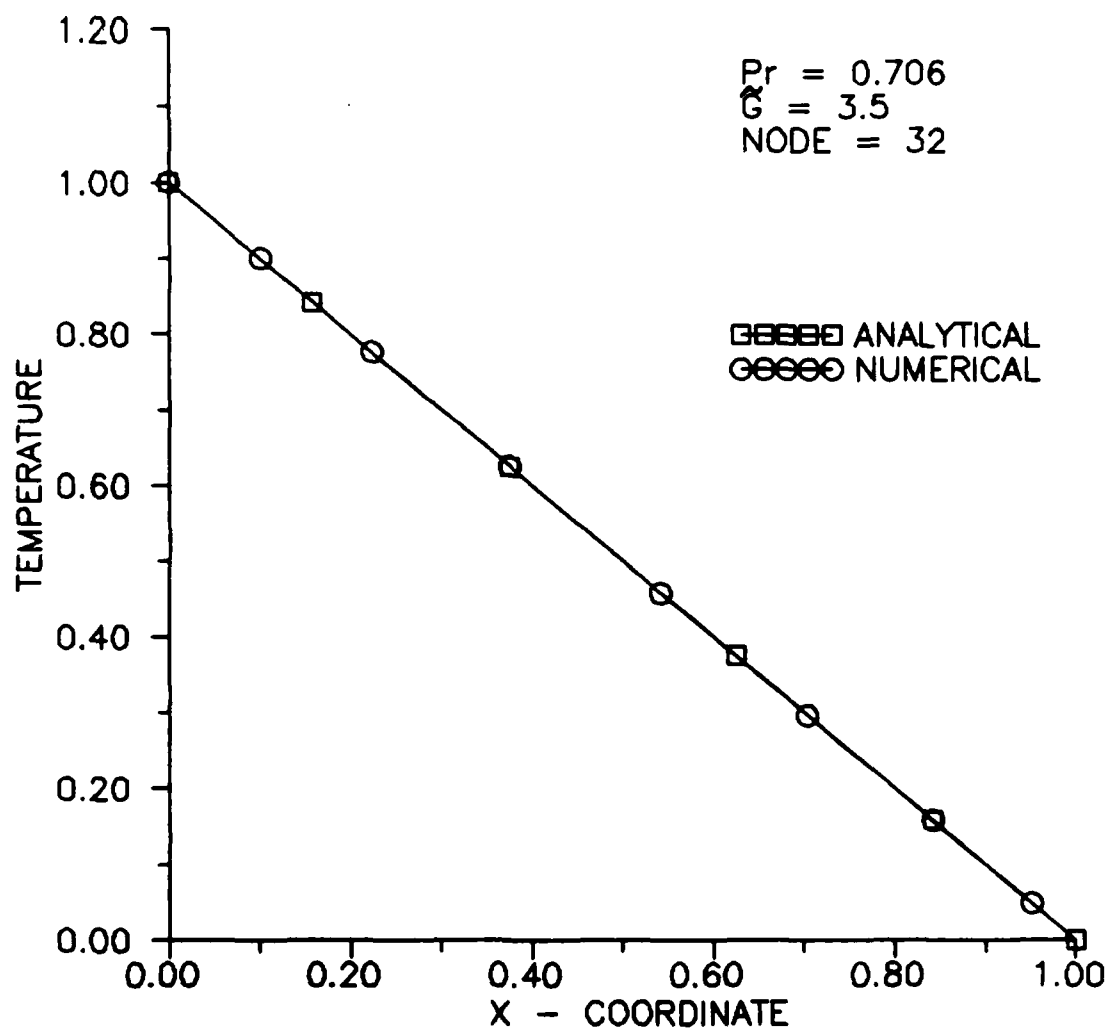


Figure 46. Temperature variation at node 32.

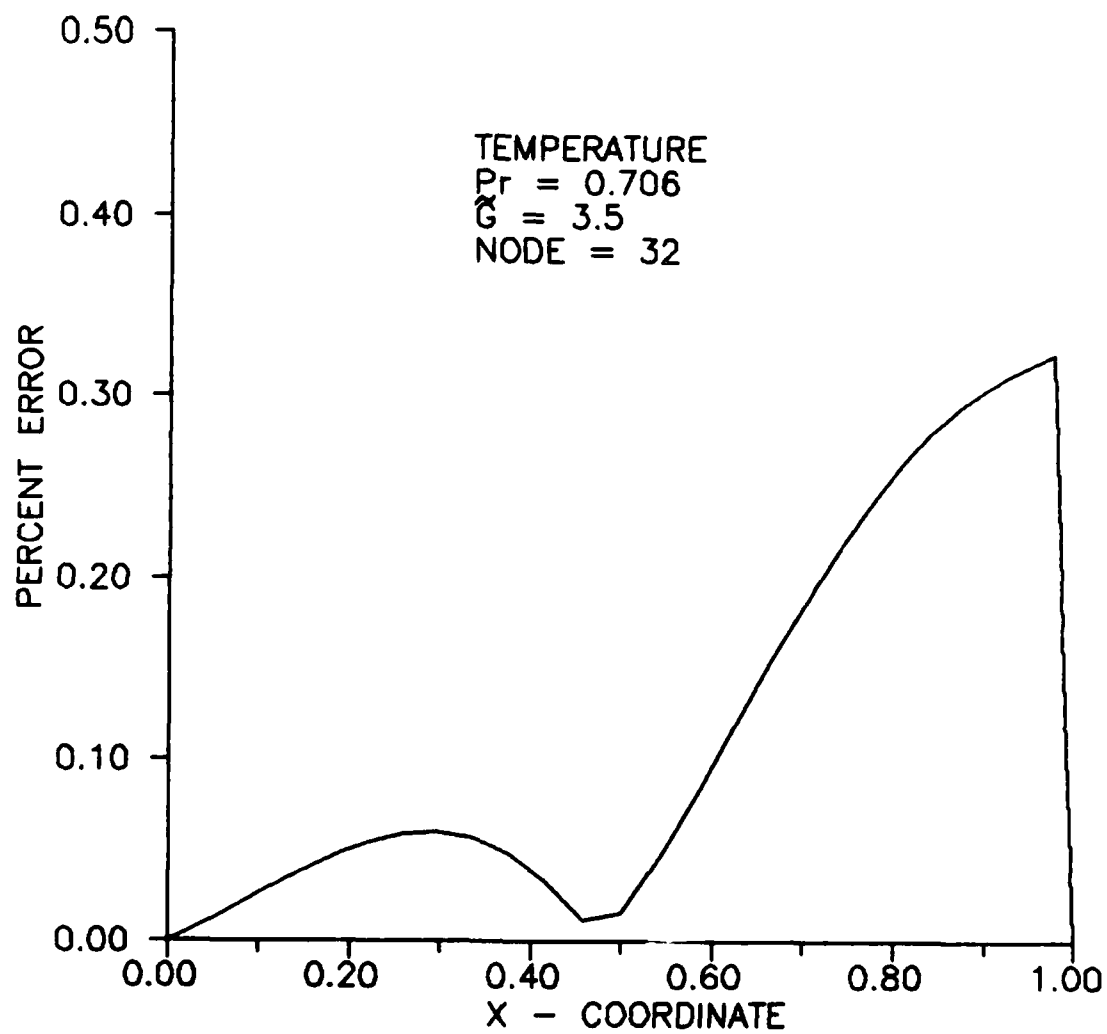


Figure 47. Temperature relative error.

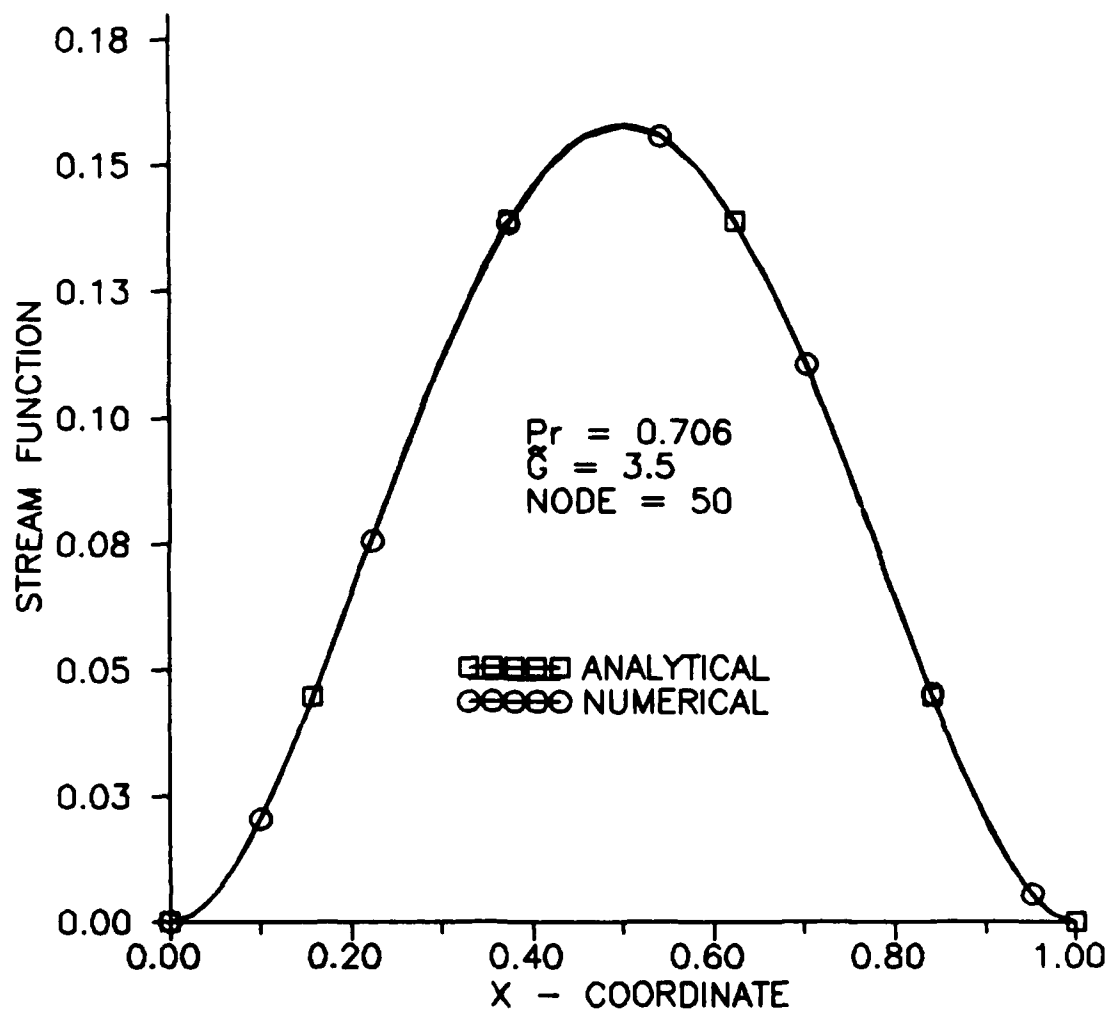


Figure 48. Stream function variation at node 50.

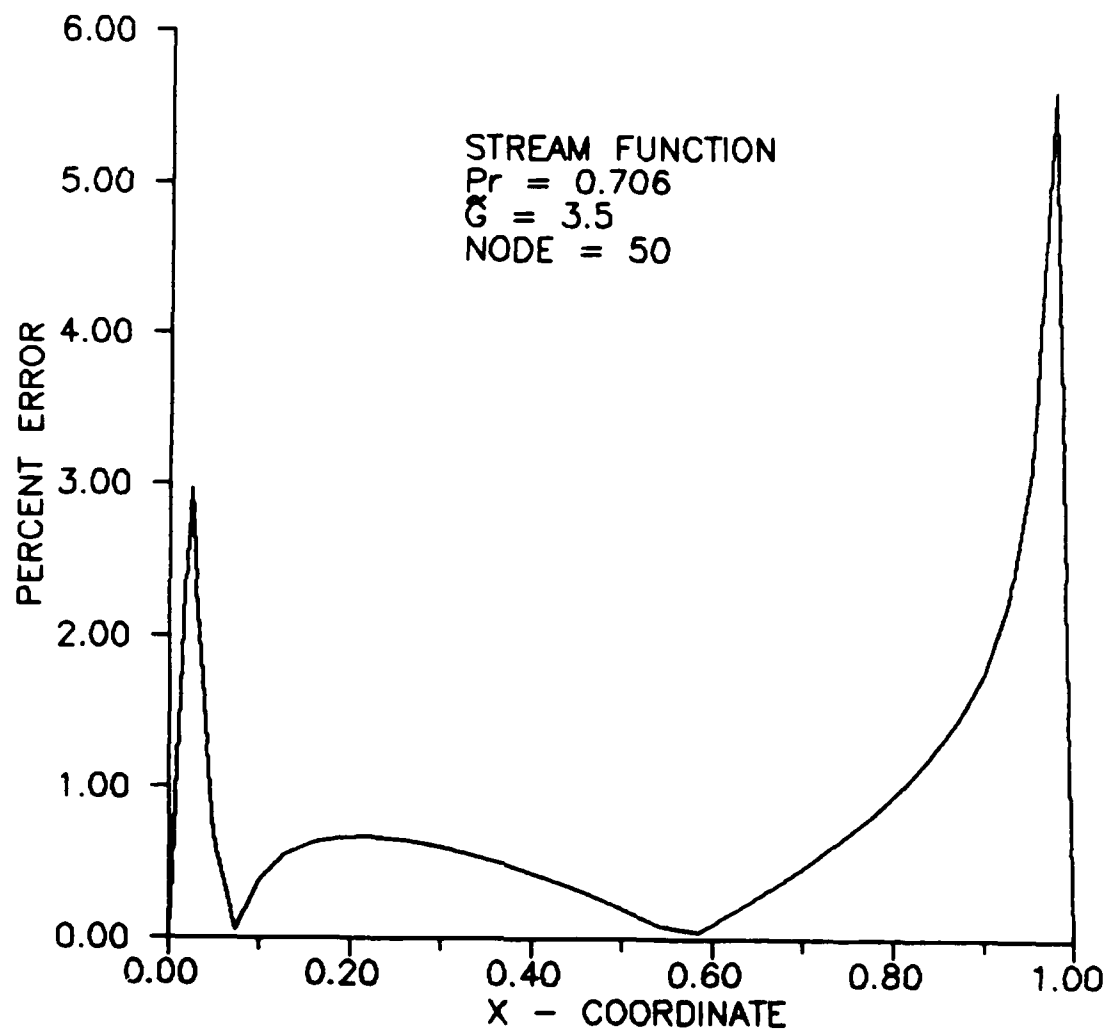


Figure 49. Stream function relative error.



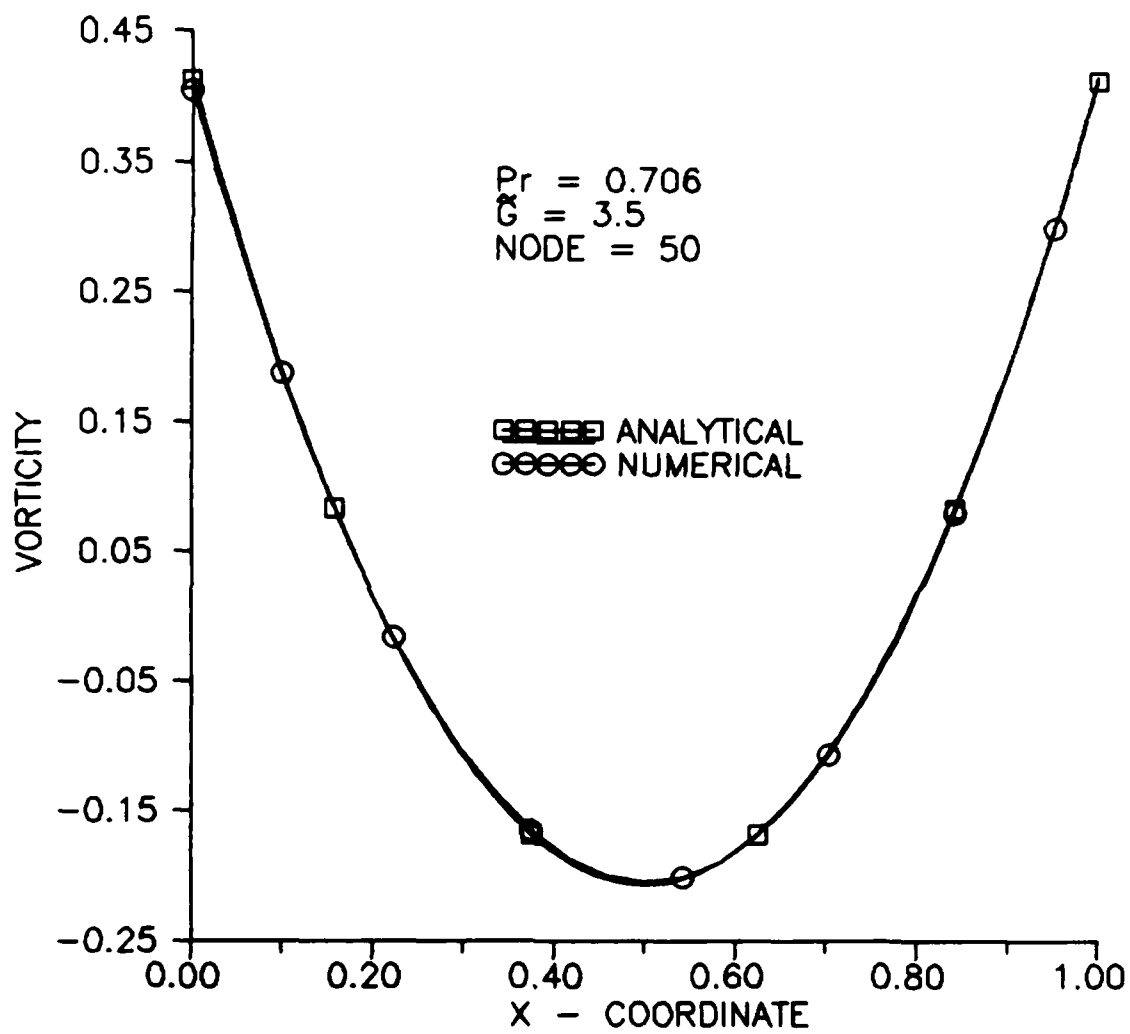


Figure 50. Vorticity variation at node 50.

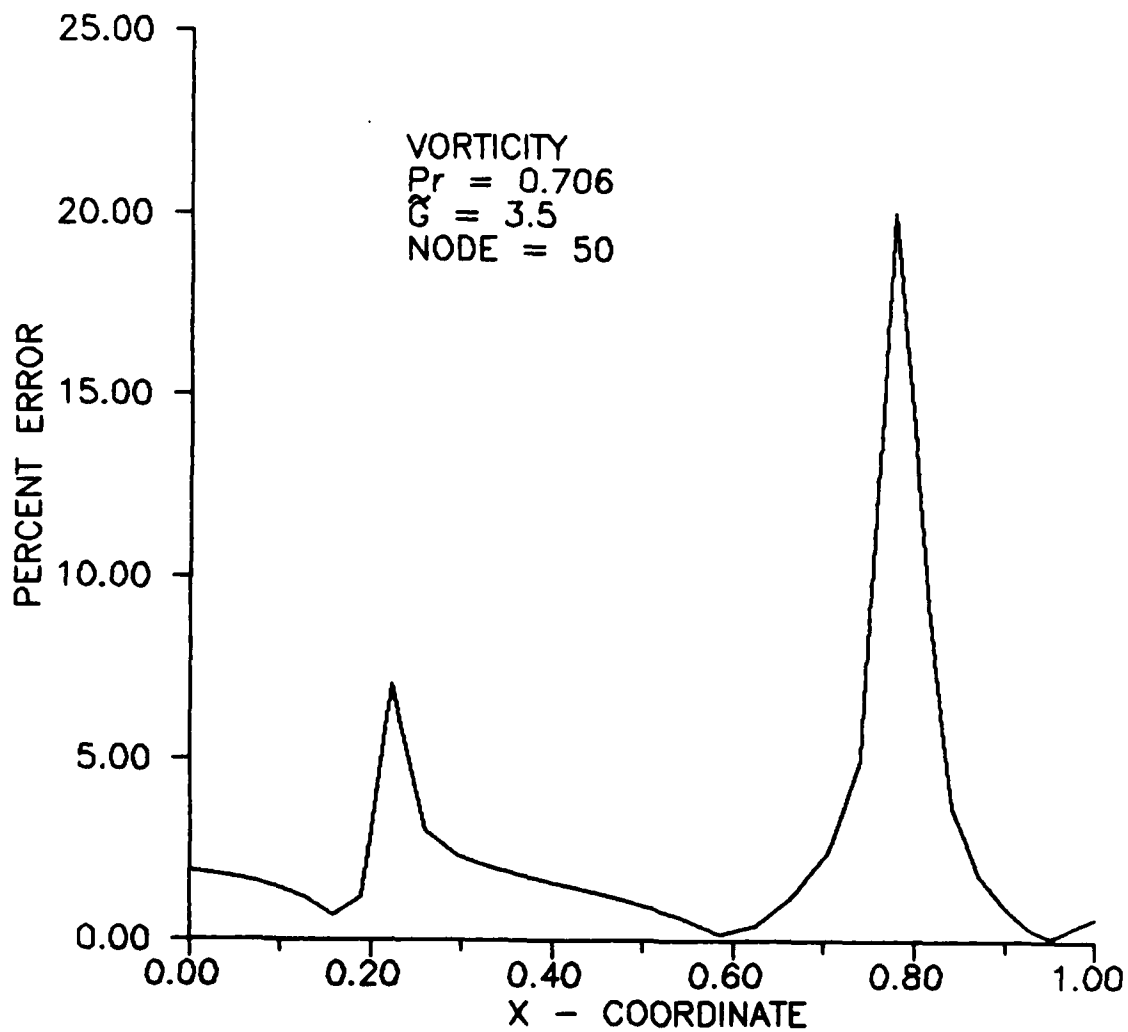


Figure 51. Vorticity relative error.

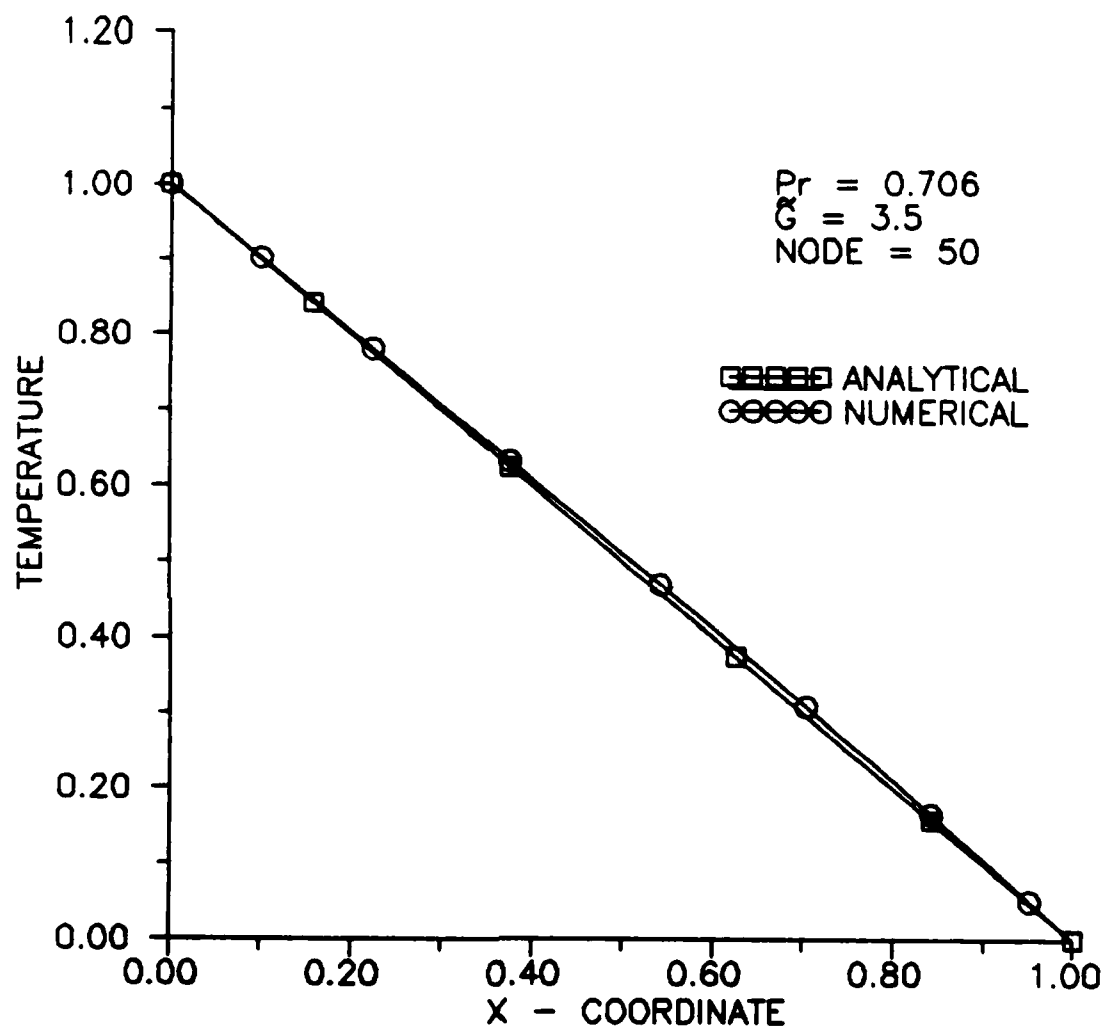


Figure 52. Temperature variation at node 50.

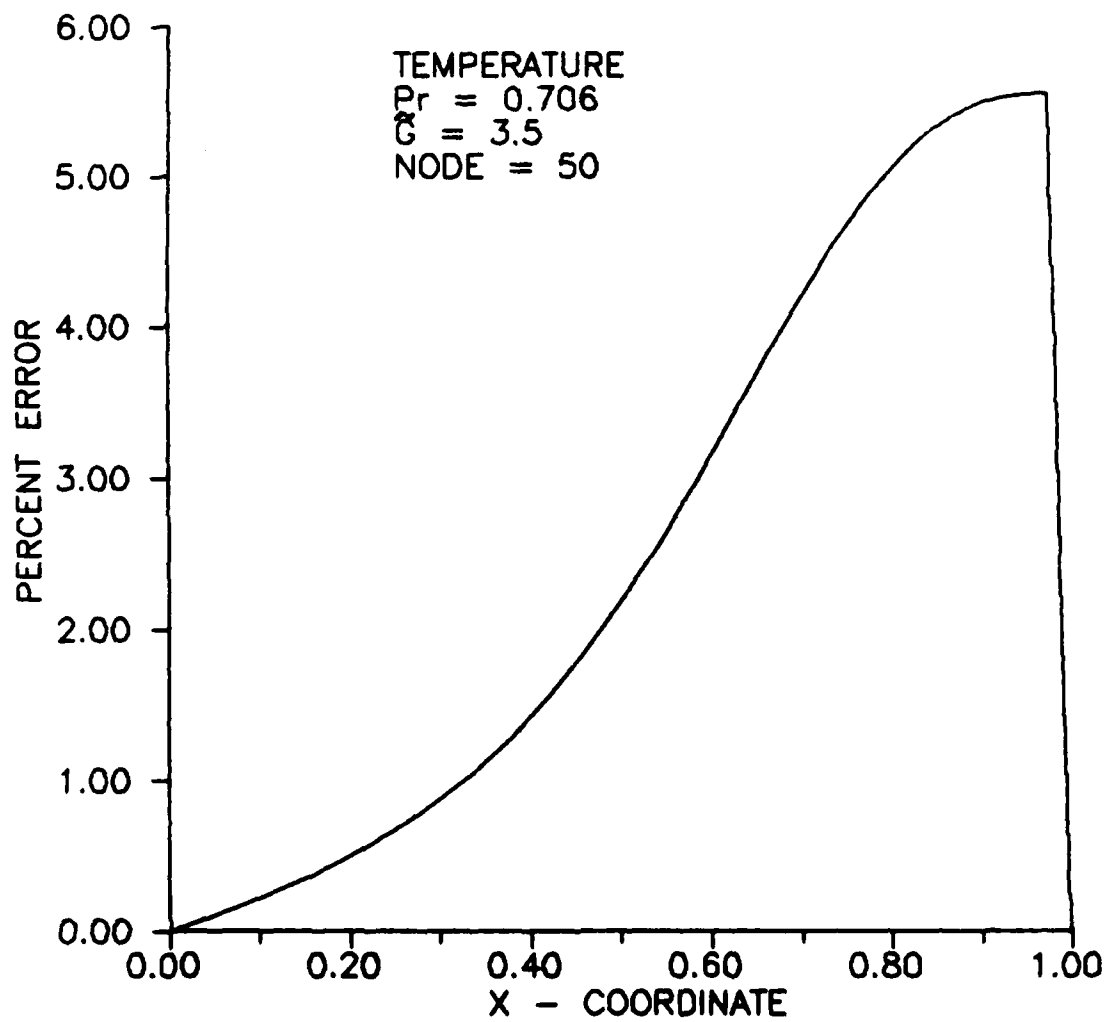


Figure 53. Temperature relative error.

### Bibliography

1. Arpaci, V. S. and P. S. Larsen. "Convection Heat Transfer," Prentice-Hall, Inc., Englewood Cliffs, New Jersey.
2. Bennett, D. L. "Variable Wall Temperature Effects on Multicellular Natural Convection in a Horizontal Annulus," Air Force Institute of Technology, AFIT/GAE/AA/88D-01 ( 1988 )
3. Chait, A. and Seppo A. Korpela. "The secondary Flow and Its Stability for Natural Convection in a Tall Vertical Enclosure," Journal of Fluid Mechanics, 200: 189-216 ( 1989 ).
4. De Vahl Davis, G. and G. D. Mallinson. "A Note on Natural Convection in a Vertical Slot," Journal of Fluid Mechanics, 72: 87 - 93 ( 1975 ).
5. Elder, J. W. "Laminar Free Convection in a Vertical Slot," Journal of Fluid Mechanics, 23: 77-98 ( 1965 ).
6. Elder, J. W. "Numerical Experiments With Free Convection in a Vertical Slot," Journal of Fluid Mechanics, 24: 823-843 ( 1966 ).
7. Fant, D. B. "Unsteady Multicellular Natural Convection in a Narrow Horizontal Cylindrical Annulus," First National Fluid Dynamics Congress, Cincinnati: American Institute of Aeronautics and Astronautics, Ohio, July 25-28, 1988.
8. Keyhani, M., V. Prasad, and R. Cox. "An Experimental Study of Natural Convection in a Vertical Cavity With Discrete Heat Sources," Transactions of the ASME, 110: 616-624 ( 1988 ).
9. Korpela, S. A., D. Gözüüm and C. B. Baxi. "On the Stability of the Conduction Regime of Natural Convection in a Vertical Slot," International Journal of Heat and Mass Transfer, 16: 1683-1690 ( 1973 ).
10. Korpela, S. A. "A Study on the Effect of Prandtl Number on the Stability of the Conduction Regime of Natural Convection in an Inclined Slot," International Journal of Heat and Mass Transfer, 17: 215-222 ( 1974 ).
11. Korpela, S. A. and Yee Lee. "Multicellular Natural Convection in a Vertical Slot," Journal of Fluid Mechanics, 126: 91-121 ( 1983 ).

12. Patton, R. L. "Incompressible Flow," Wiley & Sons, New Jersey

13. Pepper, D. W. and S. D. Harris. "Numerical Simulation of Natural Convection in Closed Containers by a Fully Implicit Method," ASME Journal of Fluids Engineering, 99: 649-656 ( 1977 )

14. Seki, N., S. Fukusako and H. Inaba. "Visual Observation of Natural Convective Flow in a Narrow Vertical Cavity," Journal of Fluid Mechanics, 84: 695-704 ( 1978 ).

Vita

Captain David C. Jarman [REDACTED]

~~He~~ He graduated from Weymouth High School in 1968 and earned an associate degree in aerospace engineering at Wentworth Institute of Technology, two years later. Upon graduation, he enlisted in the USAF. As an enlisted man, Capt. Jarman served as a scientific measurements technician and was responsible for monitoring nuclear explosions under the provisions of the 1963 Underground Nuclear Test Ban Treaty. In 1981, he was selected for the Airman Education and Commissioning Program and sent to the University Of Florida where he received the degree of Bachelor of Science in Aerospace Engineering. Upon graduation, he was commissioned as an officer of the USAF through OTS. Capt Jarman was then assigned to Wright-Patterson AFB where he worked as chief ground test engineer on the Hypersonic Glide-Vehicle Program.

## REPORT DOCUMENTATION PAGE

Form Approved  
OMB No. 0704-0188

1. REPORT SECURITY CLASSIFICATION UNCLASSIFIED		1b. RESTRICTIVE MARKINGS N/A	
2a. SECURITY CLASSIFICATION AUTHORITY		3. DISTRIBUTION / AVAILABILITY OF REPORT Approved for public release; distribution unlimited	
2b. DECLASSIFICATION / DOWNGRADING SCHEDULE		5. MONITORING ORGANIZATION REPORT NUMBER(S)	
4. PERFORMING ORGANIZATION REPORT NUMBER(S) AFIT/GAE/ENY/89D-16		7a. NAME OF MONITORING ORGANIZATION	
6a. NAME OF PERFORMING ORGANIZATION School of Engineering	6b. OFFICE SYMBOL (if applicable) AFIT/ENY	7b. ADDRESS (City, State, and ZIP Code)	
6c. ADDRESS (City, State, and ZIP Code) Air Force Institute of Technology Wright-Patterson AFB, Ohio 45433-6583		9. PROCUREMENT INSTRUMENT IDENTIFICATION NUMBER	
8a. NAME OF FUNDING / SPONSORING ORGANIZATION	8b. OFFICE SYMBOL (if applicable)	10. SOURCE OF FUNDING NUMBERS	
8c. ADDRESS (City, State, and ZIP Code)		PROGRAM ELEMENT NO.	PROJECT NO.
		TASK NO.	WORK UNIT ACCESSION NO.
11. TITLE (Include Security Classification) MULTICELLULAR NATURAL CONVECTION IN A NARROW VERTICAL SLOT (UNCLASSIFIED)			
PERSONAL AUTHOR(S) Jarman, David C., Capt, USAF			
13a. TYPE OF REPORT MS Thesis	13b. TIME COVERED FROM _____ TO _____	14. DATE OF REPORT (Year, Month, Day) 1989 December	15. PAGE COUNT 150
16. SUPPLEMENTARY NOTATION			
17. COSATI CODES		18. SUBJECT TERMS (Continue on reverse if necessary and identify by block number)	
FIELD	GROUP	SUB-GROUP	
20	13		
		Natural Convection, Narrow Vertical Slot	
19. ABSTRACT (Continue on reverse if necessary and identify by block number)			
The purpose of this study is to investigate the influence of Prandtl number on steady, or unsteady, flow behavior in a narrow vertical slot. The focus is to examine the effects of Prandtl number on natural convective flows, and the formation of single and multiple cells, over a range of Prandtl numbers from $Pr = 0$ to $Pr = \infty$ . Both numerical as well as analytical approaches are undertaken in studying these phenomena.			
20. DISTRIBUTION / AVAILABILITY OF ABSTRACT <input checked="" type="checkbox"/> UNCLASSIFIED/UNLIMITED <input type="checkbox"/> SAME AS RPT. <input type="checkbox"/> DTIC USERS		21. ABSTRACT SECURITY CLASSIFICATION UNCLASSIFIED	
22a. NAME OF RESPONSIBLE INDIVIDUAL Capt Daniel B. Fant, Instructor, AFIT		22b. TELEPHONE (Include Area Code) 513-255-3708	22c. OFFICE SYMBOL AFIT/ENY



By assuming a large Rayleigh number and small gap, the two-dimensional Navier-Stokes equations are reduced to the simpler boundary-layer form. Boundary-layer equations are then derived for both the low ( $Pr \leq 0.1$ ) and high ( $Pr \geq 10$ ) Prandtl number regimes, including the limiting conditions of  $Pr \rightarrow 0$  and  $Pr \rightarrow \infty$ . Furthermore, the equations obtained for the low Prandtl number regime also hold for any finite Prandtl number in the range  $0 < Pr \leq 1.0$ .

Numerical solutions to these equations are obtained by using a stable, second-order, fully-implicit, time-accurate, Gauss-Siedel iterative procedure. In addition to numerical solutions, steady-state analytical solutions are derived using perturbative methods.

For most of the Prandtl numbers studied, the boundary-layer approximations produced results that compared well with those obtained by other researchers using the complete Navier-Stokes equations and more sophisticated numerical and analytical techniques. The exception is in the high Prandtl number regime, which may have been due to neglecting the streamwise viscous terms. However, the results show that the boundary-layer approach captures all of the important physics of low Prandtl number fluid flows, flows where  $Pr \sim 1.0$ , and a significant portion of that involved with fluids of high Prandtl number.

Due to lack of time, the limiting condition where  $Pr \rightarrow \infty$  was not accomplished. However, the equations for this type of fluid are developed and presented in Chapter III. The  $Pr \rightarrow \infty$  case should be investigated in any follow-on studies that are conducted.